UNIVERSITY OF CALIFORNIA,
IRVINE

Cryomilled Aluminum with Diamantane: Thermal Characterization by DSC and Effects of Magnesium

DISSERTATION

submitted in partial satisfaction of the requirements

for the degree of

DOCTOR OF PHILOSOPHY

in Materials Science and Engineering

by

Michael Colin Arnold

Dissertation Committee:
Professor James C. Earthman, Chair
Professor Martha Mecartney
Assistant Professor Timothy J. Rupert

2015

DEDICATION

This work is dedicated to my wonderful wife, Corinne. The strength it took to remain so patient with me during these last several years is, I truly believe, amazing. The work I am presenting here that is dedicated to you will be a major foundation of our future life together. Although it was written by me, is based on the research I carried out, and has my name on it, this all belies the simple truth: there is just as much of you in this as there is me. I could not have done this without you. You could never get the credit you deserve for making this happen. So for this, I say with utmost sincerity, thank you.

TABLE OF CONTENTS

LIST OF FIGURES

LIST OF TABLES

LIST OF SYMBOLS

Symbol	Meaning
A	Grain boundary area
B	Number of moles of matrix metal species
D	Grain diameter (an average of a bulk material unless stated otherwise)
D_{eq}	Equilibrium grain diameter at a given temperature
D_{kin}	Characteristic kinetic grain size
D_0	Grain size at the onset of grain growth
$\bar{D}_{OBS,0}$	Grain boundary diffusivity
$FWHM$	Full width half max (XRD peak)
G	Gibbs free energy
H	Enthalpy or heat
ΔH_{seg}	Heat of segregation
IB	XRD peak integral breadth
K	Scherrer constant
M	Stress concentration in a triple junction
M_{obs}	Observable grain boundary mobility
M_0	Intrinsic grain boundary mobility
Q	Activation energy for grain growth
Q_{GB}	Activation energy for grain boundary diffusion
R	Gas constant
R^2	Correlation coefficient
T_m	Absolute melting temperature

V	Volume
V_m	Molar volume
a	Solute adsorption area
b	Burger's vector (absolute value of)
c_t	Total molar solute concentration
c_0	Molar solute concentration in grain interiors
e	XRD internal strain
k	Boltzmann constant
$k(D)$	Grain size dependent kinetic rate term
k_{max}	Maximum kinetic rate term
k_{min}	Minimum kinetic rate term
k_σ	Hall-Petch proportionality constant
k_0	Initial kinetic rate term; assumed the same as k_{max}
n	Grain growth coefficient
π	Number of moles of solute species
t	Time
t_f	Total time of integration of DSC heat signal
x	Ratio of instantaneous integrated DSC heat signal to total integrated heat signal
Γ	Grain boundary excess
Λ_i	General term for the set of parameters k_0, η, φ, D_{kin}, D_{eq}, and n
α	Defined by equation 13
γ	General grain boundary or interfacial energy
γ_0	Pure grain boundary energy
$\dot{\gamma}$	Deformation strain rate

η	Defined as $1 - k_{min}/k_{max}$
μ	Chemical potential
μ^0	Intrinsic chemical potential
σ_{obs}	Measured (and measurable) strength
σ_0	Frictional strength
τ	Applied stress
φ (or ϕ)	Rate change of $k(D)$ in the transition from k_{max} to k_{min}

ACKNOWLEDGEMENTS

I would like to thank Dr. Jim Earthman for his support, advice, and patience during this project. Certainly I would have been much more lost at times than I already was if not for his guidance. I would like to thank Dr. Ali Yousefiani for his valuable input and advocacy. His support for students' education and his appreciation of the research process in practical applications was important in structuring this work. Thank you to Dr. Martha Mecartney for support in my graduate education which, in particular, allowed my research to go a bit smoother. Thank you to Dr. Khinlay Maung for bringing me up through the program and teaching me more than anyone would ever care to know about cryomilling. Thank you to Dr. Ming-Je Sung for the help with microscopy work, for which I will perpetually owe you a cup of coffee. Likewise, thank you to Dr. Jian-Guo Zheng and the UCI Materials Characterization Center for quite excellent training on the instruments and help in making sure I could fit my work into the scheduling. Thank you to Dennis and Cheryl Carey for your loving support of Corinne and me. This work was partially funded by the UC-Discovery program with cooperation from The Boeing Company.

CURRICULUM VITAE

University of Oklahoma, Bachelors of Science in Chemical Engineering
2002 – 2007

University of Kansas, REU Program Participant
2006

University of Southern Mississippi, REU Program Participant
2007

University of Oklahoma, Undergraduate Research Assistant
2006-2007

University of California at Irvine, Masters of Science in Materials Science and Engineering
2007 – 2008

University of California at Irvine, Teaching Assistant
2008 – 2013

University of California at Irvine, Doctorate of Philosophy in Materials Science and Engineering
2008 – 2015

ABSTRACT OF THE DISSERTATION

Cryomilled Aluminum with Diamantane: Thermal Characterization by DSC and Effects of Magnesium

By

Michael Colin Arnold

Doctor of Philosophy in Materials Science and Engineering

University of California, Irvine, 2015

Professor James C. Earthman, Chair

Many structural applications require a material that is both lightweight and corrosion resistant, for which aluminum and its alloys may be considered for use if not for their relatively low strength. By improving strength of aluminum through the Hall-Petch mechanism, it could become a more suitable choice for many structural applications. Cryomilling is used as a production technique to strengthen aluminum by reduction of grain size to the 20-50 nm range. Although the powders produced by cryomilling are well within the nanocrystalline regime, the powders experience significant grain growth during consolidation to a solid body. Cryomilled powders have been shown to remain nanocrystalline by introducing a nano-diamond, diamantane to the grain boundaries. To better characterize the thermal stability of the cryomilled powder with diamantane, Differential Scanning Calorimetry (DSC) was used to measure the isothermal heat flow in the $0.6T_m$ to $0.9T_m$ range. A model was developed to correlate the isothermal DSC signal to a grain growth curve and grain growth parameters were elucidated by assuming variable boundary mobility with a sigmoidal form. The model revealed a tendency for boundary mobility to transition from an athermal grain growth mechanism to

standard thermally activated grain growth. Grain growth parameters were compared to shed light on possible mechanisms of aluminum-diamantane involvement during grain growth. Powders and consolidated samples with very low concentrations of diamantane and with magnesium were observed by TEM, SEM and XRD, and compared both separately and together to characterize the how thermal stability is affected by diamantane concentration and the presence of magnesium.

CHAPTER 1. INTRODUCTION

Since the reports by Hall and Petch in the 1950s (ref 1-2), the relationship between the strength and crystallite size in metals has become well known in the metallurgical community. The mathematical description of this correlation, called the Hall-Petch relationship, describes how average crystallite size, *D*, changes with observed strength, σ_{obs}, by:

$$\sigma_{obs} = \sigma_0 + k_\sigma D^{-½} , \qquad \text{(eq. 1)}$$

where k_σ and σ_0 are material-dependent constants. The phenomenon behind this relationship generally is understood to be due to the effect of dislocation co-interaction in confined spaces. The common thought is that as dislocations move to grain boundaries, they will have difficulty moving across the boundaries due to changes in crystallite orientation, thereby causing a pile up of dislocations generated from the same source. The pile up will then continue until enough energy is supplied for the dislocations to traverse grain boundaries and induce further deformation. Because the strain fields of the dislocations traversing the same path will interact negatively, the smaller the domain in which they pile up, the greater the energy requirement will be to move them for any given strain, thereby increasing the observed strength of the material (ref 3). It thus stands to reason that any crystalline material with permanent deformation carried by dislocation motion can be strengthened by reducing its average grain size. One such material in which this effect is expected is aluminum. Although aluminum is considered relatively low strength for a structural material, aluminum and its alloys could be made to be lightweight alternatives for some steel, titanium or nickel alloys if their strengths could be doubled (ref 4).

1.1. Grain Boundary Strengthening

Ultimately, the motivation for this work is improvement of the strength to weight ratio of metals. Increasing strength or, alternatively, decreasing weight within a fixed volume has a significant impact on cost savings and, in some cases, can make possible a material for applications before which it would not have been considered. As a general mode of improvement, several approaches might be taken. Altering chemistry to change the alloying effects may allow for some increase in strength, for example, by adding precipitation hardening elements to metals. Of course, if altering the microstructure in this matter is not called for, the other way in which bulk mechanical properties may be adjusted is by changing the way in which deformation may be carried internally within a structure. This could be done on the bulk scale, such in the case of high strength metal foams for use in compressive applications (ref 5). Deformation may also be carried differently by stabilizing or reducing an otherwise non-equilibrium phase, for instance, the reduction of embrittlement of alloy steels by eliminating retained austenite (ref 6). Alternatively, a fully dense material could be altered to change the way deformation is carried by increasing the energetic requirement for dislocation motion. Although low alloy solid solution metals are similar to precipitation hardened metals in the strict sense that they are not chemically identical to the pure metal, the basic structure is the same and it is the slight difference in chemistry from the alloying elements increasing internal strain that strengthens the metal (ref 7). The internal strain from alloying elements may then affect how dislocations carry deformation. In addition to chemical effects, the internal strain due to dislocation concentration may be increased by taking the same number of dislocations into a smaller volume (ref 3). Supposing dislocations do not easily cross a grain boundary due to

the change in crystal structure and regularity as stated before, the first to reach a grain boundary will stall until sufficient energy is supplied to do anything else, be it climb up the boundary, annihilate at a site in the boundary and generate a new dislocation elsewhere, or change directions at the boundary and propagate to the adjacent grain (ref 8). So long as the source of the initial dislocation remains active, others follow behind the initial dislocation which will then cause a pileup at the boundary behind the first dislocation after stalls. This results in many overlapping dislocation strain fields and then an increase in required energy to further propagate any of the dislocations towards the pileup. Of course, without dislocation movement, deformation is not carried as described by this standard deformation mode of a crystalline material. In other words, the pileup results in an apparent increase in strength due to the increase in the required stress to carry deformation. Because this description is that of grain boundaries impeding dislocation motion to increase observed strength, this is also often called “grain boundary strengthening” (ref 8-9). Ignoring the influence of domain size, this is also the essence of strain hardening, a dynamic deformation phenomenon (ref 8). If it is assumed that changing the domain size decreases the distance from a dislocation source to a pile-up, then it is to be expected that pile-ups would occur more quickly in a small domain and, thus, smaller crystallites in a material would make it appear stronger. This is analogous to the explanation for grain boundary strengthening given in Hall’s seminal work (ref 1).

1.2. Grain Growth Effects

Grain boundaries are known to be non-equilibrium features which means that any volume occupied by a grain boundary has a higher energy than what an ideal crystalline structure would have occupying the same volume (ref 8). This provides a driving force to eliminate grain boundaries in polycrystalline materials, although the driving force is often mitigated by kinetic inability to activate the process (ref 10). Nevertheless, as the percent volume occupied by grain boundaries increases, the amount of instability in the overall system increases as well. Although a useful way to envision why grain growth occurs, there is another factor in the driving force for grain growth. Specifically, this explanation does not provide any indication that grain growth rate would increase with a decreasing grain size, as is generally accepted to be the case. Because the effective curvature of grains must increase for their boundaries to stay continuous as the percent volume occupied by grain boundaries increases, Burke and Turnbull's curvature-driven grain growth model provides the remainder of the explanation and predicts that grain growth rate will increase with increasing boundary volume as well (ref 10). This well-known phenomenon is described by the curvature-driven equation for grain growth:

$$dD/dt = k_D/D, \qquad \text{(eq. 2)},$$

where dD/dt is the grain growth rate and D is the average grain diameter. The kinetic term in the rate equation, k_D, is typically taken to have temperature dependence of an Arrhenius form, $k_D = k_0\exp(-Q/kT)$, such that, starting from a base value of average grain size, $D_0(t = 0)$, the grain size at any given time would be:

$$D(t) = (k_D t + D_0^2)^{½} = [k_0\exp(-Q/kT)t + D_0^2]^{½}, \qquad \text{(eq. 3)}.$$

Combining equations 1 and 3 and condensing the Arrhenius term, the observed strength becomes time-dependent from $t = 0$ in the form:

$$\sigma_{obs} = \sigma_0 + k_\sigma(k_D t + D_0^2)^{-¼}, \quad \text{(eq. 4)}.$$

Because measurements of strength require instruments with finite sensitivity to observe and measure material behavior, polycrystalline materials may appear to have no change in properties over even the order of decades, either because D_0 is so large, k_D is small enough, or both, and there is no detectable change of the value contained in the brackets. If, however, k_D is significantly large compared to D_0, the observable strength could decrease at a very high rate, such that it decreases by a large portion in the time between producing the small-grain structure and characterizing it. As k_D is said to have Arrhenius temperature dependence, the loss in observable strength would be exacerbated by a thermal treatment when k_0 is large compared to D_0. Care must thus be taken when considering how to produce very small grain sizes that can take advantage of Hall-Petch strengthening. Otherwise, the time, energy and resources spent to produce a nanocrystalline material would be for naught as unstable grain growth would lead to softening.

1.3. Producing Nanocrystalline Metals

Ignoring any possibility of measurable grain growth at room temperature, one approach to utilizing a nanocrystalline structure in a metal that is not normally nanocrystalline, i.e. that is intentionally grain boundary strengthened, is to introduce the nanograins in the as-used conditions. The advantage of this approach would be that the structure would need no forming, joining or other operation that requires heat. Bottom-up fabrication approaches that take

advantage of printing technologies and sol-gel synthesis are promising example applications that may be able to create nanocrystalline structures from non-heat treatable materials in an end use form, assuming the technology is further developed (ref 11-12). Furthermore, powder extrusion may be able to take advantage of nanocrystalline non-heat treatable alloys for applications that require wire stock, so long as the frictional heat produced during the powder extrusion does not induce grain growth (ref 13). Heat treatable alloys could be used in a similar manner, although the effects of heat treatment must be considered along with any loss in strength due to grain growth. However, with the observation that room temperature or even cryogenic grain growth can occur in some cases (ref 14-15), avoiding thermal treatment may not be enough to maintain strength in a structure. This approach also limits the service temperature of the nanocrystalline product to regimes in which grain growth will not occur. The applicability of a material for an application would need to be demonstrated for each case as a matter of safety.

If exposure to heat could not be avoided, an alternative approach to maintaining a high strength nanocrystalline structure is to prevent grain growth during thermal treatments and high temperature service. In essence, it is the same approach as before, specifically, to avoid providing enough thermal energy to activate grain growth, except in this case the goal is to induce a change in the material that makes it more tolerant to heat, pressure, or both. Ideally, the energy required for any measurable grain growth would be so great that, at atmospheric pressure, the material would break down, melt, or the like before undergoing grain growth. This approach to maintain strength by maintaining a nanocrystalline structure relies on either

significantly slowing the diffusive processes necessary for grain growth, or making other processes thermodynamically more favorable in the temperature range of concern. Slowing the diffusive process would be more desirable, as the grain growth process would be active but very slow, which would impart stability against grain growth up to relatively high temperatures and for periods of time that could impart a long service life on working part. Introducing other thermodynamically favorable processes would impart some stability in a microstructure, but the approach comes with a natural risk that the stability would be limited in time and temperature ranges and that the other process or processes introduced could have other deleterious effects on the material.

The cryomilling of aluminum provides an excellent case study of how grain growth is altered to maintain a very small grain size with a corresponding increase in strength. Mechanical milling is a method to produce a nanocrystalline metal by crushing a powder using a milling medium such as hardened steel balls, whereafter the crushed powder is mechanically welded back together by the same milling medium once it cannot be crushed any more (ref 16). The repeated fracturing and welding of powder ultimately produces a powder with a much smaller average grain size than the starting powder, owing to the random orientation of particles during the welding stage. A pictograph of the process can be found in [16]. The energy input is significant so as to cause such extreme amounts of powder fracture and welding, and so by performing the milling at cryogenic temperatures, sufficient energy for grain growth and recovery is not available. Milling in a cold environment is effective enough that the final average grain size of the powders is kept very small. This method of milling is called “cryomilling” and aluminum is

typically cryomilled by constant immersion of all milling media and powder in liquid nitrogen. Contrary to the initial expectations when the method was first gaining wide use, it is the supposedly un-reactive milling liquid that helps to impart thermal stability to cryomilled aluminum (ref 17).

1.4. Cryomilling Aluminum

According to the curvature driven grain growth description of equation 2, grain growth will be very slow once the average grain size becomes very large, even at a high homologous temperature. However, the quantitative definition of "very large" for many materials may be on the order of millimeters, sizes below which grain growth should be observable when heated (ref 18). In the case of aluminum, grain growth at an average grain sizes in, for example, the tens of microns has been reported at elevated temperatures and should be expected upon heating (ref 18). Simply as a *gedankenexperiment*, it should also be expected from equation 2 that, if 35 µm powders are cryomilled to have an average grain size of 35 nm, there should be nothing to prevent the cryomilled powders from undergoing grain growth to eventually revert back to their 35 µm grain size after being heated. Furthermore, regarding this *gedankenexperiment*, equation 3 predicts that the initial grain growth should be very relatively fast compared to grain growth observed in coarse grained aluminum. However, this is not what is observed (ref 4). Cryomilled aluminum typically has an average grain size of 20-25 nm and when heated to a high homologous temperature will not exceed an average grain size of about 300 nm after consolidation and thermal treatment (ref 17,19). Lavernia and coworkers first reported this phenomenon to be due to small aluminum nitrides, oxides and carbides present

after milling. These hard ceramic particles were postulated to pin grain boundaries from moving, which imparts thermal stability to the structure (ref 17).

Cryomilling of aluminum has been extended to the cryomilling of aluminum alloys as well. Thermal stability of alloys generally has been observed to be about the same as with pure aluminum, with the average grain size of 25nm in Al6061 to 150 nm after consolidation by sintering and Al7075 growing from approximately 50nm to 250 nm, and so forth (ref 20-21). As expected from equation 1, the strengths imparted in the final materials were greater than those of the coarse-grained counterparts. In comparison, the strength of Ti-6Al-4V is about 825 MPa (approximately 25% greater than cryomilled and consolidated Al7075) while the density is about 70% greater than that of aluminum (ref 22). Thus, the strengthening of cryomilled aluminum has been initially demonstrated, and equation 1 predicts the milled product's strength could stand to be improved by as much as an additional 50% by reducing average grain size below 100 nm into the nanocrystalline regime.

The mechanism of hard ceramic particles slowing grain growth is understood to be by the particles pinning grain boundaries by acting as an obstacle to diffusion (ref 23). If grain growth is assumed to be a mechanism by which atoms desorb from one grain edge, diffuse through the boundary with the adjacent grain, and adsorb to the opposite edge, then the hard particles slow grain growth by impeding the diffusion step, literally acting as a physical barrier (ref 10, 24). Thus, it should be expected that the grain size at which pinning occurs would depend on the size of the hard ceramic particles. This was indeed the case reported by Lavernia and

coworkers, with the precipitates 10-33% of the average grain size. To maintain a grain size under 100 nm, it would be expected as a simplification that the type of hard particles that could pin grain boundaries would scale the same amount, or under 2 nm.

Maung and coworkers took the approach of utilizing smaller, hard pinning particles by using diamantane in aluminum to pin boundaries, rather than aluminum-based ceramic particles (ref 4, 25). Diamantane is an organic molecule in a class of diamond-like molecules called *diamondoids*. Diamondoids are simple hydrocarbons that form cages in the diamond cubic structure and terminate in hydrogen (ref 26). Because their bulk form is held together only by weak van der Waals forces, they seem waxy when handled, however, they are expected to be extremely rigid as a molecule due to the diamond-cubic covalent bonds (ref 27). Thus, if sitting on a grain boundary in aluminum and the system energy is kept low enough for them to remain un-reactive with the aluminum, they should act as diffusion barriers. Diamondoids may also be understood as being oligomeric units of diamond, such that if many were to react, bulk diamond may be formed. In that sense, diamondoids may be classified by the number of diamond cubic cages that would contribute to the bulk form, with a single diamond-cubic cage called *adamantane*, two diamond-cubic cages called *diamantane*, three cages called *triamantane*, and so forth. Again, this description imparts an expectation that they must be considered “hard” since they are units of an extremely hard substance. How diamantane and the other diamondoids are classified aside, diamantane is the second smallest of the group, composed of two diamond cubic cages (ref 26). In this work, diamantane was the primary

diamondoid introduced into the aluminum host, however, adamantane was used at some points as well.

Introducing diamantane into aluminum grain boundaries was accomplished by taking advantage of the fact that the grain boundaries created during cryomilling form by welding two previously free surfaces together. By adding diamantane to the milling mixture, it can coat the surface of the milling powders and subsequently be welded into the newly created grain boundaries (ref 25). Several hours are given for the milling to approach the minimum possible final average grain size, and it is expected that the initial milling period in which the starting powders are broken down also allows for diamantane to be reduced from its bulk wax-like form to a fine powder coating the aluminum surfaces so that the diamantane is evenly distributed along the grain boundaries in the produced powder (ref 20, 25, 28). To determine the amount of diamantane to add to the cryomilling mixture, a model was assumed to approximate the volume of the bulk occupied by grain boundaries, and the diamantane volume was chosen to fill some portion of the grain boundary volume (ref 25, 29). The initial estimate was that, for an as-milled grain size of 20-25 nm, the amount of diamantane necessary to fill all grain boundaries would be just less than 1 weight percent. Some thermal stability was imparted to the cryomilled powders with diamantane added in small weight percents, as was expected. The stabilized grain size after annealing at $0.8T_m$ was less than 60 nm after the addition of 1 wt% diamantane to the milling mixture (ref 25). Furthermore, after consolidation by hot isostatic pressing, high speed cold extrusion, and annealing, the average grain size remained under 100 nm. Surprisingly, the addition of diamantane did not strengthen the consolidated form. Rather

the material with diamantane had a lower strength than the control material without diamantane (ref 4). This was attributed to a change in deformation mechanism to grain boundary sliding accommodated by dislocations in the nanocrystalline regime (ref 4, 30).

This work begins where Maung, et al. left off. It begins by describing the techniques used in detail and describes a how a technique typically used for characterization of phase transformations can be used to measure grain growth in real time. A model is then introduced to describe grain growth in cryomilled aluminum. The possibility of grain boundary sliding occurring below 100 nm grain size is reintroduced and discussed in grain growth model terms as well. The work also investigates a solid solution strengthened aluminum matrix with a small amount of magnesium added, cryomilled in the same manner as the pure aluminum. The aluminum-magnesium solid solution is discussed in the context of a grain boundary sliding deformation mechanism. Finally, questions are introduced from this point in the work with hypotheses introduced to guide future work.

CHAPTER 2. METHODS AND PRELIMINARY RESULTS

2.1. Cryomilling

2.1.1. Stock Powder

The powder used in cryomilling, referred to in the as-purchased condition as *stock* powder, had a minimum 3N level of purity, or 99.9%, for what would be the "pure" components and 99% purity as 1100 series aluminum for all other powders. The stock powder of alloy powder was not verified chemically as all stock powder was purchased with known composition, such as a composition meeting the composition ranges designated for the alloy by the International Alloy Designation System, UNS, or the appropriate governing body. Although every reasonable effort was taken to ensure the stock powder was kept from contamination, it was not practical to take extreme measures to do so. Even with care taken in the storage and handling of stock powders, it is usually not certain that a stock powder from its supplier would have been handled as delicately. As such, the powder was stored and handled so as not to introduce significant contamination, and it was assumed that there was some oxide present in the final powder that originated as surface oxide in the stock powder. If, however, it is desired in future works to remove surface oxide, it can be removed from aluminum by chemically by etching in dilute acid, such 0.1N sulfuric acid. The acid will attack the oxide quickly but has a low dissolution rate of bare aluminum. Concentration of the acid may be increased to increase the etch rate, however, this will also increase the rate at which the bare aluminum surface is etched. The process must be carried out in an inert atmosphere, rinsed in a non-oxidizing medium, and sealed before removing to air. This extra step would be desirable if a high purity powder such as 5N (99.999%)

is used to reduce the influence of contaminants at later points. Even with alloy powders, this extra processing step may prove useful when attempting to completely remove the influence of precipitates in solution alloys. Although this step was not taken for the powders used in the current project, it is recommended when exceptional purity in the final powders is a concern, and care must be taken when selecting an etchant for other metals.

The stock powders used in the current project are as shown in Table 1.

Table 1 Powders Used for Cryomilling

Powder	Size	Source
99.9% Aluminum	325 mesh	Atlantic Equipment Engineers
99.8% Magnesium	325 mesh	Alfa Aesar
1100 Aluminum *("Commercially Pure")*	17 - 30 µm	Alfa Aesar
50% Aluminum - 50% Magnesium	270 mesh	Valimet

2.1.2. Equipment

The primary production equipment of the cryomilling work was a Union Process Svegari-type attrition mill, as seen in Figure 1.

Figure 1 Cryomilling Apparatus. *Shown are the body and motor casing, liquid nitrogen connection, and milling container with bottom valve attached. Not shown is the attrition arm or lid.*

The primary milling action was performed by driving a shaft rotationally. The shaft that was driven had 12 arms, divided into four rows of three arms, each row 90 degrees apart and each adjacent row staggered from the neighboring rows; opposite rows of arms were at identical positions with respect to the length of the shaft. The shaft and its arms were contained within a round vessel with double-layer walls and contained by a lid. The main vessel was flanged by a rounded-corner square and the lid bolted to the tank flange at the four corners. The lid had several ports, most of which were 1/8” and sealed with a swage-locking cap. When used in the current project, only one of the 1/8” ports was left open, and that was to allow access of a thermocouple. In addition, a 3/4" port was positioned on a side of the lid, which acted as an

inlet for gas or liquid. It is also important to note that the center-hole allowing access to the shaft was a nipple-type port approximately two inches in diameter.

The bottom of the vessel had a single hole cut into it, aligned with the mid length of one of the flange's edges and spaced approximately two thirds of the way from the center of the vessel and its edge. A round stopper fit into this hole and was connected to a threaded rod that adjusted its position so that it acted as a valve. The position of the rod was determined by two screws 180° apart that fit into sigmoidal-shaped slots in an outer valve casing. At the top part of the slot, the stopper was held in the high position and the valve was closed. By turning the body of the outer casing, the screws holding the center rod dropped as they fell into the lower position of the slots, which subsequently caused the center rod and stopper to drop. This opened the bottom hole and, effectively, the valve to allow contents to vacate the vessel. The entire valve casing was kept in place by a cylindrical shaft bolted to the bottom of the main vessel so that the stopper fit into the hole. When the valve was installed, the stopper position was able to be fine-tuned with two indentations in the top of the stopper head by using a special two-pronged tool to screw the stopper up or down along the center rod. Care was taken to ensure the valve closed flush to the main vessel. If there would have been gaps in the seal, it was at risk of leaking. If the valve stuck up into the vessel, it was at risk of being deformed during milling such that it would freeze into place (requiring repair and ruining the product of a run) or excessively wearing during milling (requiring more frequent replacement).

The milling was carried out in a liquid nitrogen environment. Liquid nitrogen was purchased from Airgas, typically at 22 psi. The necessary amount to mill for 8 hours was approximately 500L, and up to 100L was kept for use after the milling is complete. As such, three 200L cylinders were typically needed for each 8 hour milling run. If the run was particularly efficient, up to 150L may have been left over, and an inefficient run may have used all 600L. The liquid nitrogen was carried through a jacketed tube to a pneumatic valve. The valve was controlled by solenoid switch, which opened the valve in a certain band, typically -160°F to -180°F. This required that the thermocouple position through the vessel's lid be nearly the same each run. As nitrogen boils at about -195°F, a temperature reading of -180°F assumed the thermocouple was reading at a few inches above the liquid level. Thus, if the thermocouple sat a few inches above the contents, the contents of the vessel should have been approximately immersed entirely in liquid nitrogen. If the position of thermocouple would have changed, then the band of the controller would need to be changed accordingly or the liquid level would have been affected. Also, this meant that the liquid nitrogen had to be flowed in manually above -160°F, which acted as a kind of safety feature to the nitrogen level. In addition to the pneumatic valve, a manual butterfly valve acted as a bypass. Not only was this used for the initial filling of the tank, it was a convenient aid in fine-tuning the controller, and it was also sometimes used to provide a constant trickle in the bypass. After the junction of the bypass and line out from the pneumatic valve, another jacketed pipe connected to the inlet on the tank's lid. This connection was swaged as well.

The last equipment necessary to cryomill in this setup was the milling media. The media used were 2mm balls, which were cleaned after each use and reused. Although they were not thoroughly sorted after each cleaning, it was important to remove balls that clearly misshapen, rusting, discolored, or reduced in size. The smooth, spherical surface of the balls allowed for the milling action to occur without severe damage to the vessel or shaft; however misshapen balls would have had the potential to damage any of this. Balls showing rusting or other discoloration were usually removed as both were likely to increase contamination in the produced powder. Finally, the design of the valve was such that the stopper should have kept the 2mm balls from being trapped between the stopper and the bottom of the vessel when it was in the down position. If the balls were reduced in size, this feature was not guaranteed and if balls were trapped in that gap then the valve would be effectively stuck open after it was first opened. For this reason, balls were occasionally replenished. The typical ratio of balls to milled powder was 30-32 to 1, i.e. one kg of starting powder required 30 to 32 kg of balls.

The vessel, shaft, shaft's arms, and milling balls were all constructed of 316L stainless steel.

2.1.3. Handling and Sealing of Cryomilled Powders

After cryomilling was complete, the powders kept from contacting air. There was likely to already be oxide present because of what was on the powders prior to the milling, however effort was made to keep the amount of oxide in the final powder to a minimum amount. Some of the milled powders' surfaces would have been bare aluminum coming out and, if quenched with air at any point, these surfaces could have reacted with the available oxygen enough to

make airborne powder explosive. While this was unlikely to happen in most cases after milling, it was a simple enough task to protect the freshly milled powders that these precautions were taken for safety reasons as well.

The primary means to protect the powders was the liquid nitrogen. This was what protected the powders during milling and, if enough was on hand to have excess at the end of the 8 hour cycle (the extra 100L mentioned previously), the extra was used to keep milled powders in a slurry. The slurry—while extremely cold to handle and requiring its own precautions to prevent burning of skin—very effectively kept out oxygen and allowed transport of the powder so long as the liquid level stayed above the powder level. If the liquid level did drop, very little time remained for handling the powder in air. Evaporating nitrogen would continue to protect powders, but that protective layer flows out of the holding vessel. More liquid nitrogen was at times introduced to increase the handling time in an open environment, however, gaseous nitrogen was used to flush the top of the powder first so that the action of pouring the liquid nitrogen did not push oxygen onto the powders. It was found that the most efficient way to transfer powders was to first open the bottom valve at the end of milling and allow the slurry to drain into stainless steel beakers. So long as the valve was not stuck open, it could be closed and more liquid nitrogen added to the vessel while it the attritor remained powered off. Once filled to the point that it was being read by the thermocouple, the attritor would be turned back on and let run for only a few minutes. The purpose of this was to break off any powders stuck to the milling balls and reintroduce them back into the liquid nitrogen slurry. With the machine still running, the valve would be carefully opened and the slurry collected again. When needed,

the slurries in different beakers were combined, but it is important to note that some liquid was always kept on the top. Closing the valve and flushing with liquid nitrogen was repeated until the liquid nitrogen that is collected was clear.

While the milled powder was in slurry form with liquid nitrogen, it was transferred to a glove box, although in future experimentation any other means of containment that is able to keep out air may be used. That said, a glove box is preferable as it allows for ready handling of milled powders and is designed to purge gas. The glove boxed used in the present work was set up with an oxygen monitor and purging gas source, so that it could hold powders for an extended time without significant contamination. The gas purge was particularly useful when the powders were in slurry form as the evaporating nitrogen effectively purged any air that was in the glove box when the powders were placed into it. Once in the glove box and the liquid level dropped below the powder level, clean instruments were used to gently stir the powders to bring out the remaining nitrogen. When the powders were finally free of the liquid, they were carefully poured into another sealed vessel, which was then taken out of the glove box for further processing.

As the powders were typically consolidated after milling, the ideal vessel in which to transfer freshly milled powders inside the glove box was a Hot Isostatic Pressing canister. The canister was selected to have sufficient volume to contain the powder and have an inner diameter appropriate for the starting diameter of every intended consolidation step. The wall thickness of the canister was selected to be thick enough to not warp under compression but thin enough

to allow for compression. The top and bottom caps of the canister used in the present project had an interference fit, and the seam between the caps and body were welded for a tight seal. Note, however, that an alternative design was developed but not implemented for the current work and it is highly recommended in any future work that this design be used. The new design consisted of top and bottom caps that would be tightly threaded and all other design aspects would be the same, including being welded at the seam between the cap and canister body. The top cap also contained a smaller tube at its center through which the powder was loaded into the canister. Careful consideration was given to selection of this tube. It was selected such that it did not have walls so thin that they deformed under the compressive pressure during processing, but they were thin enough to be able to be crimped either with or without heat. Furthermore, the inner diameter was selected to be large enough to fit a funnel for loading powders while still being appropriate for the vacuum system used later to evacuate gas from the powders. Because of these requirements, the deciding factors in the design of this loading tube were the inner diameter and wall thickness, with the outer diameter a consequence of those two factors. The limit of the outer diameter was also dependent upon the main canister diameter. The canister material was selected so that it was similar to the powders being milled, but because the can is not fabricated as a single piece, the material selected had to be easily welded. The 2XXX series of aluminum was considered for its high strength but was not suitably weldable. The 7XXX series offers was considered for its high strength as well, but was cost prohibitive. The next best option was, thus, a 6XXX series alloy. For the current project, the main body was constructed of 1 ¾" OD 6061 aluminum with 0.065" wall thickness. The loading tube construction was 0.370" ID 6061 aluminum with 0.065" wall thickness, although a larger

inner diameter (at least 0.500”) is recommended for future work because most lab funnels do not suitably match the 0.240” inner diameter.

Once the can was initially constructed, it was immediately checked for weld integrity. Because a high vacuum level would be applied to the canister first and a large compressive pressure would be applied later, leaks would kill the vacuum level and could cause explosion (respectively, for each step). To check for leaks, the cans were immersed in a liquid, either water or methanol; all welds were in the liquid. When in the liquid, a positive pressure was applied which caused the evolution of bubbles at leaks. As a matter of practicality, this was done by using compressed lab air and placing the nozzle into the canister’s tube with very light pressure applied manually to form a seal and build pressure in the tube. If bubbles were observed, the canister was tilted and rotated to determine the point from which they were emerging. The leak was marked and the canister returned for patching the hole or holes. Towards the end of the current work, significant bending was observed in consolidated canisters, which was determined to likely be due to pinholes opening in welds during the consolidated. As such, once the canister was leak-free, it was annealed to relieve any residual stresses, particularly welding stresses. As the weld integrity may have been affected by, the canisters were leak checked again to verify no holes opened. Once verified to be leak-free, including after annealing, the final preparation step for use was to attach a valve. In the current project, a simple ball-valve from SwageLok was used. In the current project, duct tape was wrapped around the valve handle such that resistance prevented it from opening without cutting the tape. In future works, a valve with a locking mechanism is recommended, however,

any method that prevents a closed valve from opening may be used. Given the lack of difficulty in keeping the valve closed, the method used in the current project proved effective. During the loading of powders into canisters, the valve did not need to stay connected to the canister, but the valve was fitted beforehand on the loading neck so that the ferrule was in the proper position. A temporary fitting was put in place of the valve to aid with loading powder, however, this may not necessary in future works. Once ready for use, completed canisters with all ferrules swaged into place were stored in the glove box used for loading powders.

With useable canisters on hand and an evaporating powder slurry ready for loading, a funnel was used to aid in pouring powder into the canister. Because of the extreme cold of the powder slurry, oversized cold gloves were worn over the gloves in the box so that the powders could be transferred immediately. However, this would not be necessary in other cases and, instead, time could have been given for the holding container to warm, which would also aid in handling. In the current work, it was decided that powders need to be transferred immediately, to ensure the least amount of contamination by limiting the time spent in the glove box. It was decided that better results would be obtained by not allowing the collection vessel to warm. When the canister was filled and space inside eliminated as much as is practically possible, the top of the powder level should was protected by a mesh. In the current work, 200 mesh aluminum was used due to its ready availability. However, in general, the mesh should be smaller than the powder size to prevent loss of powder later. In some cases, ensuring this may be impractical as the size of milled powders may vary to some degree from run to run, in which case the size distribution would be much wider than that of the stock powders. A general

guideline would be to take known values of powder size and size distribution after consolidation from already characterized work, for example, at least 20 µm (ref 20). In the case of stock powder with 325 mesh size, any smaller mesh size would suffice. Because of the expected wide distribution of powder sizes and the size of the mesh available, the aluminum 200 mesh was used in multiple layers as follows. The mesh was put in place through the loading tube, so that it would expand once out of the tube and into the canister body to cover the loading tube hole. Even if the mesh had not expanded and instead stayed folded, crumpled, or remained in the loading tube, this also would have served the purpose of preventing powder from flowing up and out of the canister body. Because the final placement of each meshing could not be verified visually and could only somewhat be verified tactilely, it is a reasonable assumption that there is only a chance it would have been placed correctly. This was the reasoning for using several bits of meshing for each loaded canister. Furthermore, the loaded canister was finished off by loading aluminum wool above the powder surface so that it rested at the bottom of the loading tube. Once the canister was loaded, the valve was replaced back onto the loading tube of the canister and it was sealed in the off position. Once the valve was replaced to the canister and sealed off, the canister was removed from the glove box without a risk of contamination of the powders. The final step in preparing the canister was to place a filter on the other side of the valve. This filter, also supplied by SwageLok, was reused by attaching pieces of piping on either side so that one piece attached to the valve and the other piece attached to a vacuum setup later. The filter was reusable and not replaced during the course of the current work. Although reusable, in future works this type of filter should be replaced when it becomes evident that gas flow through it is being restricted. By placing it on

the outward flow of the valve, the filter was actually protecting the vacuum system itself and not the valve. In fact, slight contamination of the valve may not likely have been a problem so long as it was flushed occasionally to ensure it fully closes. Similarly, the mesh, aluminum wool and filter were all used for protecting the vacuum system and not the valve. The canister, valve, and filter are what were delivered for degassing in the following step when outsourced.

2.2. Consolidation of Powders

2.2.1. Removal of Residual Gas

When the powders were fully sealed, the only gasses that absolutely needed be removed were the air and nitrogen trapped between the powders. Consolidation only requires that the canister stabilize under the kind of vacuum level achieved by a small rotary lab pump. If contamination was not a concern, the low vacuum level supplied by a small pump would be all that was needed and no further degassing would be required. However, as contamination by hydrogen or water were of concern, full degassing in the current work was necessary. As such, a staged heating and vacuum cycle was needed. Once the canister (with valve and filter) was attached to the vacuum setup and that setup was pulling against the closed valve, the valve was slowly opened. Although not absolutely necessary to open slowly, evaporation of nitrogen may have built a positive pressure in the canister and which could have overloaded or blown out powder with enough back pressure that it could escape the filters and contaminate the vacuum system. When the valve was fully open, the canister was being lightly degassed to remove air and nitrogen. If this was all that was necessary, pressure would have been brought down for preparing the canister for consolidation. As this was not the case for the current project, the

pressure was brought down to approximately 1 torr and the process continued for full degassing.

The vacuum system used for in-house degassing was constructed of all stainless steel tubing and SwageLok fittings. The system first connected to the canister with a low vacuum gage near the connection. This measured the vacuum pulled by a roughing pump, down to approximately 1 torr. Next along the line was a turbo vacuum followed by an ion gauge. In addition, a bypass line was split from the main line before the ion gauge so that the roughing pump could optionally pull on the powder canister with the turbo pump isolated. While not absolutely necessary, it was done each time and allowed the majority of any gas to be evacuated from the canister before removing the rest of the gas with the turbo pump. The turbo pump could have been kept on the whole time, however, it had minimal startup time so there was no need for this. With the roughing pressure in the appropriate range, the back connection of the turbo pump opened without risk of damaging the turbo pump, the bypass was closed off, and then the front connection of the turbo pump line was slowly opened. Note that the back must connection was required to be opened first to prevent backflow caused by the roughing pump. The roughing pump was able to pull the pressure down further than the recommended 1 torr, so the spike in pressure felt by the turbo pump was negligible. In other words damage to the pump was not a concern in this setup. When the turbo pump line was completely open, the system was left alone while the pressure dropped. A schematic of the degassing setup of the degassing setup used in the current work is shown in Figure 2.

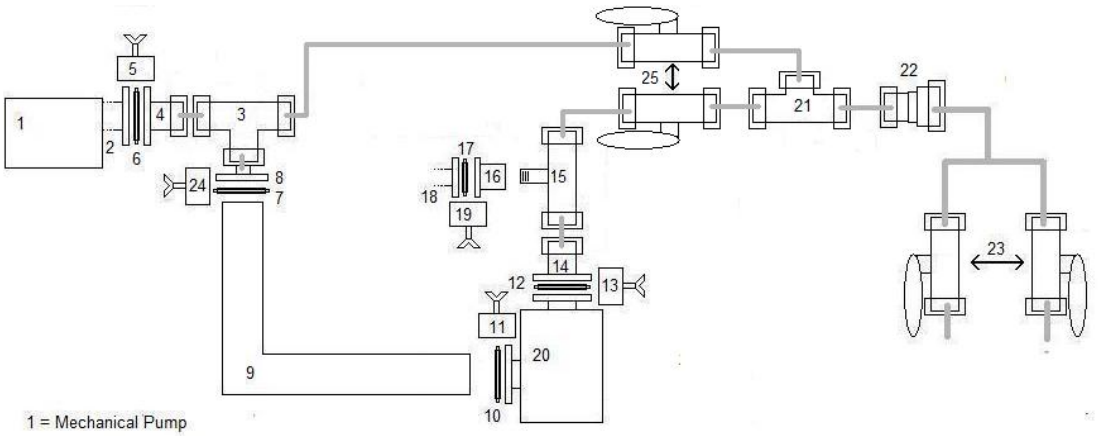

1 = Mechanical Pump			
2 = PG	8 = JNWSWAG4014 (KF40-SL)	14 = JNWSWAG1614 (KF16-SL)	20 = Turbo Pump
3 = -400-3 (T union)	9 = KF16 metal hose	15 = -400-3-4TTM (T union w/ mNPT)	21 = -400-3 (T union)
4 = JNSWAG1614 (KF16-SL)	10 = KF40 centering & O-ring	16 = fNPT to KF40	22 = -810-6-4 (0.25"-0.5" recuding U)
5 = KF16 clamp	11 = KF40 clamp	17 = KF40 centering & O-ring	23 = -83TS8 (ball valve)
6 = KF16 centering & O-ring	12 = KF16 centering & O-ring	18 = IG	24 = KF16 clamp
7 = KF16 centering & O-ring	13 = KF16 clamp	19 = KF40 clamp	25 = -83TS4 (2-way ball valve)

Figure 2 Powder Degassing Schematic *The numbers indicate vacuum hardware used, including the Swagelok part number where applicable. PG = pressure gage (low vacuum), IG = ion gage. Not shown is the particulate filter below the valves (#23).*

The ideal pressure range for full degassing was less than 10^{-5} torr, with 10^{-6} or better for the heating step. If this pressure was not reached, it was first assumed to be due to a leak in the canister small enough to be undetectable by the preliminary check. Methanol was lightly sprayed on the can welds and, if a pressure spike was observed, the leak was identified. A filled canister should not be discarded, of course, so any on-the-spot fix was the best option to fix small leaks. If a leak could not be identified, the canister was sealed off and the vacuum system connections were checked. Once the canister reached 10^{-5} torr it could have been closed off for consolidation, which would have provided better results than a 1 torr vacuum level. As full degassing was desired, heating was required at this point.

At 10^{-6} torr, tramp contaminants and some water will be outgassed. Any water that is released is likely not chemically bonded to powders, but only physically attached through weaker interactions. To fully liberate water, light hydrocarbons, and hydrogen, heat is applied. This would have been best done by using a case furnace, however because this was not conducive to the setup a well-insulated tube furnace was used with extreme caution instead. The temperature was measured at the can surface using thermocouple leads. The temperature ramping was slow and in three stages with a soak at each stage. The first stage, 135°C, liberated the remaining physically absorbed water. The second stage, 290°C, liberated chemically absorbed water. The third stage, 400°C, liberated hydrogen. After pressure stabilization at each soak, the canister was held longer to ensure maximum removal of gasses. However, if time or exposure to temperature is of any concern in future works, ramping may continue once the vacuum level recovers with an acceptable level of confidence the powders are sufficiently degassed. After the vacuum level recovered during hydrogen degassing and was shown to be stable, the can was slowly cooled. Rather than continue holding vacuum using the valve, the loading tube was sealed with a hot crimp over a length of about four to six inches. Care was taken not to crack the tube as this would make compressive consolidation in a fluid not possible and the powder would essentially be wasted. To ensure the crimp stayed, it was cut towards its top (away from the canister) and the top and sides of the crimp were welded. No other work was needed to prepare the powders for consolidation. Any outsourced degassing was carried out at Aegis Technologies (Santa Ana, CA) or California Nanotechnologies (Cerritos, CA) with similar methods. The degassing of cryomilled aluminum powders is discussed much more extensively in (ref 31).

2.2.2. Initial Consolidation

All initial consolidation work in the current project was outsourced to Kittyhawk Inc (Garden Grove, CA). The consolidation was by Hot Isostatic Pressing (HIP or HIPing). In isostatic pressing, a pressurized fluid delivers pressure to the contents of a chamber. If the pressure is built by compression of a piston in a cylinder containing an inert gas such as argon, the gas acts as the fluid and is able to deliver the pressure equally, in other words, isostatically. The fluid may also carry heat, which increases diffusion rates and effectively expedites consolidation. This was chosen for initial consolidation over other consolidation methods because the isostatic compression eliminates directional properties resulting from directional consolidation. The standard HIPing profile used was 520°C at 15 ksi for 2 hours. All HIP consolidation was carried out as *piggybacking*, in other words the relatively small canisters were secondary to large pieces in the commercial HIP chamber. This is unlikely to affect results of the work, however, it should be noted that a devoted laboratory scale HIP setup would eliminate any unknown variables resulting from consolidation with other work pieces. After completion of the HIP cycle, the can material was removed to access the inner consolidated billet. It should also be noted that HIPing bonds the consolidated powder to the can material as well. For this reason, the ideal can material would be a consolidated form of the inner material, however, as the powder is of experimental design this is not possible. The 6061 material would have had some interdiffusion between powder at its inner surface and the can walls and to account for this, the can material was always removed in addition to 0.25” of the apparent consolidated billet surface.

The dimensions of HIP billets, after removing can material, typically were 1 to 1.25 inches in diameter. The consolidated density can be estimated to be approaching the theoretical density at this point such that further consolidation will achieve more than 99% of the theoretical density (ref 4). As such, to further consolidate towards almost full density, a secondary consolidation is needed.

2.2.3. Final Consolidation

Extrusion may be considered an option at this point, although extrusion typically leads to elongation of grains which, as mentioned before, may lend to directional properties. Two methods of final consolidation were used in this project, one being *trap extrusion* and the other swaging. Trap extrusion is a room temperature process carried out at a very high rate such that the only heat experienced by the material is from internal heating. The trap extrusion was carried out at California Nanotechnologies (Cerritos, CA) and the exact parameters were unknown due to the process being proprietary. The starting pieces for trap extrusion were 0.5" diameter cylinders of 1" length, which were extruded to 0.25" diameters. Swaging was carried out at Sophisticated Alloys, Inc (Buttler, PA) at a temperature of 350°C. The starting rods for swaging ranged from 0.7" to 0.8" in diameter and were reduced to 0.5" diameter. Starting rod lengths ranged from 8" to 12". Between the two final consolidation methods, trap extrusion proved much more successful due to the brittle nature of the consolidated forms, which often caused cracking in swaged rods. Note that in the following analyses, only certain powders with a final consolidation of swaging were compared because some as-HIPed rods could not be successfully swaged. Following final consolidation, the rods and extruded pieces were either

machined as threaded, round tensile specimens for mechanical testing or prepared accordingly for other analyses. Consolidated and turned down billets with the remaining can material are shown in Figure 3.

Figure 3 Billets Consolidated from Cryomilled Powders. *The portions at the top left and right of the image are still in the HIP canister. Other sections have had the can removed by lathing.*

2.3. Differential Scanning Calorimetry to Measure Grain Growth

2.3.1. Initial Theoretical Development

The evolution of microstructure in polycrystalline metals is an important consideration given that it is entirely the chemistry and microstructure of a material that determines its properties in any given environment. Given that material performance is dependent upon material properties, the change in performance observed in different environments is thus related to evolution in microstructure and chemistry. Any means by which the changing microstructure can be observed with environmental changes would be useful in predicting changes in performance. One such important example of the observation of the evolution of material

microstructure in polycrystalline metals is the change in average grain size during processing, annealing, and any other number of procedures that require the application of heat. Perhaps the most commonly used method to observe the change in average grain size during heat treatment is to heat material samples in an oven at different temperatures for different amounts of time and measure the average grain size as a function of time and temperature. However, the heat treatment with this method can in practice be highly variable due to the uncertainty of the heat transfer processes in many lab ovens. In fact, the sample size and geometry, temperature equilibration in the oven, and sample loading would all have to be ideal to ensure that the time-temperature profile intended for a sample is even close to the heat treatment that the sample received. If the microstructural evolution in a material is slow, then such possible discrepancies likely wouldn't be significant for extended heating profiles, however this may not always be the case. In fact, if significant grain growth or other microstructural changes occur on the same time scale in which a sample is likely to come to full thermal equilibrium, then information about the initiation of microstructural evolution is lost. This makes in-situ observation of grain sizes during heat treatment a valuable tool in determining the full evolution of microstructure. In-situ x-ray diffraction (XRD) measurements may be performed, but may also require specialized equipment to heat the sample, in addition to the problem that the range over which grain sizes can be measured accurately by XRD is limited (ref 32). In-situ transmission electron microscopy (TEM) measurements may be made as well, but again this requires specialized equipment and arduous setup compared to the other available options (ref 33). Furthermore, the high energy electron beam used in TEM measurements may be enough to alter the grain growth behavior and obscure the results of the experiment. Given

that grain growth is a thermally activated process, a thermal analysis technique that takes data in real time might prove to be more accurate, convenient and cost-effective than other in-situ techniques.

Lu (ref 34) showed that differential scanning calorimetry (DSC) can be used to indirectly measure grain growth in some polycrystalline materials systems by directly measuring the evolution of heat during the growth process. By increasing the homologous temperature of a polycrystal to a high value and measuring the heat flow, Lu showed that it is possible to determine the grain size at any time if the average grain size before and after heating is known. The functional equation from Lu's study can be derived by differentiating the product of the specific grain boundary energy and grain boundary area, assuming the grain boundary energy remains constant,

$$dG = \gamma dA, \qquad \text{(eq. 5)},$$

where G is the average free energy of a boundary, γ is the average specific grain boundary energy, and A is the average grain boundary area. Assuming the average grain to be perfectly spherical and equating the heat evolution to the average free energy per unit volume, $dH = dG/V$, one obtains the result

$$dH = (12\gamma/D^2)dD, \qquad \text{(eq. 6)},$$

where D is reintroduced as the average grain diameter. Assuming the average grain size to start at some value, D_0, prior to heating the material, equation 6 may be integrated to show the heat evolved during grain growth

$$\Delta H(t) = -12\gamma[D(t)^{-1} - D_0^{-1}], \qquad \text{(eq. 7)},$$

where $\Delta H(t)$ is the heat evolved at any time and $D(t)$ is the average grain size in the material corresponding to the time at which the heat evolution is $\Delta H(t)$. If the average grain size after heating the material is known and taken to be D_f, then the heat evolved at this point would be $\Delta H(t_f)$, also a known value. By taking the heat evolution at any time in proportion to the final value of the heat evolution, a new term may be defined as $x(t)$ so that

$$x(t) = \Delta H(t)/\Delta H(t_f) = [D(t)^{-1} - D_0^{-1}]/[D(t_f)^{-1} - D_0^{-1}], \qquad \text{(eq. 8)},$$

which is equivalent to Lu's equation 4 (ref 34). Of course, this assumes that growth during the increase to and decrease from the high homologous temperature is negligible, an assumption that can be tested with knowledge of the growth kinetics. Neglecting any grain growth occurring during the heating and cooling times, knowing $x(t)$ over time in addition to the initial and final average grain sizes measured allows inference of the grain size over the same time period.

2.3.2. Improvement of the Theory

Weissmuller's relationship between solute excess in a multiphase system (ref 35) can be used along with the Gibbs absorption isotherm and a simple chemical mixing potential to yield a relationship between grain boundary energy and grain size of

$$c_t = c_0 + (3\Gamma V_m/D), \qquad \text{(eq. 9)},$$

where c_t is the total solute concentration, c_0 is the solute concentration away from the boundaries or "matrix concentration", and V_m is the molar volume of the mixed system. The term Γ in equation 9 is defined as the solute excess at the grain boundaries, and deserves extra attention in its explanation. Kirchheim describes an earlier though experiment in which a

container holds a liquid and a gas that is only partly soluble in the liquid. In the "upright" orientation, there will be some equilibrium at the interface that depends on the amount of gas dissolved in the liquid and the surface area of the liquid such that and that, when the container is tilted onto its "side" orientation, the amount of gas adsorbed at the surface will change due to the change in interfacial area (ref 36). Kirchheim then notes that the same thought experiment can be applied to a solid system in which solute atoms are adsorbed at a grain boundary such that, as the boundary moves and grain boundary area is reduced, equilibrium of the entire system must shift accordingly. The thought experiment described thusly is initially put in terms of the differential change in the moles of gas at the interface with respect to change in interfacial area and by way of Maxwell relations is equated to differential change in interfacial energy with respect to chemical potential, in other words, the Gibbs adsorption isotherm. From this, the solute excess is defined as

$$\Gamma = (\partial \pi/\partial a)|_{T,V,\mu,B} = -(\partial \gamma/d\mu)|_{V,T,a,B,} \qquad \text{(eq. 10)}$$

where π is the number of moles of the solute or alloying species, a is the interfacial area, γ is the specific interfacial energy, μ is the chemical potential of the solute or alloying species, B is the number of moles of the host or matrix species, V is the system volume, and T is the temperature (ref 36). From the definition given in equation 10, equation 9 can be seen much more simply as a mass balance.

The Gibbs isotherm in equation 10 can be integrated with respect to a pure matrix material such that $\gamma = \gamma_0$ and $\mu \rightarrow \mu^0$. Rearranging the isotherm such that $d\gamma = -\Gamma d\mu$ can yield the change

in interfacial energy at low solute or alloying concentrations by integration with respect to the pure state as such:

$\gamma - \gamma_0 = -\Gamma[RTc_0\ln(c_0) + RT(1 - c_0)\ln(1- c_0) + \Delta H_{seg}]$, (eq. 11),

where the chemical potential is integrated by introducing a heat of mixing term with ΔH_{seg} the heat of segregation of solute or alloying atoms in the grain boundary. The grain boundary energy can then be determined for small amounts of solute or alloying atoms by rearranging equation 11 and substituting in equation 9:

$\gamma = \gamma_0 - \alpha D$, (eq. 12)

where

$\alpha = [(c_t - c_0)/3V_m]/[RTc_0\ln(c_0) + RT(1 - c_0)\ln(1 - c_0) + \Delta H_{seg}]$, (eq. 13).

From the derivation of the grain boundary excess, it is clear that c_0 must change as grain size changes and, thus, α is not a constant. However, if it is assumed that a solute or alloying species has similar solubility in the grain boundary as it has away from the grain boundary, then c_0 will not change appreciably and α may be approximated as a constant. In that case, equation 12 may expressed in differential form with respect to average grain size to yield the simple relationship

$d\gamma = -\alpha dD$, (eq. 14).

Supposing now that α will be positive, equation 12 states simply an approximation of how grain boundary energy will be decreased by small solute additions. If, then, the average grain size reaches some critical value, γ will become zero and the driving force for grain growth will have disappeared. That is to say that equation 12 predicts that some equilibrium grain size exists due to a difference in solubility of a solute or alloying species between the grain boundary and grain

interior and that γ will become zero at this average equilibrium grain size, D_{eq} (ref 36). In this case, equation 12 predicts that $\gamma_0 = \alpha D_{eq}$. Equation 12 may then be rewritten in either of the following:

$$\gamma = \alpha(D_{eq} - D) = \gamma_0(1 - D/D_{eq}), \qquad \text{(eq. 15)}.$$

It has been postulated that equation 9 can be stated in a more general case in which grain boundary concentration of a solute or alloying species is not inversely proportional to the average grain size, but is proportional to D^{-n} such that (ref 37)

$$c_t = c_0 + (3\Gamma V_m/D^n), \qquad \text{(eq. 16)}.$$

By selecting n = 1, the grain boundary energy is expressed by equation 15 and the Burke equation of grain growth, equation 2, results. By selecting n = 2, the grain growth equation of Michels results (ref 37). Without specifying the physical reason for n taking a particular value, equation 16 is thusly taken instead of equation 9 such that equation 15 becomes

$$\gamma = \alpha(D_{eq}^{\,n} - D^n) = \gamma_0(1 - D^n/D_{eq}^{\,n}), \qquad \text{(eq. 17)},$$

and equation 14 becomes

$$d\gamma = -\alpha n D^{n-1} dD, \qquad \text{(eq. 18)}.$$

With an understanding of how grain boundary energy and its differential change with grain size, a new approach to the measurement of grain growth with DSC may be taken. By modifying the differential Gibbs free energy change to include changes in the boundary energy, $dG = \gamma dA + A d\gamma$, and by keeping the assumption of the average grain being perfectly spherical, equations 17 and 18 can be used with the differential Gibbs free energy equation to give the heat evolution with grain size as

$$dH = -6\alpha[(n + 2)D^{n-2} - 2(D_{eq}^{n}/D^{2})]dD, \quad \text{(eq. 19).}$$

Integration of equation 19 gives the heat evolution at any time as

$$\Delta H(t) = -6\alpha[(n + 2)/(n - 1)(D(t)^{n-1} - D_0^{n-1}) + 2D_{eq}^{n}(1/D(t) - 1/D_0)], \quad \text{(eq. 20)}$$

so that equation 8 becomes

$$x(t) = [(n + 2)/(n - 1)(D(t)^{n-1} - D_0^{n-1}) + 2D_{eq}^{n}(1/D(t) - 1/D_0)] \div$$

$$[(n + 2)/(n - 1)(D_f^{n-1} - D_0^{n-1}) + 2D_{eq}^{n}(1/D_f - 1/D_0)], \quad \text{(eq. 21a)}$$

for $n \neq 1$. For $n = 1$, equation 1 will integrate to yield the result

$$x(t) = [(n + 2)\ln(D(t)/D_0) + 2D_{eq}^{n}(1/D(t) - 1/D_0)]/[(n + 2)\ln(D_f/D_0) +$$

$$2D_{eq}^{n}(1/D_f - 1/D_0)], \quad \text{(eq. 21b).}$$

Thus, with $\Delta H(t)$ measured over time, $x(t)$ can be calculated and, with D_0 and D_f known, n and D_{eq} can be estimated to find $D(t)$. Alternatively, the grain growth kinetics can be assumed as well to solve for $D(t)$and $x(t)$ subsequently so that the calculated form of $x(t)$ can be compared to the measured one. The fit of the calculated form to the measured form can be improved by changing the value of n and the form of the grain growth kinetics until a least-squares fit is obtained. This inherently allows one to both determine the form of the grain growth kinetics and the values of n and D_{eq}. This is the approach that will be taken in this study. Note that the value n used in the development is one less than what is typically considered a "grain growth exponent" and, mathematically, becomes equivalent to the usual definition of a grain growth exponent when the chosen form of dD/dt is integrated with respect to D.

2.3.3. Thermokinetic Combined Equation for Grain Growth

The definition of the boundary excess, *Γ*, with a general dependence upon grain size can be determined by rearranging equation 16:

$\Gamma = [(c_t - c_0)/3V_m]D^n$, (eq. 22).

This relates the changing concentration of impurities in the grain boundary as the volume of the boundaries change. As a single grain boundary sweeps through the interior of a material and its total line length (or equivalent circumference if approximated as a spherical cross-section) increases by consuming smaller grains, the overall sum of all grain boundary lengths must decrease to conserve volume in the entire system. Equation 22 shows that a non-zero *Γ* requires that the boundary concentration of impurities must change and that the direction of change will be the same as the sign of *Γ*. Thus, depending on the sign of *Γ*, a sweeping boundary will either pick up or drop off impurities. So long as the impurities remain mixed into the host atoms at the boundary, then as the concentration of impurities changes at the boundaries, the diffusivity of host atoms through and along the grain boundaries is likely to change (ref 39). To describe exactly how the average boundary mobility changes with grain size, one would have to have a detailed knowledge of how the host and impurity atoms diffuse in and along grain boundaries in the changing atomic atmosphere, something which requires significant—and possibly not easily measurable—knowledge of any system at hand. Furthermore, the relationship can be complicated by multiple types of impurities and other factors influencing diffusivity such as internal stresses. Whatever the case, the general requirements of how boundary mobility changes with grain size are that the mobility should saturate at upper and lower bounds and that the transition between the upper and lower bounds be continuous. A

mathematical expression often found in nature that describes such a transition is the sigmoidal function. In some situations, it may be possible that the mobility is dependent upon an increasing adsorption of impurities into the grain boundaries, which could then lead to a sigmoidal change in mobility with grain size. In other situations, it may be the case that, at some grain size, the growth mechanism changes to a more energetically favorable one. Similarly, the movement of boundaries could be initiated by some process such as a concentration gradient that terminates once the driving force—a chemical potential in this example—is removed. At that point a secondary mechanism would remain.

Regardless of why the mobility of a grain boundary might change as grain size increases, the sigmoidal form of $M(D)$ requires a minimum mobility, maximum mobility and transition point. All of this is encompassed by the equation

$$M_{obs} = M_0[1 - \eta/(1 + e^{-\phi\Delta D}{}_{kin})], \qquad \text{(eq. 23)}.$$

In equation 23, M_0 is the maximum mobility of the boundary and assumed to be the starting mobility at the onset of grain growth. The term η is then effectively the ratio of the maximum and minimum mobility where $M_0(1 - \eta)$ is the minimum or "final" mobility. ΔD_{kin} is the difference between the instantaneous grain size and D_{kin}, which is a kinetically defined grain size at which the mobility is mid way between its minimum and maximum values. The parameter φ is then defined as the rate of transition between the maximum and minimum mobility; note that the rate in this case is with respect to grain size. Although the equation is not derived from first principles, it is a convenient tool for describing how mobility can change continuously between two values during grain growth. Also note that it is defined in terms of

average grain size, D, due to the only variable being $\Delta D_{kin} = D_{kin} - D(t)$, it may be related to any other changing physical property or phenomenon that itself can be described in terms of average grain size, for instance grain boundary solute concentration by equation 16. By defining $k_D = M_{obs}\gamma$ (ref 10) in equation 2 and $k_0 = M_0\gamma$, equations 2, 17 and 23 may be combined to give the final form of the thermokinetic grain growth equation as

$$dD/dt = k_0[1 - \eta/e^{-\phi\Delta D_{kin}}](1/D - D^{n-1}/D_{eq}^{n}), \qquad \text{(eq. 24)}.$$

If grain sizes have been measured over time at a given temperature, values for n, k_0, η, φ, D_{kin}, and D_{eq} can be assumed and $D(t)$ found from them by doing stepwise integration of equation 24. The true values of those parameters can then be found by a least squares fit between the measured and calculated $D(t)$ values. Although it is very likely that several local minima will exist for the chosen 6-parameter data sets n, k_0, η, φ, D_{kin}, D_{eq}, if reasonable bounds are selected for several or all of these parameters, then the correct set of parameters may be deduced or estimated equally reasonably. Furthermore, it should be noted that the theory presented leading to equation 24 assumes that grain growth is entirely driven by the motion of grain boundaries in a polycrystal. However, equations 13, 17, and 18 may be modified to account for grain growth by other means and by determining the relationship between grain size and the kinetic pre-factors of the other processes, the result of equation 24 may be altered to account for the other means of grain growth. For the remainder of this work, equation 24 is assumed correct unless stated otherwise.

With grain growth description chosen as equation 24 and the set of parameters n, k_0, η, φ, D_{kin}, D_{eq} selected, the starting grain size may be measured independently and equation 24 may be integrated to yield the grain size at any time. The calculated grain size along with the initial grain size, n, and D_{eq} may then be used to solve equation 21. As $x(t)$ is a measured parameter, any error in the instantaneous grain size $D(t)$ will be known by comparing the measured and calculated $x(t)$ values, and the set of parameters n, k_0, η, φ, D_{kin}, D_{eq} may be adjusted accordingly to yield a better fit of the calculated $x(t)$ curve to the measured one, assuming the final grain size is known as well. If grain size is not measured for comparison, the $x(t)$ curve yielded form DSC then may be used to measure grain growth by curve fitting to $x(t)$ and adjust the set of parameters n, k_0, η, φ, D_{kin}, D_{eq}. Thus, equations 21 and 24 provide a general means to use DSC to measure grain growth in real time, if D_0 and D_f are known. In particular, this has the potential to be quite useful for demonstrating the shape of a grain growth curve, and knowledge of the value of D_{eq} is helpful in design purposes as it indicates the grain size to which a structure should stabilize while in higher temperature service.

2.4. Powder Characterization

2.4.1. Thermal Characterization (DSC, TGA)

After cryomilling, commercially pure (CP) powders both with and without diamantane or adamantane were thermally characterized with a TA Instruments Q500 Thermal Gravimetric Analyzer (TGA) and a TA Instruments Q2000 Differential Scanning Calorimeter (DSC). The TGA pan used was the stock platinum pan provided with the instrument, the balance was flushed with dry nitrogen at 40 mL/min, and the analysis was carried out in a dry nitrogen flow of 60

mL/min. The standard and sample pans used for DSC were both Tzero type aluminum pans and heating of the pans was carried out in a 50 mL/min flow of dry nitrogen. The heating and cooling profiles of TGA and DSC varied from run to run and will be stated as needed in this work.

Prior to any observation of grain growth, CP cryomilled powders with any diamondoids, CP cryomilled powders with adamantane and CP cryomilled powders with diamantane were characterized with TGA and DSC. Several of the heating and cooling steps were to *equilibrate*, which benefits from some explanation. Often, the measured temperature of the sample would lag behind the driving temperature, which is to be expected due to heat transfer. The equilibration step is meant to allow the sample to stabilize at a set temperature. The effect of this step of a heating program is typically to allow a sample to finish its approach to the set temperature. With this in mind, the preliminary thermal characteristics of each powder are as follows:

CP Cryomilled Aluminum. The TGA heating profile was to ramp from room temperature to 100°C at a rate of 20°C per minute, equilibrate at 100°C, hold isothermally for 2 minutes, ramp to 273°C at a rate of 20°C per minute, equilibrate at 273°C, hold isothermally for 2 minutes, and ramp to 500°C at a rate of 20°C per minute. The sample weight and temperature during the heating are shown in Figure 4.

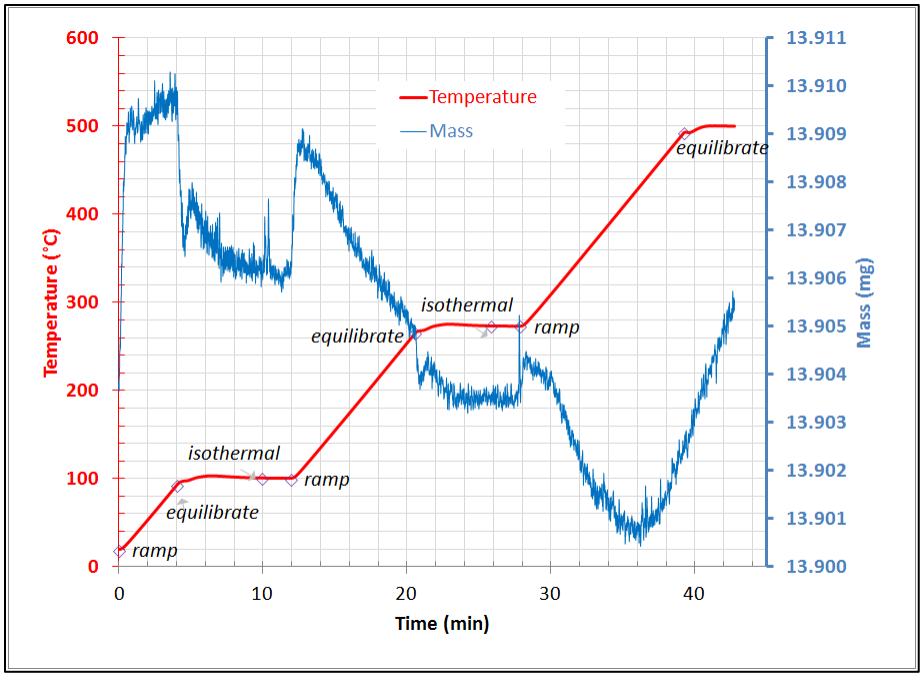

Figure 4 TGA Trace of Commercially Pure Cryomilled Powder Heated to 500°C. *Shown are the programmed steps of the run are indicated.*

Several DSC heating profiles were used. The initial DSC heating profile for capturing thermally activated processes was to ramp from 40°C (chosen to represent room temperature) to 500°C at a rate of 30°C per minute, equilibrate at 500°C, ramp at a rate of 30°C per minute back to 40°C, equilibrate at 40°C, hold at 40°C for two minutes, then use the same ramp and equilibrate profile to again heat to 500°C and return to 40°C. The sample temperature and heat flow during this process is shown in Figure 5. Shown in Figure 6 is the heat flow trace as the sample temperature is raised and lowered both times; as indicated in the figure, the heating is the bottom part of the trace while the cooling is the top part, and the positive heat flow direction indicates exothermal release of energy from the sample. By comparing Figure 5 with Figure 6, it can be seen that more heat input is required to raise the temperature of the sample to 500°C the first time than it is the second time. Except for this difference in heat input, the first and

second heat flow traces appear to coincide well. The direction of exothermic heat flow (up) and location of the heating (bottom) versus cooling (top) part of the trace is the same for the curves recorded for other samples below.

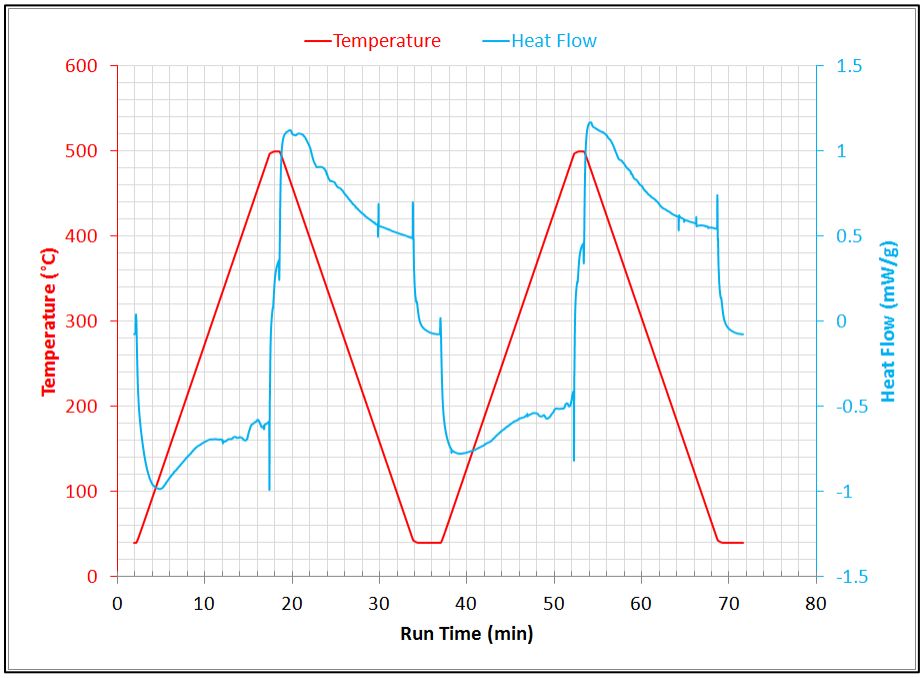

Figure 5 DSC *Q*/*T* vs. *t* Trace of Commercially Pure Cryomilled Powder Heated and Reheated to 500°C. *In this run, the sample was heat twice to 500°C consecutively. Upward heat flow represents exothermic heat flow.*

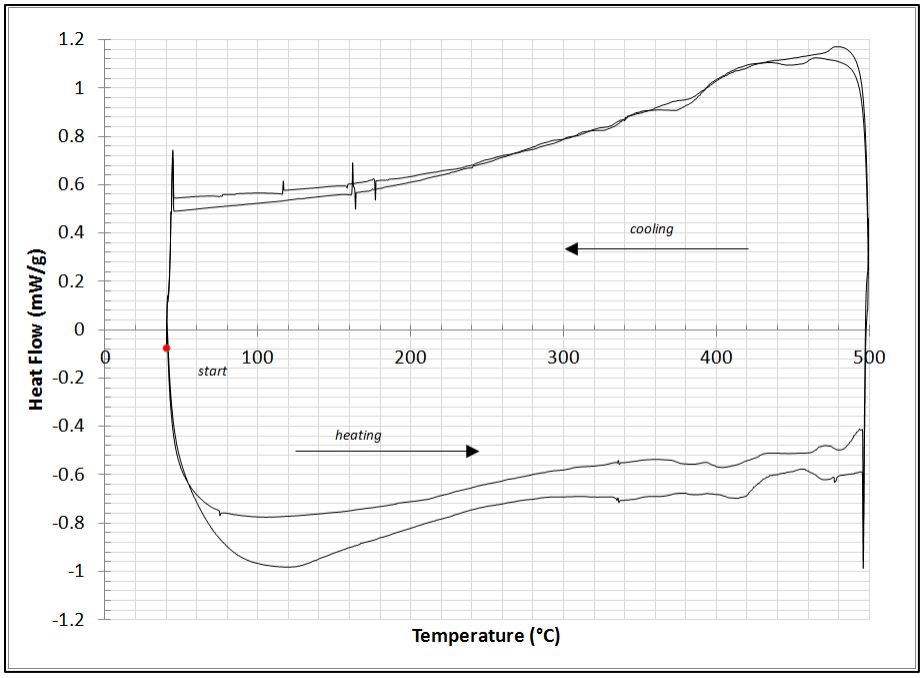

Figure 6 DSC *Q* vs. *T* Trace of Commercially Pure Cryomilled Powder Heated and Reheated to 500°C. *This is the same run as in Figure 5. The bottom portion of the trace shows the heating of the sample and the top portion shows the cooling. The start of the run is marked as such. The second time heating the sample is the trace requiring less heat input.*

An example heating profile used for an isothermal DSC heating experiment is shown in Figure 7. In this example, the sample was heated from 40°C to 300°C at a rate of 120°C per minute, allowed to equilibrate at 300°C, then held isothermally at 300°C for 40 minutes. Following the isothermal hold, the sample was cooled at a rate of 30°C per minute back to 40°C. Figure 7a shows the temperature and heat flow during the run, and Figure 7b shows the heat flow as the temperature is increased, held, and decreased.

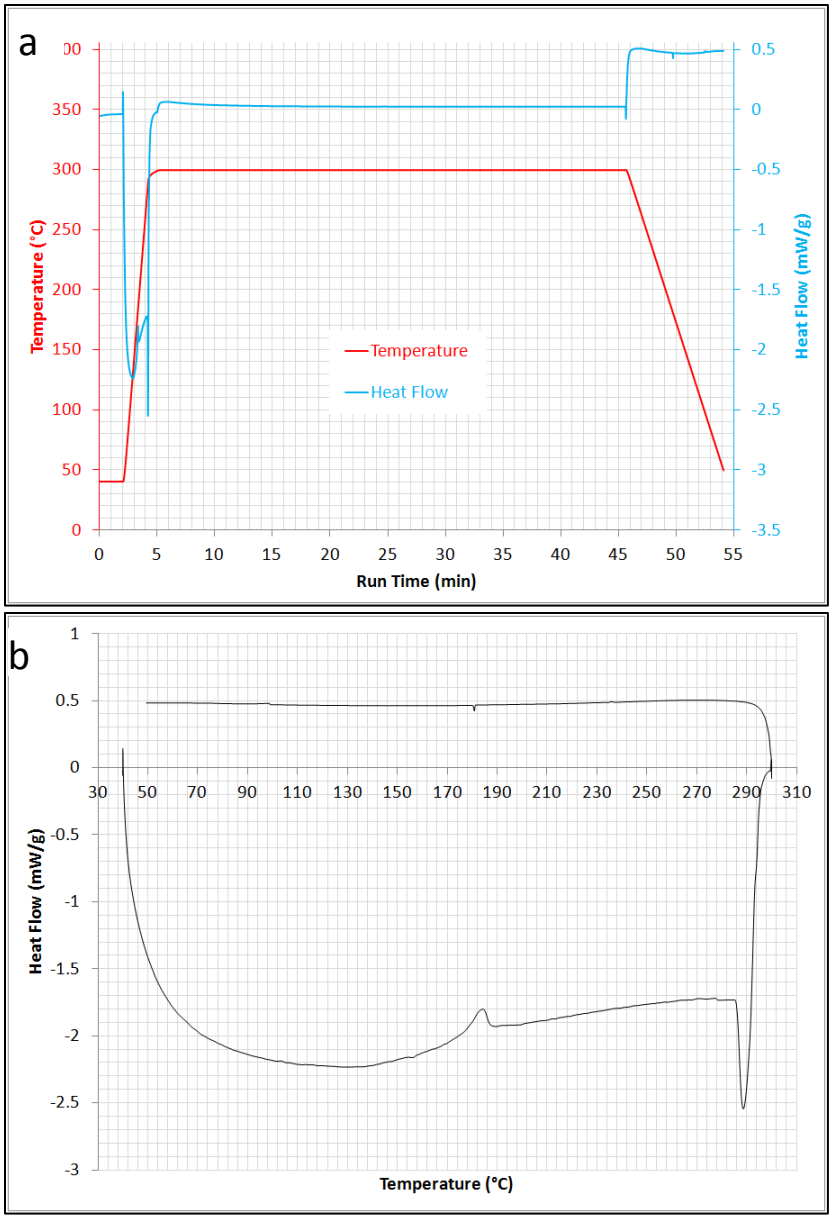

Figure 7 Isothermal DSC Traces of Commercially Pure Cryomilled Powders Heated at 300°C. *(a) The temperature and heat traces. (b) The heat-temperature trace of the same isothermal DSC run. The heating profile is to ramp from 40°C to 300°C at 120°C per minute, equilibrate, hold for 40 minutes, and ramp back to 40°C at 40°C per minute.*

It is worth noting as well that the sample was held isothermally at 40°C prior to the heating ramp, despite not being programmed; likely, this is part of the DSC software to ensure the sample is heated evenly prior to ramping. In this case, the sample ramping was held off for two

minutes while the sample sat at 40°C. The actual temperature ramping rate and heat flow for the first four minutes is shown in Figure 8. In each case, an un-programmed isothermal hold was added prior to the initial ramping and the length generally correlated to the initial ramp rate. In all of the following curves, it can be assumed that there is a short un-programmed—and, thus, unmentioned—isothermal hold prior to the initial ramp.

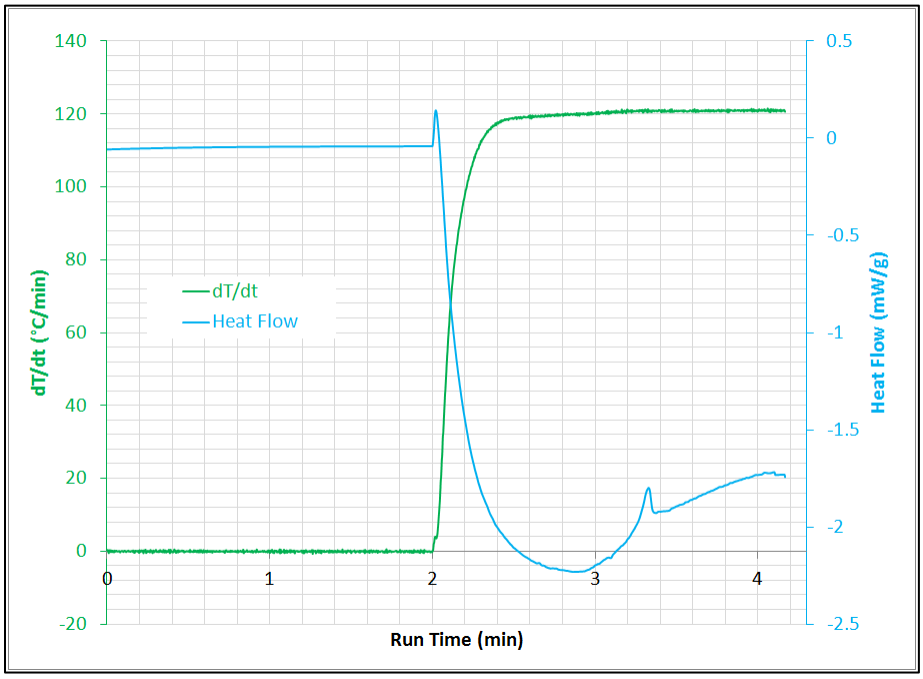

Figure 8 Example Heating Rate and Heat Flow Lag in First Several Minutes Due to DSC Software. *Despite not being programmed, a two minute isothermal hold is applied to the sample prior to a "fast" ramping of 120°C per minute. The same isothermal equilibration of samples can be expected in other DSC runs with "fast" ramping.*

2.4.2. X-Ray Diffraction (XRD)

As-cryomilled powder was analyzed by XRD first by scanning the entire expected range of aluminum reflections, 36° to 80° (2θ) with a Siemens/Bruker D5000 X-Ray Diffractometer and a copper X-Ray tube. The range was scanned at an interval of 0.02° with a dwell time of 1 second

at each angle. Following the full scan, the primary peaks were identified and select peaks were scanned at a slower rate for grain size analysis.

2.4.3. Electron Microscopy (TEM, SEM, EDS)

As-cryomilled 3N aluminum + 5% 3N magnesium + 0.2% diamantane (DM) powders were characterized by SEM using a Philips XL-30 FEG microscope for the purposes of determining morphology of as-milled powders. EDS mounted in the SEM chamber was used for determining the effectiveness of the process in mechanically alloying the starting powders. Shown in Figure 9 is an example SEM micrograph of the as-milled powders showing typical scanning parameters. In the upper left corner of the micrograph, a powder particle (indicated by the arrow) can be seen that appears as an agglomeration of smaller particles welded together. Figure 10 shows an as-milled micrograph of powders along with EDS elemental maps of aluminum, magnesium, and oxygen. The pixels in each of the elemental maps become colored once the radiation count at the location exceeds the threshold indicated just above each image. As the threshold for aluminum is 13 counts and magnesium is 10 counts, the colored pixels in those respective maps represent approximately the same concentrations of the respective elements and the difference in pixel density approximates the difference in concentration. Thus, Figure 10 indicates a relatively well-distributed concentration of both aluminum and magnesium across the image, with aluminum clearly of higher concentration than magnesium. The one exception is what appears to be a particle of magnesium, indicated by the arrow. Also shown in Figure 10 is the oxygen map, with a lower radiation count threshold than what was applied to magnesium and aluminum. The oxygen is evenly distributed as well, which is to be expected, and the

magnesium particle appears to preferentially oxidize more than the aluminum. Note that at no point was there a significant amount of iron, nickel, chromium, molybdenum, lead, or any other alloying element detected in powders or consolidated pieces, thus indicating the milling media did not contaminate the powders.

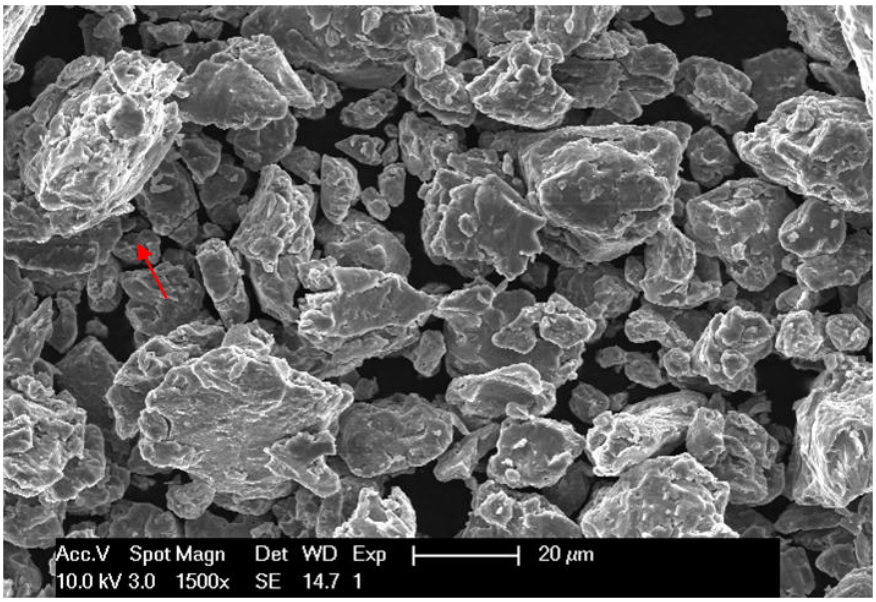

Figure 9 SEM Micrograph of As-Cryomilled Aluminum + 5% Magnesium. *The red arrow indicates a particle that appears to be made of a large number of particle fragments welded together.*

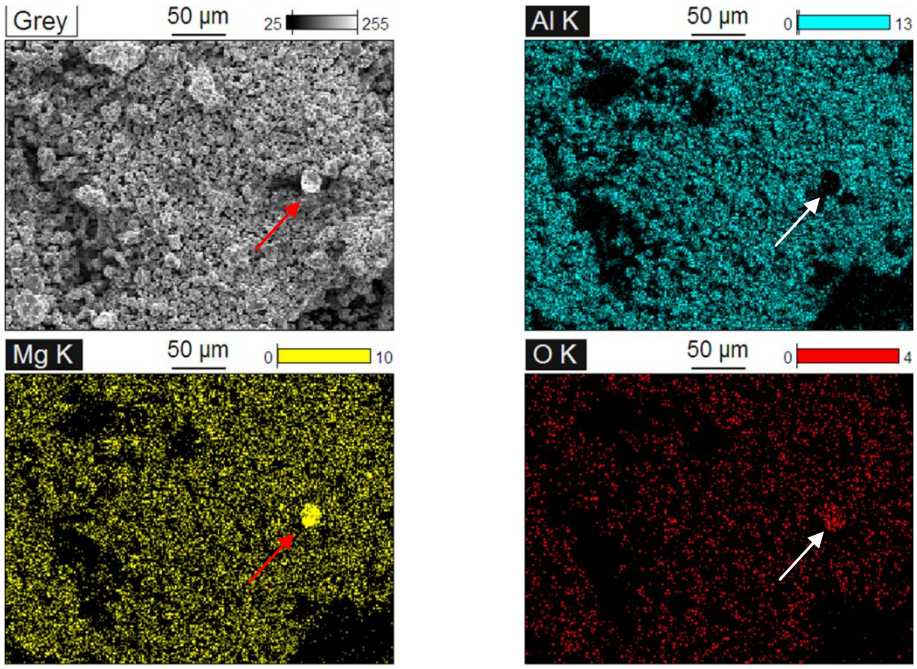

Figure 10 EDS Maps of Aluminum, Magnesium, and Oxygen in As-Cryomilled Aluminum + 5% Magnesium Powders. *The color bars indicate the minimum number of radiation counts at the pixel location to be colored (e.g. 13 or more aluminum K-α counts per blue). The arrows are pointing to a particle with a high magnesium concentration and an absence of aluminum.*

Transmission electron microscopy (TEM) was performed on as-milled particles using a FEI/Philips CM-20 microscope to characterize grain size. Powders were deposited onto PELCO copper TEM grids by Ted Pella by suspending in methanol and drying with a standard laboratory countertop light. An example TEM micrograph is Figure 11 of cryomilled commercially pure aluminum with 5% diamantane.

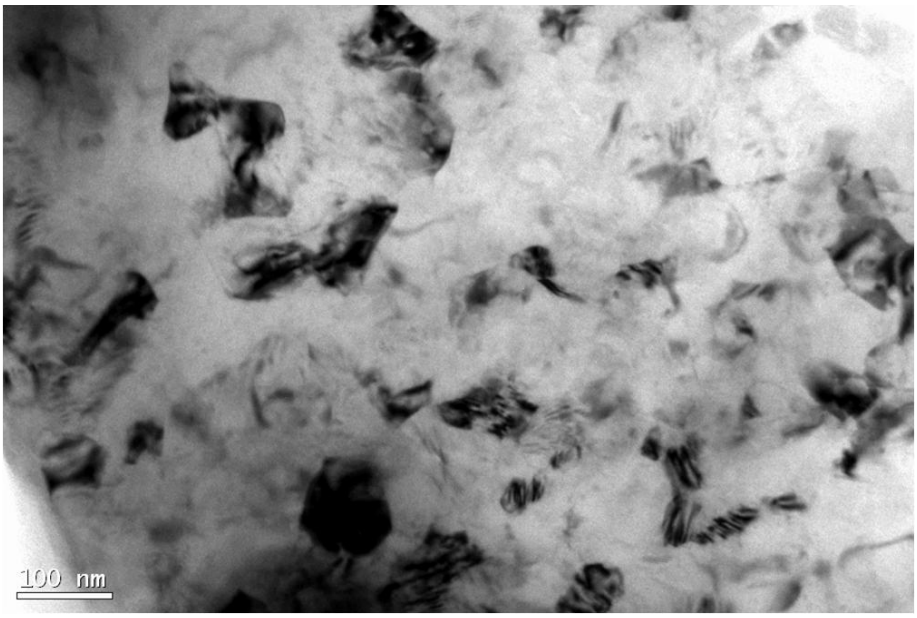

Figure 11 TEM Micrograph of As-Cryomilled Aluminum + 0.5% Diamantane Powder

Grain size was measured in each TEM image using the ImageJ program from the National Institute of Health. The measurement tool in ImageJ was first calibrated to the scale bar in the image and the grains were then traced with the polygon selection tool. Once outlined, the program would calculate the area of the grain based on the number of pixels in the enclosed polygon area. The equivalent grain diameter was then calculated by approximating each grain as a random cross-section circle in a spherical grain, or $D_{eq} = [(Area/\pi)^{0.5}]/\cos(\pi/4)$. The correction factor, $1/\cos(\pi/4)$, is applied because of the assumption that the equivalent circle representing each measured grain cross-section is a random cut through the equivalent grain sphere, thus making the measured average grain size less than the actual average grain size. Given an infinite number of measurements, the measured average will be $\cos(\pi/4)$ of the actual grain size, and so the reciprocal of this value is used as the correction.

2.5. Bulk Characterization

2.5.1. XRD

Following consolidation, samples were scanned with the same equipment as was used for the powders between the angles of 36° and 41°, and between 42° and 47° to characterize the (111) and (200) peaks, respectively. Because each of the solid pieces was mounted in commercially available clay (Hasbro Play-Doh), the clay was scanned as well, and these peaks were identified in each trace as applicable. The XRD traces of the (111) and (200) peaks for cryomilled powders of: CP aluminum, CP aluminum + 0.5% DM, 3N aluminum + 0.2% DM, 3N aluminum + 5% 3N magnesium, and 3N aluminum + 5% 3N magnesium + 0.5% DM are shown in Figures 12 and 13. The diffraction profiles taken in Figures 12 and 13 were scanned at 0.03° intervals with a 1 second dwell time at each angle.

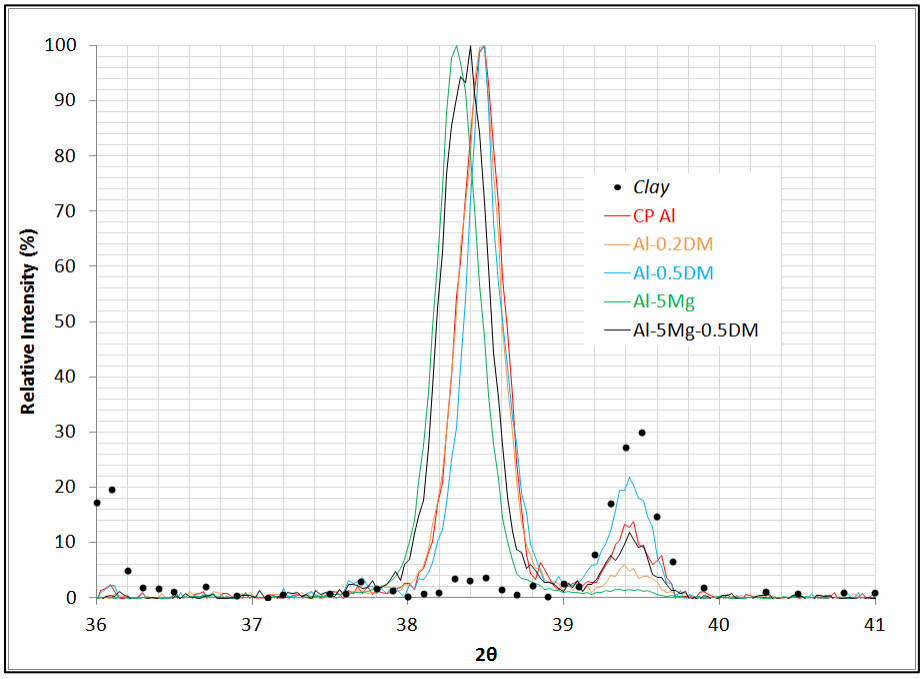

Figure 12 Comparison of (111) XRD Peaks of As-Cryomilled Powders. *Black circles indicate the XRD signal of the clay used to hold the samples.*

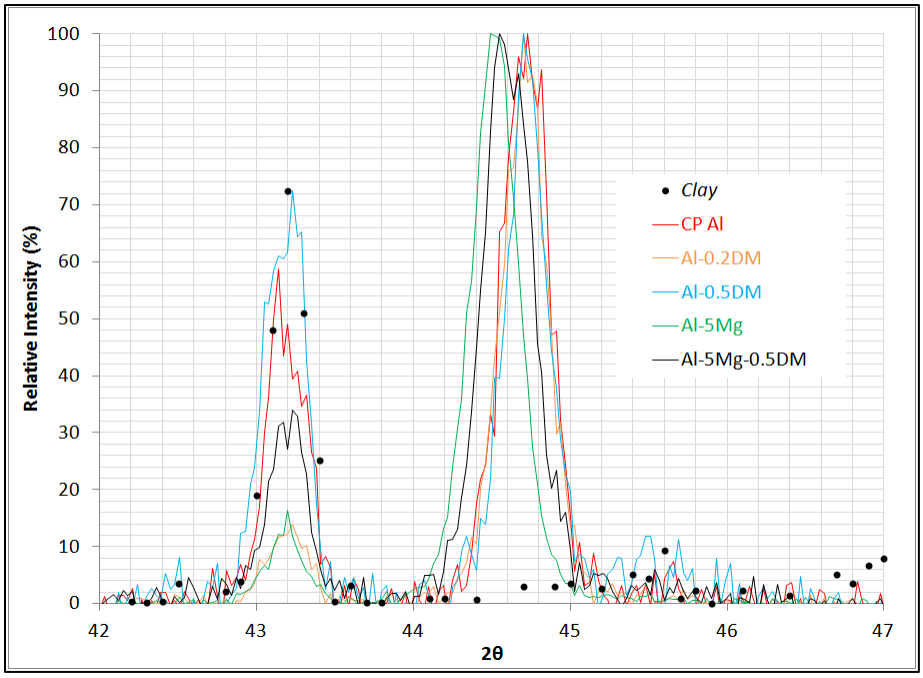

Figure 13 Comparison of (200) XRD Peaks of As-Cryomilled Powders. *Black circles indicate the XRD signal of the clay used to hold the samples.*

2.5.2. TEM

Following the consolidation of powders by HIPing and trap extrusion or swaging, TEM micrographs were taken with the same FEI/Philips CM-20 microscope used for characterization of powders. Samples were ground to a thickness of approximately 0.1 mm and polished to a smooth finish using standard metallographic techniques. The thin samples were then cored into 3mm discs and thinned for TEM observation with a Struers Tenupol-3 double jet electropolisher. A 25% solution of nitric acid in methanol was used as the polishing media at a temperature of -30 ± 5°C. Before polishing, discs were sonicated in isopropyl alcohol for approximately 2 minutes.

2.5.3. Hardness

Hardness of consolidated samples was measured with a Buehler Micromet microhardness machine with various test loads, 15 second dwell, and a Vickers tip. Rockwell B hardness was also measured on a Buehler Macromet hardness tester for select samples with a 15 second dwell as validation of Vickers measurements. Vickers Hardness values were determined from an average of five to eight measurements. The Rockwell B measurements are not shown in this report as they were only used for comparison of measurements with coarse-grained materials. The Rockwell B measurements did not reveal any discrepant Vickers hardness values.

2.5.4. Tensile Testing

Tensile testing was carried out on consolidated specimens of cryomilled aluminum with and without diamantane, and on coarse grained commercially pure diamantane. The results were have been published in the work of Maung, et al., and will be referenced where needed in this work (ref 4). A typical tensile specimen is shown in Figure 14 along with the setup of the test with an attached strain gage. Several of the tensile specimens fractured in the threads during the test. Because of the difficulty in obtaining an accurate test and because the brittleness of many of the consolidated samples made machining threaded sections difficult, tensile testing was abandoned in favor of hardness testing mid-way through the work carried out in the current project. The primary conclusion drawn from the work was that consolidated tensile specimens with diamantane were lower strength but considerably more ductile than without it (ref 4).

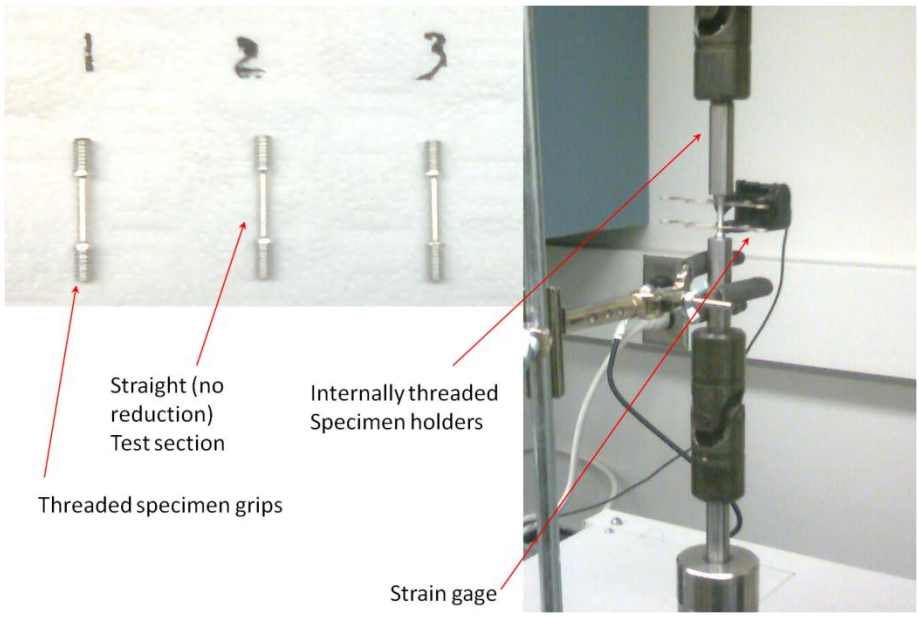

Figure 14 Round Dogbone Tensile Specimens of Consolidated Cryomilled Powders and Tensile Test Setup

CHAPTER 3. EXPERIMENTAL DATA

3.1. XRD Characterization of Powders

The resulting diffraction profiles of as-cryomilled powders are shown in Figures 15 to 19.

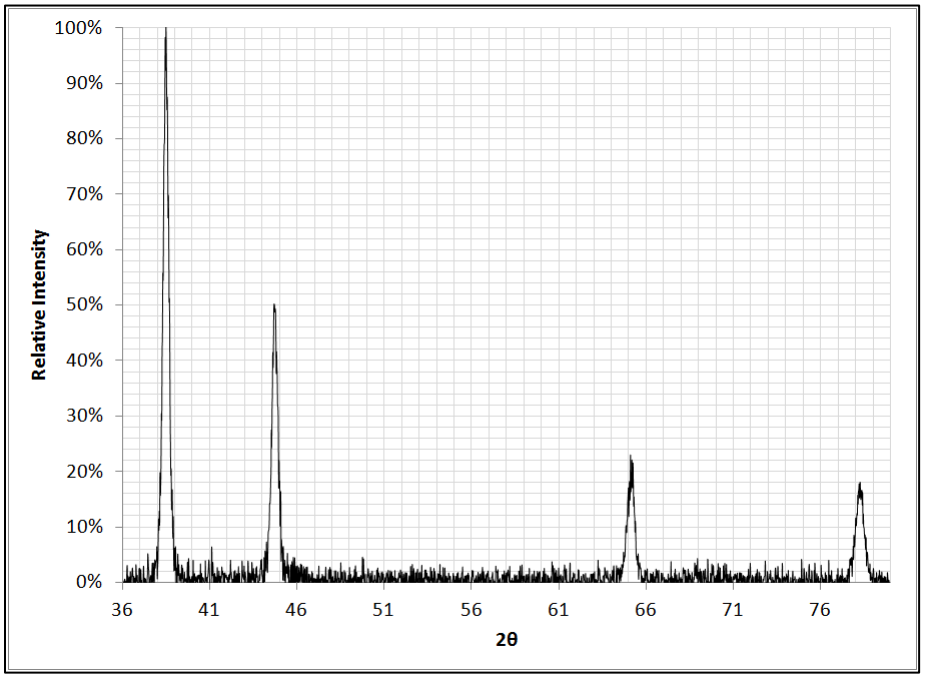

Figure 15 XRD Trace of As-Cryomilled Commercially Pure Aluminum Powder

The diffraction trace of as-milled commercially pure aluminum is shown in Figure 15. The peak centers were identified to be at 2θ values of 38.48°, 44.68°, 65.10°, and 78.26°, corresponding to the (111), (200), (220), and (311) peaks, respectively.

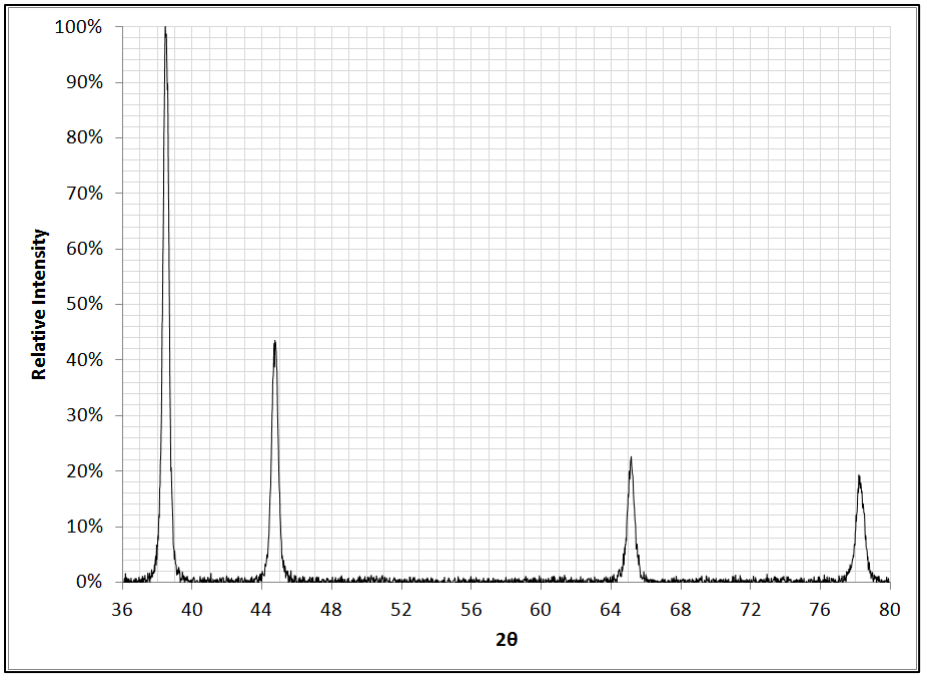

Figure 16 XRD Trace of As-Cryomilled Aluminum + 0.5% Diamantane Powder

The diffraction trace of as-cryomilled aluminum with 0.5 wt% diamantane is shown in Figure 16. The peak centers were identified to be at 2θ values of 38.44°, 44.72°, 65.14°, and 78.18°, corresponding to the same peaks as in Figure 15.

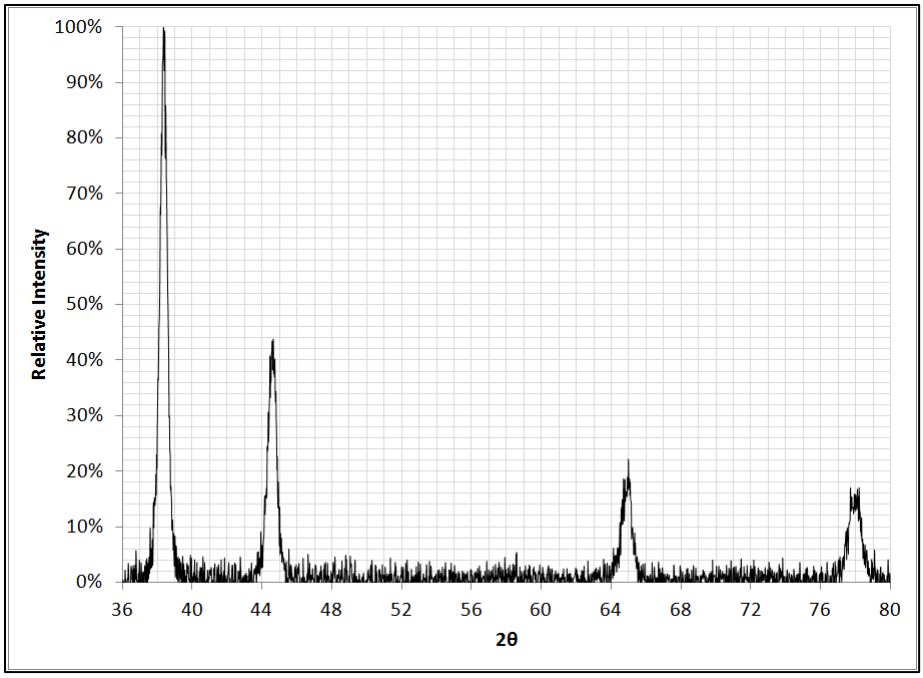

Figure 17 XRD Trace of As-Cryomilled Aluminum + 5% Magnesium Powder

The diffraction trace of as cryomilled 3N aluminum with 5 wt% 3N magnesium is shown in Figure 17. The peak centers were identified to be at 2θ values of 38.34°, 44.62°, 64.98°, and 78.20°, corresponding to the same peaks as in Figure 15.

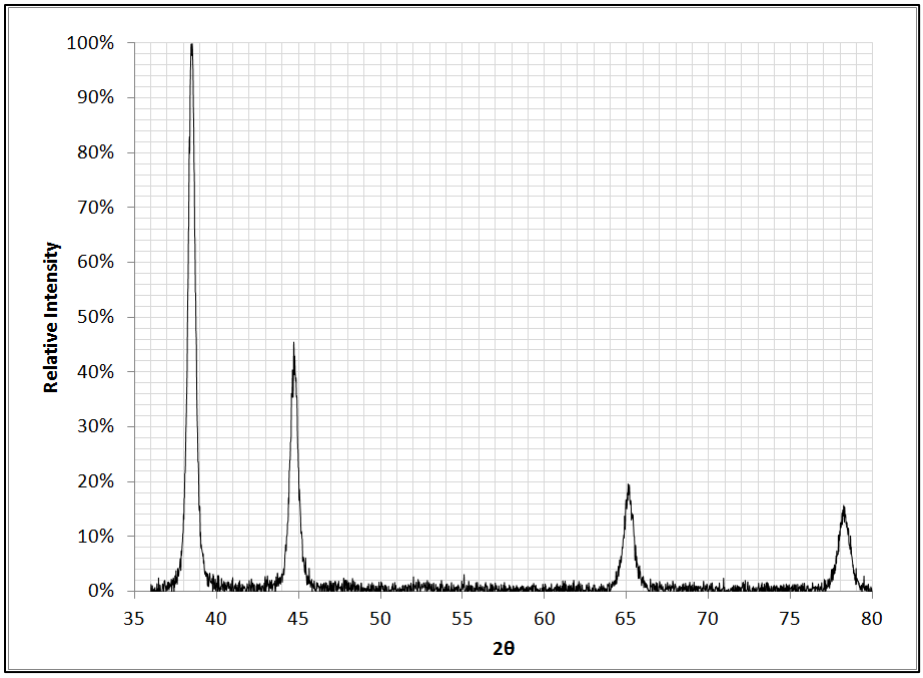

Figure 18 XRD Trace of As-Cryomilled Aluminum + 5% Magnesium +0.2% Diamantane Powder

The diffraction trace of as-cryomilled 3N aluminum with 5 wt% 3N magnesium and 0.2 wt% diamantane is shown in Figure 18. The peak centers were identified to be at 2θ values of 38.52°, 44.72°, 65.10°, and 78.24°, corresponding to the same peaks as in Figure 15.

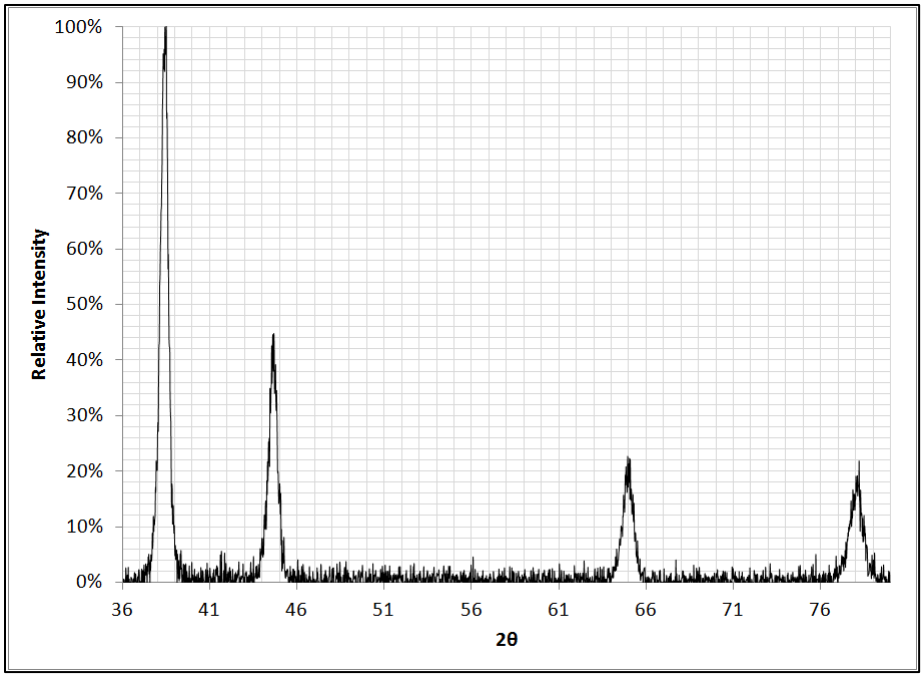

Figure 19 XRD Trace of As-Cryomilled Aluminum + 5% Magnesium +0.5% Diamantane Powder

The diffraction trace of as-cryomilled 3N aluminum with 5 wt% 3N magnesium and 0.5 wt% diamantane is shown in Figure 19. The peak centers were identified to be at 2θ values of 38.46°, 44.66°, 64.94°, and 78.20°, corresponding to the same peaks as in Figure 15.

Powders were primarily analyzed by XRD for comparative grain size analysis. Following subtraction of background and beta radiation from the machine software, the width of each peak was analyzed at half of the maximum by identifying the angles corresponding to half of a peak's maximum intensity, or by dividing the integrated area under each peak by its height. The difference in angles was taken as the full width at half maximum intensity (FWHM) and used to characterize grain size and the peak area divided by height was taken as integral breadth (IB). The FWHM and IB were generally in approximate agreement of each other as a measure of peak width, with IB being 10-20% larger than FWHM. Because of the cryomilling induces a high

concentration of dislocations, it is to be expected that strain in addition to small crystallite size would cause peak broadening (ref 16). For this reason, the method used in [20] for the determination of cryomilled powder grain size by XRD was evaluated for use according to the equation:

$$(IB)^{-1} = D - 4De^2[(2\sin\theta/\lambda_{Cu\text{-}K\alpha})/(IB)]^2 \qquad \text{(eq. 25)},$$

where *e* is taken as the internal strain and the source radiation has a wavelength, $\lambda_{Cu\text{-}K\alpha}$, of 0.154 nm. The reciprocal peak width, $(IB)^{-1}$, was plotted against $[(2\sin\theta/\lambda_{Cu\text{-}K\alpha})/(IB)]^2$ and a linear trend determined from the plot by a least-squares fit. The intercept of the trend line was taken as the average grain size, *D*, and the strain was determined from its slope. The results for cryomilled aluminum-magnesium powders with and without diamantane as well as a coarse grain counterpart are shown in Table 2. Because of the lack of sensitivity in the XRD instrument, as-cryomilled grain size was determined to be unreasonably large and internal strain unreasonably small. For this reason, the Scherrer equation was used to estimate as-milled grain size as well:

$$D_{avg} = K\lambda_{Cu\text{-}K\alpha}/(FWHM)\cos\theta, \qquad \text{(eq. 26)},$$

where the *K* is assumed a value of 0.9 and the remaining terms have the same definitions as in equation 25 (ref 8). Table 2 shows the average grain size calculated from the same four peaks used for equation 25 as well as the standard deviation. Although lacking the strain information, Scherrer grain sizes are much more reasonable.

Table 2 XRD Grain Size of Cryomilled Powders. *"Mg" = Aluminum + 5% Magnesium, "CG" = coarse grained, "DM" = diamantane. The calculated grain size and internal strain by the Integral Breadth method, and calculated grain size by the Scherrer equation are shown.*

Sample	D_{IB} (nm)	e	$D_{Scherrer}$ (nm)
5Mg-CG	569	*	70 ± 20
5Mg	220	0.00013	31 ± 4
5Mg-0.2DMa	312	0.00032	31 ± 4
5Mg-0.2DMb	296	0.00035	26 ± 4
5Mg-0.5DM	375	0.00017	42 ± 2
*Result was an imaginary number			

The grain size was measured by equation 26 for another cryomilled aluminum + 5 wt% magnesium + 0.5 wt% diamantane sample and for cryomilled commercially pure aluminum as 31 ± 2 nm and 42 ± 2 nm, respectively.

3.2. TEM Characterization of Powders

Grain size was determined from TEM micrographs by measuring the area with ImageJ software as mentioned above. The grain sizes of some of the investigated powders are shown in Table 3.

Table 3 TEM Grain Size of Cryomilled Powders. *The grain sizes are larger than what is typically reported for the as-cryomilled condition, however, they are consistent and indicative that as-cryomilled grain size is relatively independent of diamantane concentration.*

% Diamantane	Grain Size
0	40 ± 14
0	37 ± 8
0.5	34 ± 10
0.5	34 ± 7
1	35 ± 7

3.3. TEM Characterization of Bulk Samples

Shown in Figures 20 and 21 are examples of a consolidated sample TEM micrographs, of extruded and swaged materials, respectively. Figures 22 and 23 show consolidated samples after extrusion and swaging, respectively, and for both an additional 100 hours of heating at 500°C.

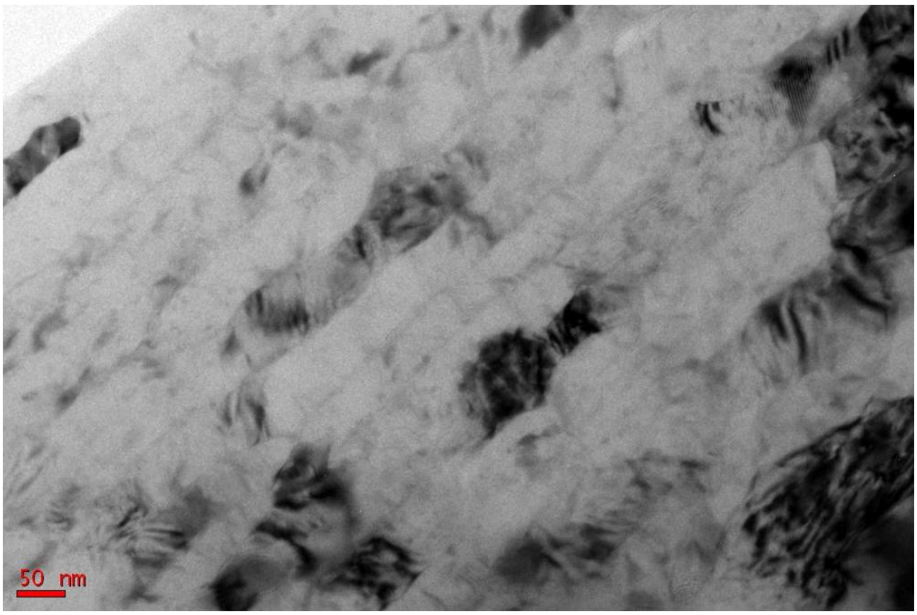

Figure 20 TEM Micrograph of Cryomilled Aluminum + 0.2% Diamantane Powder Consolidated by HIP and Trap Extrusion

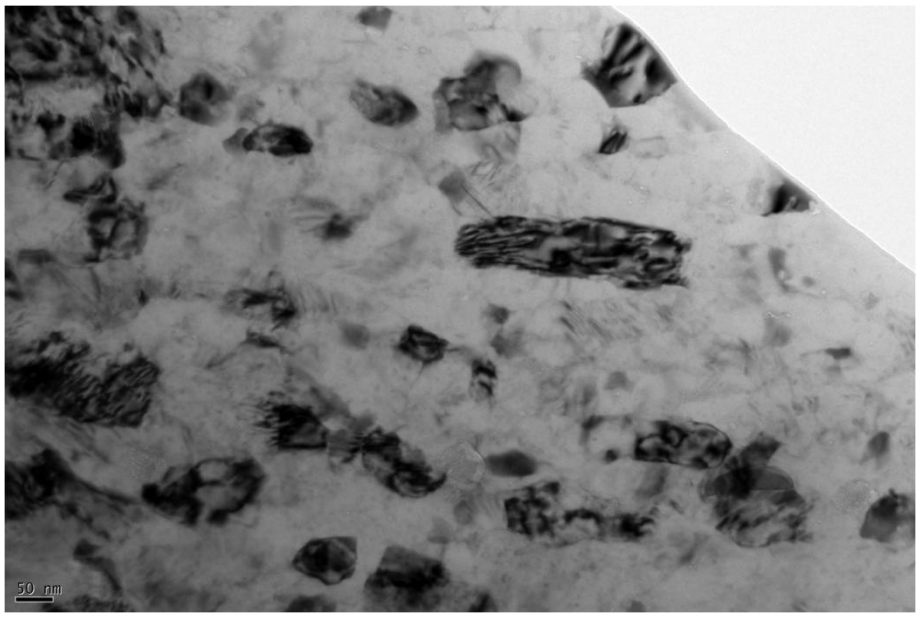

Figure 21 TEM Micrograph of Cryomilled Aluminum + 0.2% Diamantane Powder Consolidated by HIP and Swaging

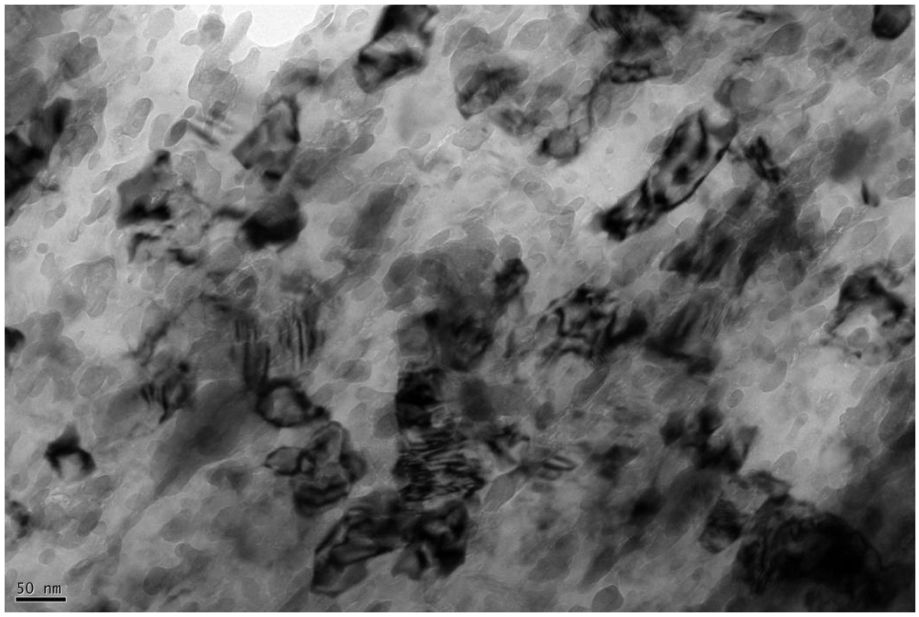

Figure 22 TEM Micrograph of Cryomilled Aluminum Powder Consolidated by HIP and Trap Extrusion, and Annealing 100hr at 500°C

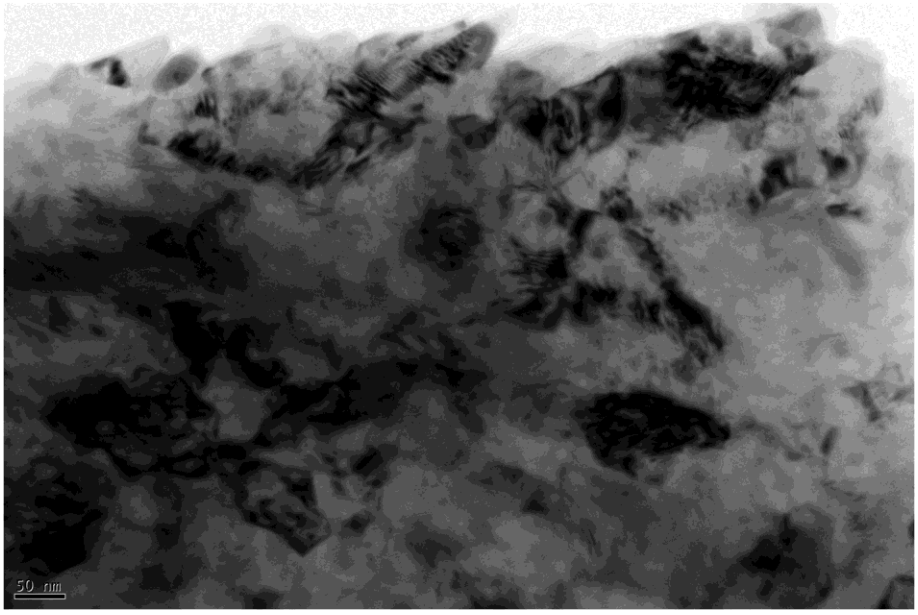

Figure 23 TEM Micrograph of Cryomilled Aluminum Powder Consolidated by HIP and Swaging, and Annealing for 100 hr at 500°C

Grain sizes were determined on consolidated samples by the same method as used for powders. The grain sizes of several of the consolidated samples as well as comparisons from published data are shown in Table 4.

Table 4 TEM Grain Size of Consolidated Cryomilled Material

Wt % Diamantane	Wt % Mg	Consolidation	Avg Grain Size (nm)	Comments
0	0	HIP + Trap Extrude	155 ± 125	Ref 4
0	0	HIP + Trap Extrude	61 ± 18	100 hr anneal
0	0	HIP + Swage	85 ± 21	
0	0	HIP + Swage	58 ± 16	100 hr anneal
0	5	HIP + Trap Extrude	110 ± 38	
			109 ± 35	
0	7.5	Sintered	125	Al6061; Ref 20
0.1	0	HIP + Trap Extrude	61 ± 23	
0.2	0	HIP + Trap Extrude	75 ± 23	
0.2	0	HIP + Swage	81 ± 24	
0.5	0	HIP + Trap Extrude	74 ± 30	
0.5	0	HIP + Trap Extrude	75 ± 32	Ref 4
0.5	5	HIP + Trap Extrude	88 ± 28	

3.4. Hardness Results

The hardness measured by 500g Vickers indentation of several commercially pure samples with and without diamantane, and either trap extruded or swaged, are shown in Table 5. Several of the samples were heated at the indicated temperature and time to measure the evolution of measured hardness. Hardness measured after heating is shown in Table 5 as well.

Table 5 Vickers Hardness of Consolidated Cryomilled Material

Wt % Diamantane	Consolidation	Heating Temp (°C)	Heating Time (min)	Vickers Hardness
0	HIP + Trap Extrusion	--	--	115 ± 4
0	HIP + Trap Extrusion	300	40	116 ± 7
0	HIP + Trap Extrusion	300	120	112 ± 8
0	HIP + Trap Extrusion	500	40	118 ± 11
0	HIP + Trap Extrusion	500	120	104 ± 7
0	HIP + Swaged	--	--	136 ± 3
0	HIP + Swaged	300	40	141 ± 9
0	HIP + Swaged	300	120	145 ± 1
0.1	HIP + Trap Extrusion	--	--	126 ± 6
0.1	HIP + Trap Extrusion	300	40	125 ± 4
0.1	HIP + Trap Extrusion	300	120	122 ± 4
0.1	HIP + Swaged	--	--	118 ± 7
0.1	HIP + Swaged	300	40	123 ± 6
0.1	HIP + Swaged	300	120	122 ± 8
0.2	HIP + Swaged	300	40	122 ± 6
0.2	HIP + Swaged	300	120	125 ± 6
Aluminum with 5% Magnesium				
0	HIP + Trap Extrusion	--	--	151 ± 20
0.5	HIP + Trap Extrusion	--	--	162 ± 10

3.5. DSC and TGA Characterization of Powders

Cryomilled CP Aluminum with No Diamantane Shown in Figure 24 are the temperature and heat traces during an isothermal DSC heating cycle at 500°C and the heat flow with temperature, similar to what is shown in Figure 7. The TGA trace is shown in Figure 4.

Cryomilled CP Aluminum + Diamantane ("DM") The TGA temperature and mass traces are plotted against time for cryomilled CP aluminum with 0.5% DM, 1% DM and 7% DM are shown in Figures 25 through 27. The DSC temperature and heat traces are plotted against time and heat is plotted against temperature for the same sample formulations in Figures 28 through 30 for a 300°C isothermal hold and Figures 31 through 33 for a 500°C isothermal hold.

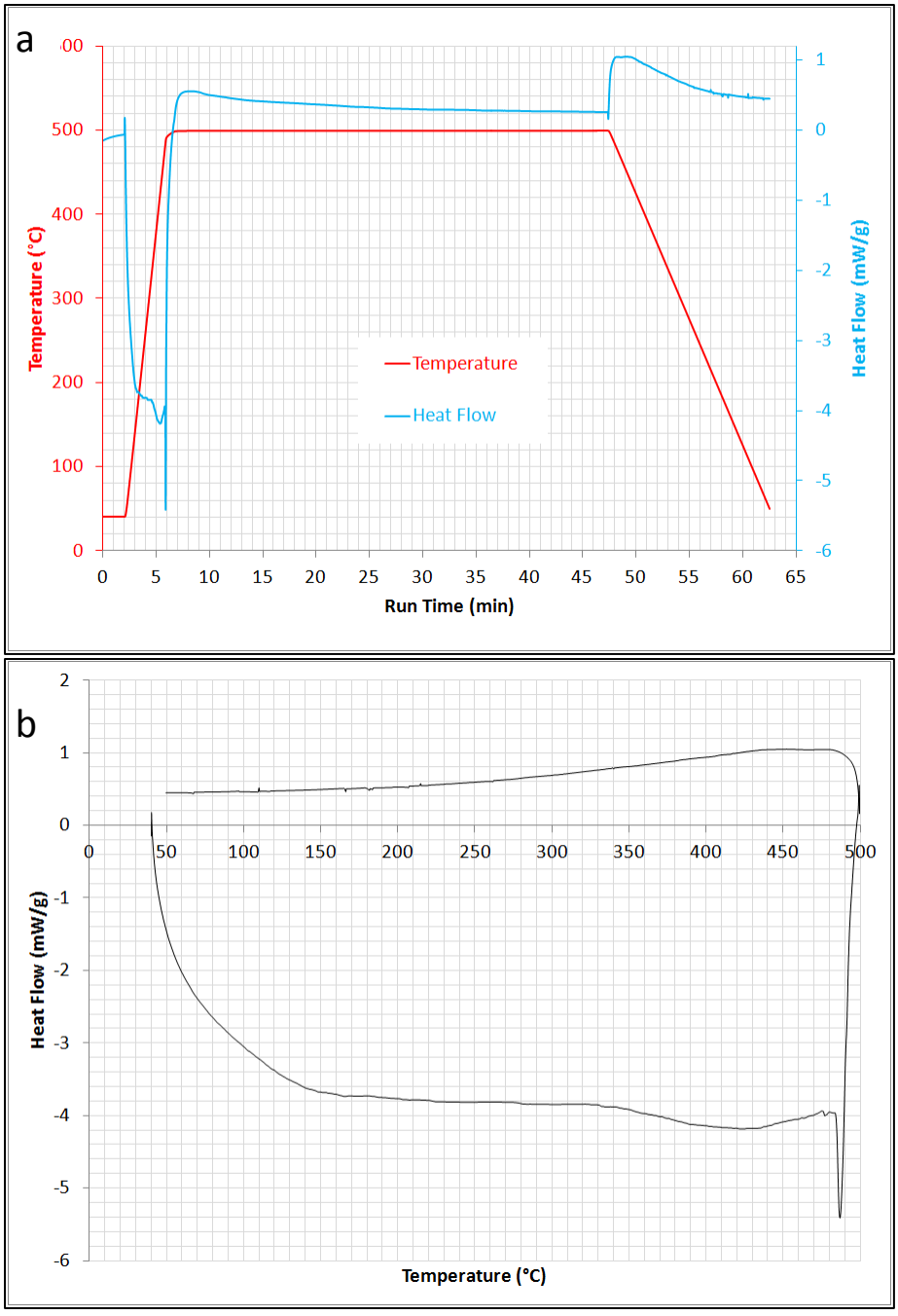

Figure 24 Isothermal DSC Traces of Commercially Pure Cryomilled Powders Heated at 500°C. *(a) The temperature and heat traces. (b) The heat-temperature trace of the same isothermal DSC run. The heating profile is to ramp from 40°C to 500°C at 120°C per minute, equilibrate, hold for 40 minutes, and ramp back to 40°C at 40°C per minute.*

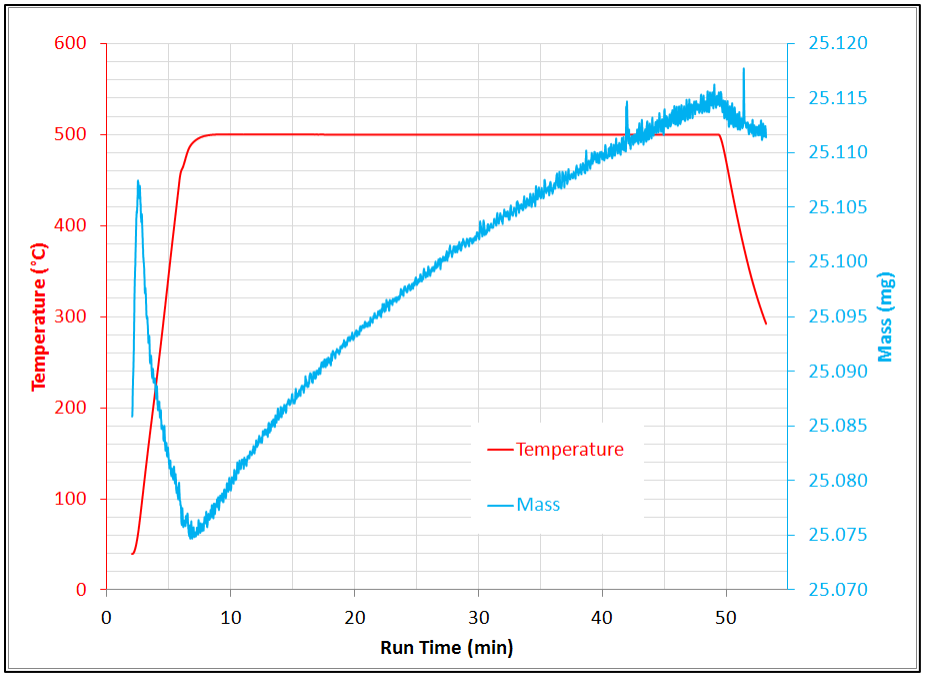

Figure 25 TGA Trace of Aluminum + 0.5% Diamantane Powder Heated to 500°C. *The sample was equilibrated at room temperature, ramped at 120°C per minute to 500°C, equilibrated, held at 500°C and ramped at 40°C per minute to 40°C (data collection stopped before reaching 40°C).*

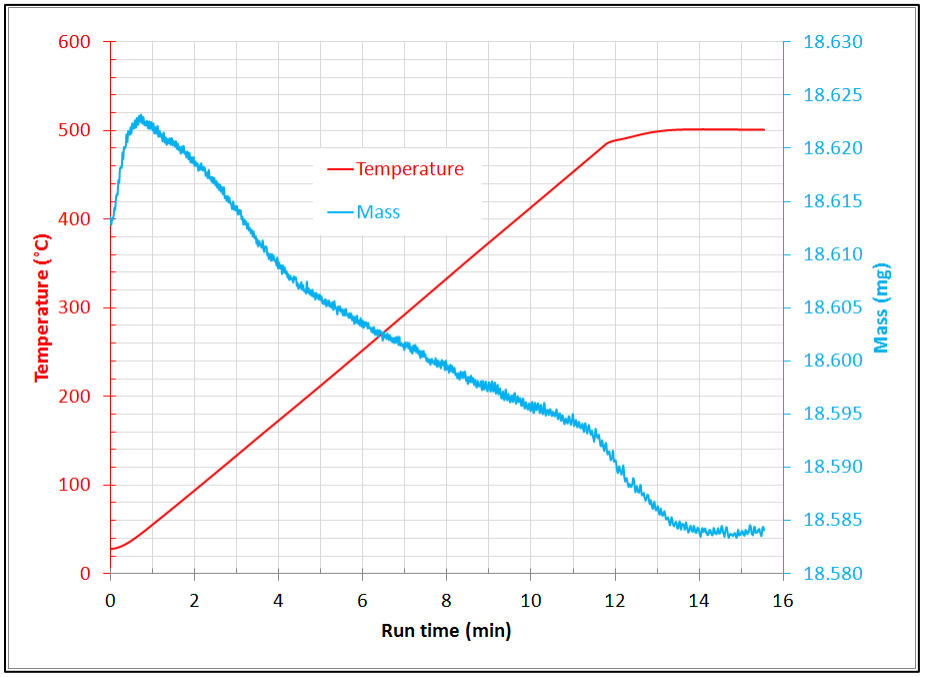

Figure 26 TGA Trace of Aluminum + 1% Diamantane Powder Heated to 500°C. *The sample was equilibrated at room temperature and heated at 40°C per minute to 500°C, equilibrated, and held for 2 minutes at 500°C.*

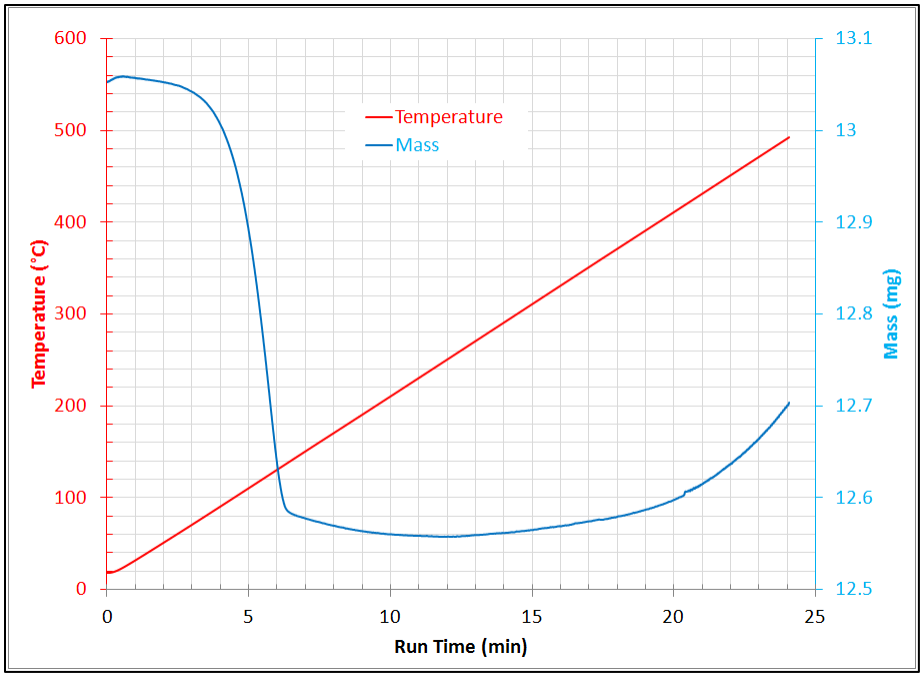

Figure 27 TGA Trace of Aluminum + 7% Adamantane Powder Heated to 500°C. *The sample was equilibrated at room temperature and ramped at 20°C per minute to 500°C.*

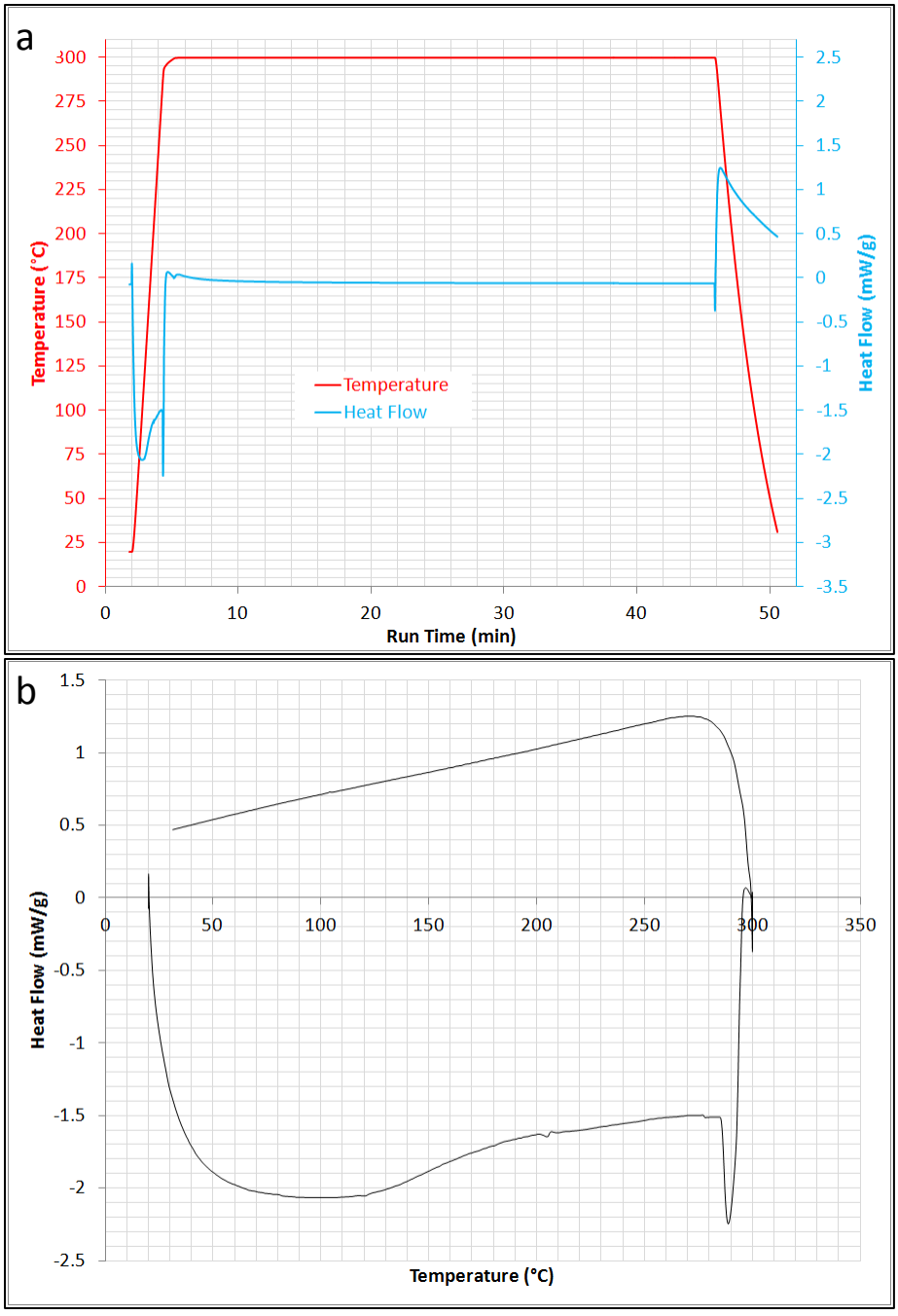

Figure 28 Isothermal DSC Traces of Aluminum + 0.5% Diamantane Powders Heated at 300°C. *(a) The temperature and heat traces. (b) The heat-temperature trace of the same isothermal DSC run. The heating profile is to ramp from 40°C to 300°C at 120°C per minute, equilibrate, hold for 40 minutes, and ramp back to 40°C at 120°C per minute.*

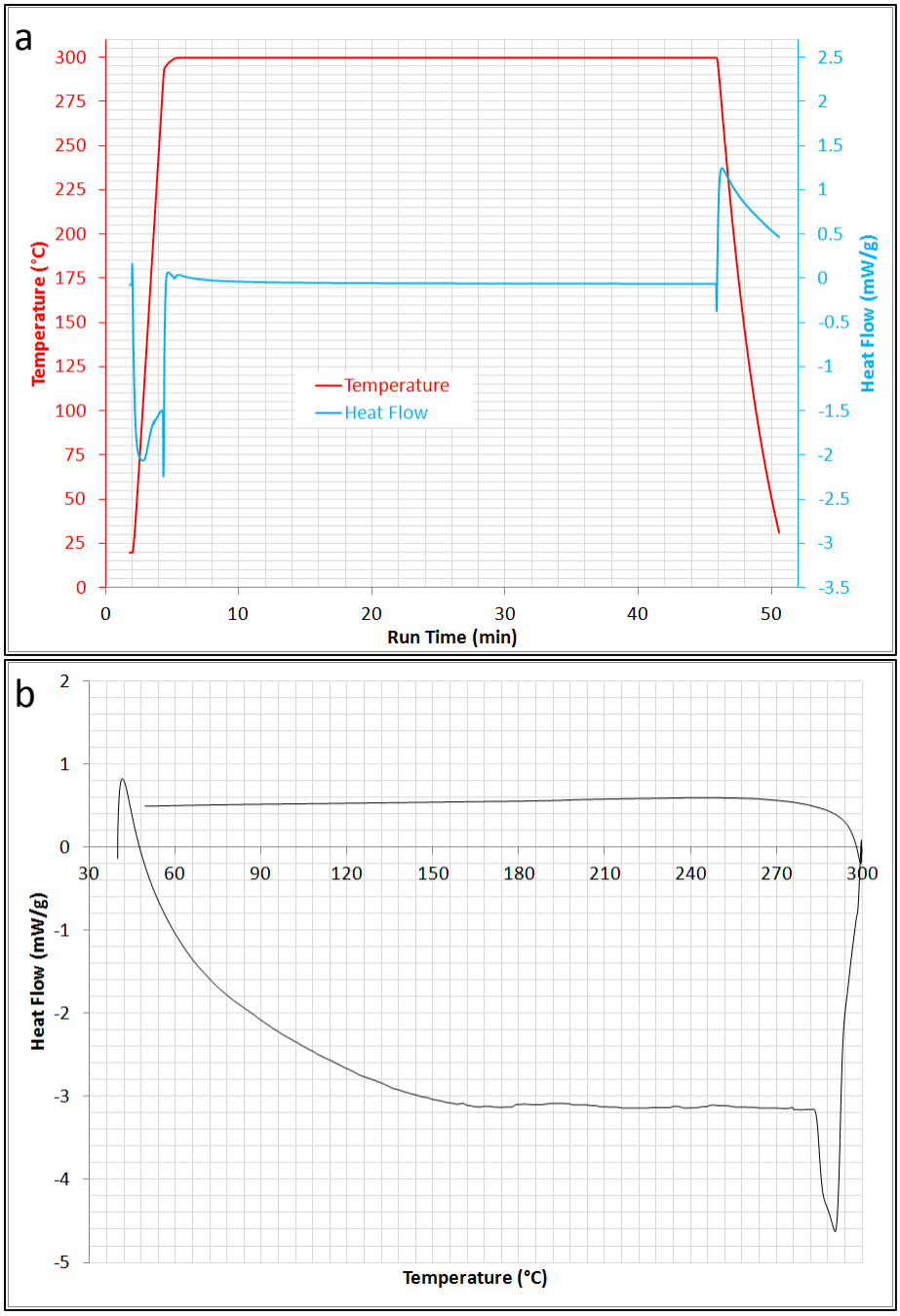

Figure 29 Isothermal DSC Traces of Aluminum + 1% Diamantane Powders Heated at 300°C. *(a) The temperature and heat traces. (b) The heat-temperature trace of the same isothermal DSC run. The heating profile is to ramp from 40°C to 300°C at 120°C per minute, equilibrate, hold for 40 minutes, and ramp back to 40°C at 40°C per minute.*

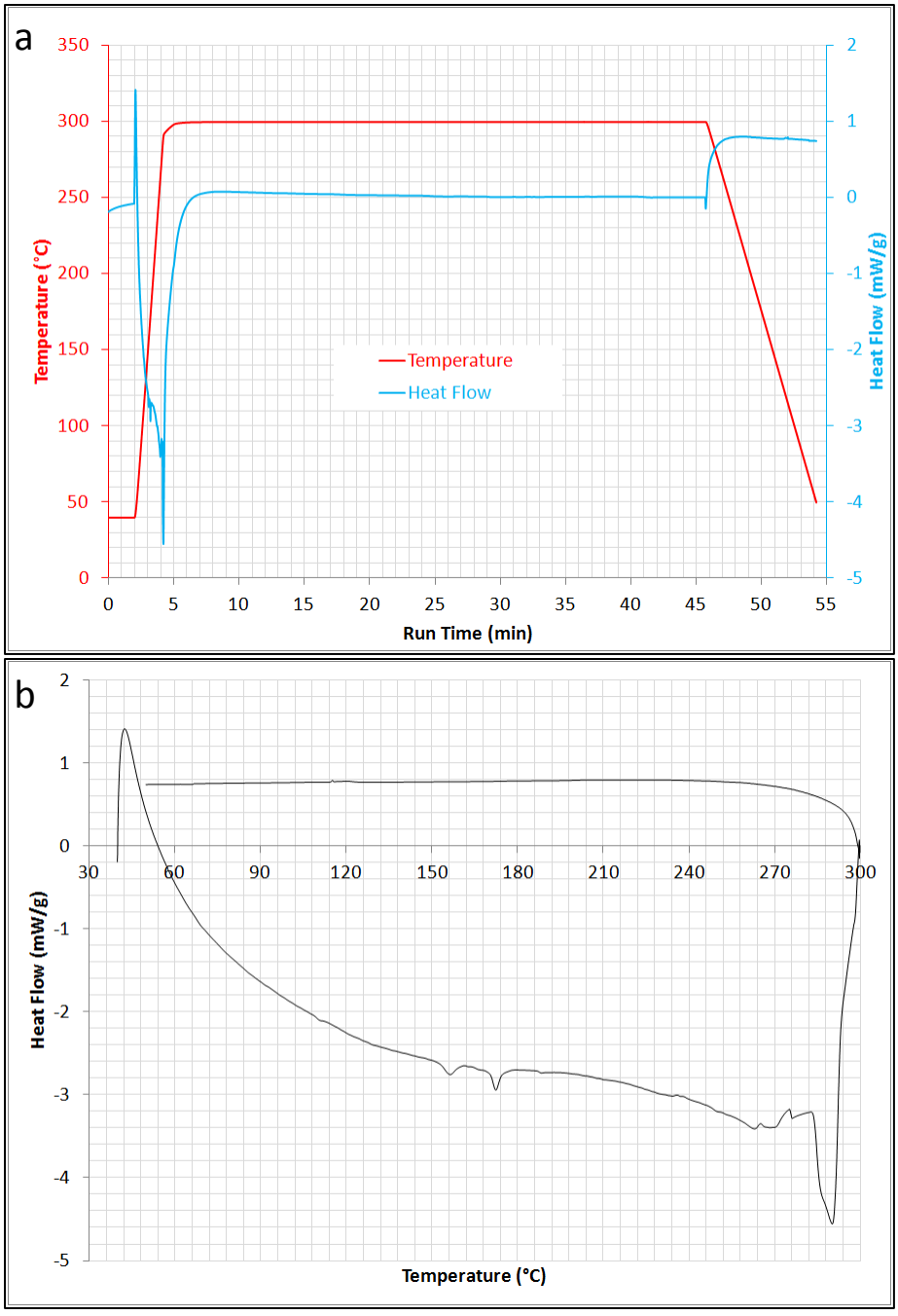

Figure 30 Isothermal DSC Traces of Aluminum + 7% Diamantane Powders Heated at 300°C. *(a) The temperature and heat traces. (b) The heat-temperature trace of the same isothermal DSC run. The heating profile is to ramp from 40°C to 300°C at 120°C per minute, equilibrate, hold for 40 minutes, and ramp back to 40°C at 40°C per minute.*

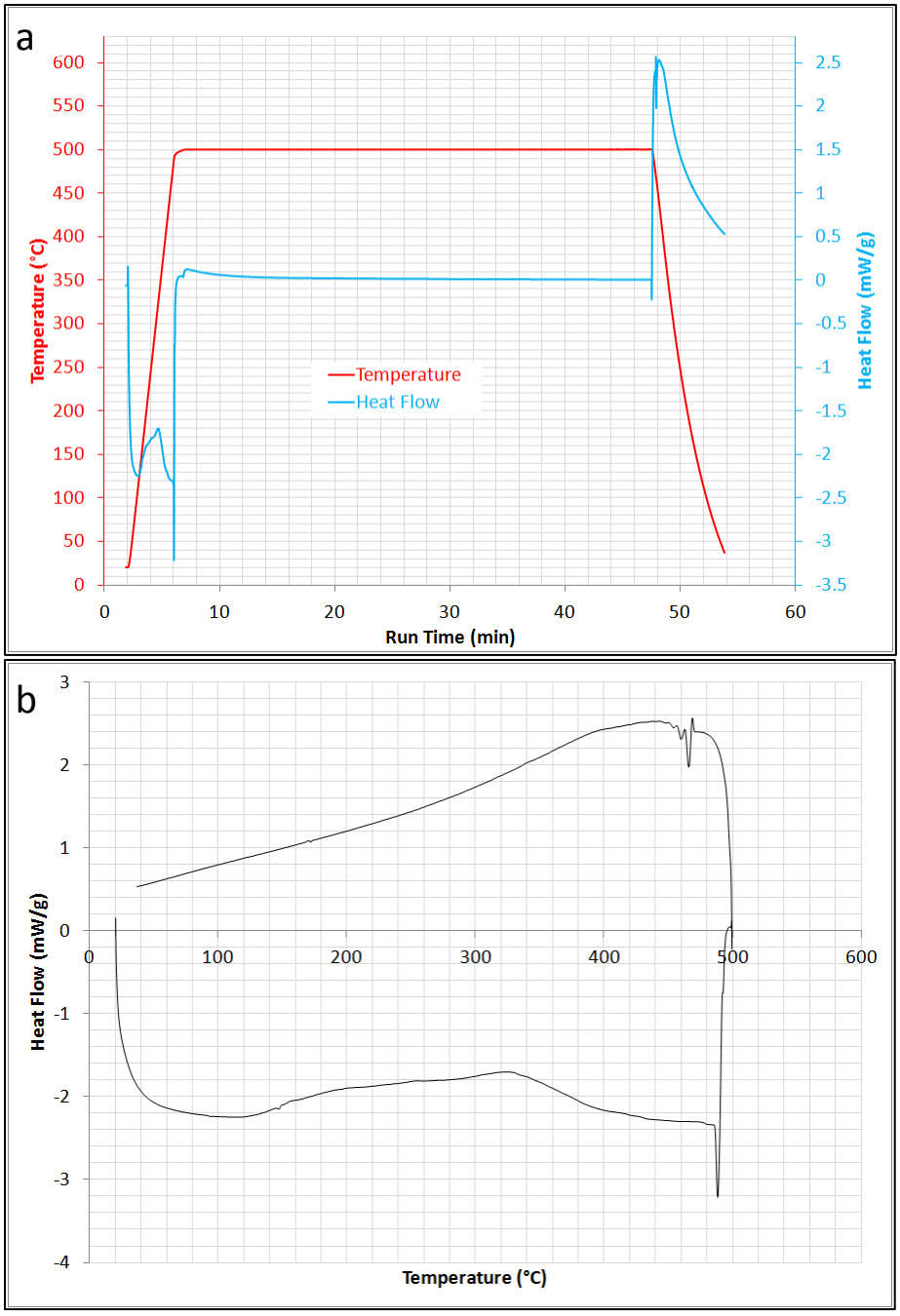

Figure 31 Isothermal DSC Traces of Aluminum + 0.5% Diamantane Powders Heated at 500°C. *(a) The temperature and heat traces. (b) The heat-temperature trace of the same isothermal DSC run. The heating profile is to ramp from 40°C to 500°C at 120°C per minute, equilibrate, hold for 40 minutes, and ramp back to 40°C at 120°C per minute.*

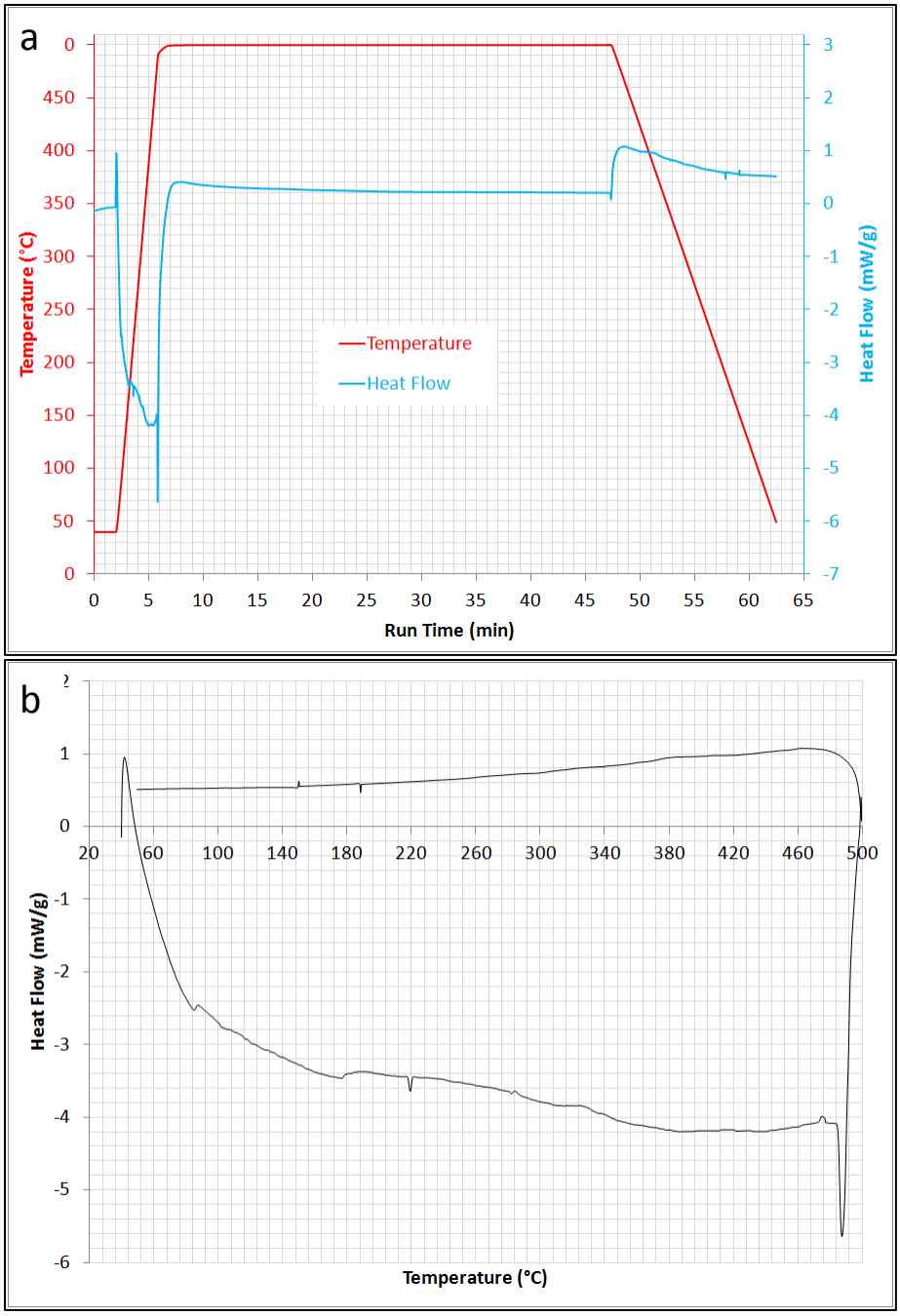

Figure 32 Isothermal DSC Traces of Aluminum + 1% Diamantane Powders Heated at 500°C. *(a) The temperature and heat traces. (b) The heat-temperature trace of the same isothermal DSC run. The heating profile is to ramp from 40°C to 500°C at 120°C per minute, equilibrate, hold for 40 minutes, and ramp back to 40°C at 40°C per minute.*

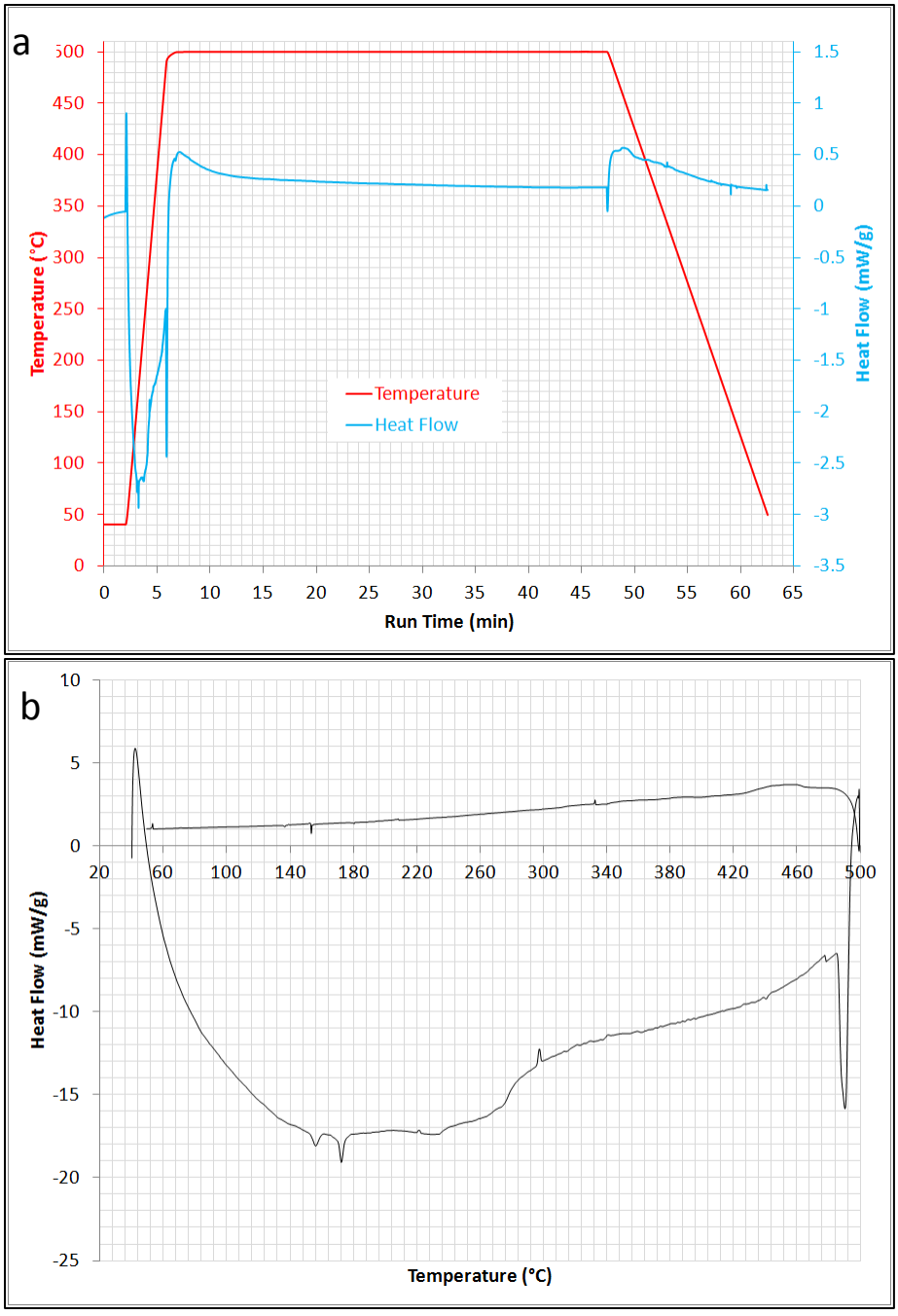

Figure 33 Isothermal DSC Traces of Aluminum + 7% Diamantane Powders Heated at 500°C. *(a) The temperature and heat. (b) The heat-temperature trace of the same isothermal DSC run. The heating profile is to ramp from 40°C to 500°C at 120°C per minute, equilibrate, hold for 40 minutes, and ramp back to 40°C at 40°C per minute.*

Cryomilled Aluminum + Adamantane ("AD") The TGA temperature and mass traces against time are shown in Figure 34. The DSC temperature and heat flow traces against time, and heat flow against temperature are shown in Figures 35 and 36 for isothermal holds at 300°C and 500°C, respectively.

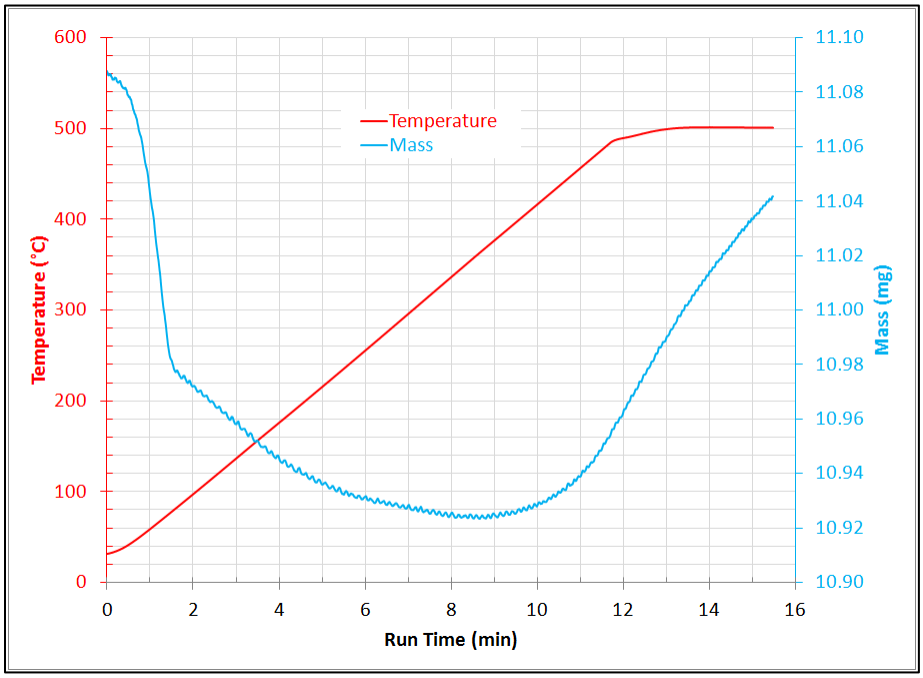

Figure 34 TGA Trace of Aluminum + 5% Adamantane Powders Heated to 500°C. *The sample was equilibrated at room temperature, ramped at 400°C per minute to 500°C, equilibrated, and held at 500°C for 2 minutes.*

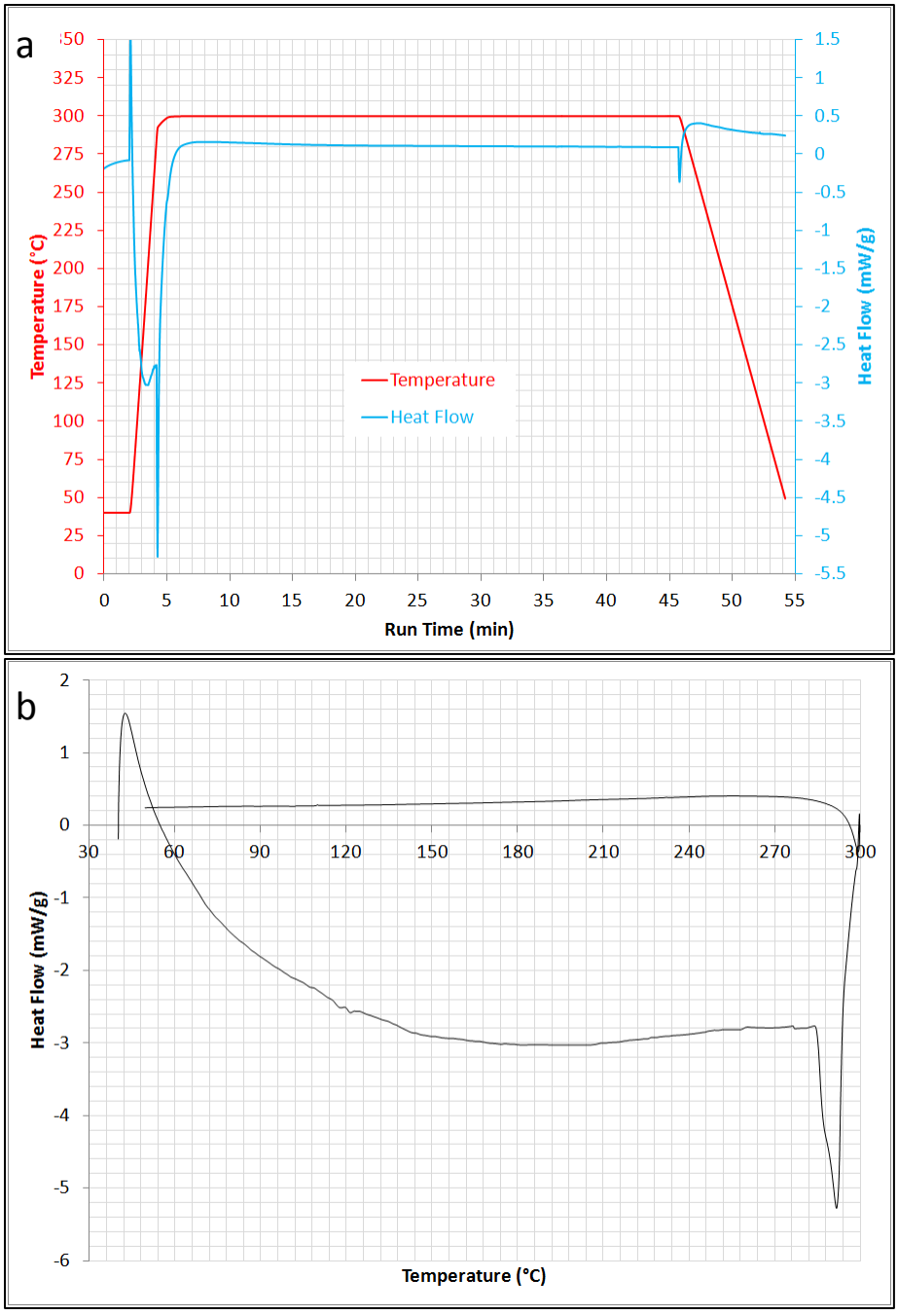

Figure 35 Isothermal DSC Traces of Aluminum + 5% Adamantane Powders Heated at 300°C. *(a) The temperature and heat traces. (b) The heat-temperature trace of the same isothermal DSC run. The heating profile is to ramp from 40°C to 300°C at 120°C per minute, equilibrate, hold for 40 minutes, and ramp back to 40°C at 40°C per minute.*

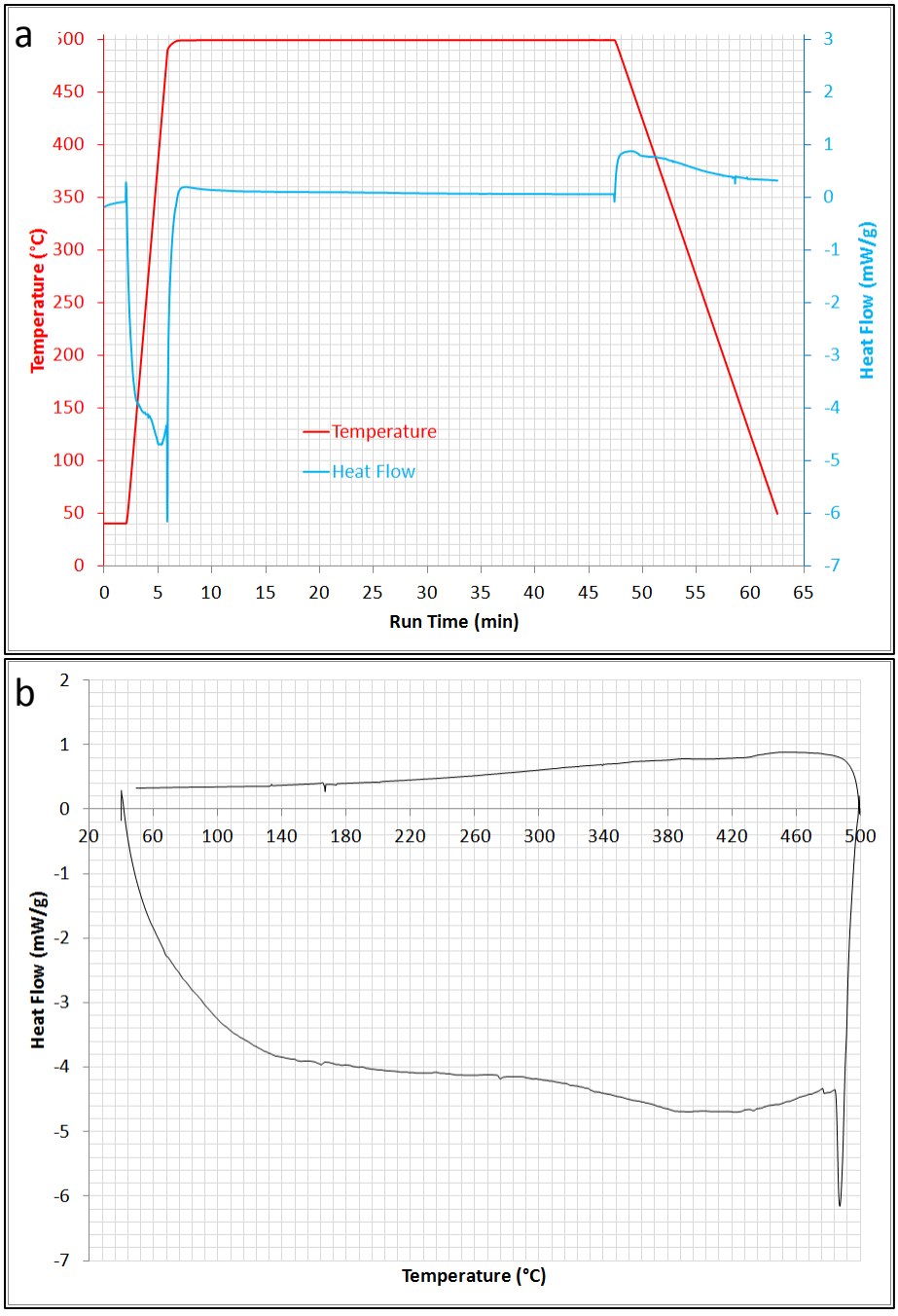

Figure 36 Isothermal DSC Traces of Aluminum + 5% Adamantane Powders Heated at 500°C. *(a) The temperature and heat traces. (b) The heat-temperature trace of the same isothermal DSC run. The heating profile is to ramp from 40°C to 500°C at 120°C per minute, equilibrate, hold for 40 minutes, and ramp back to 40°C at 40°C per minute.*

Shown in Figure 37 is the heat flow of the DSC run during the isothermal portion of Figure 7. The heat flow trace shows a very large exothermic heat flow in the first several minutes, followed by a tapering to a relatively constant flow beginning around 20 minutes. The heat flow during the isothermal period is integrated over time and shown as the cut red line in Figure 38.

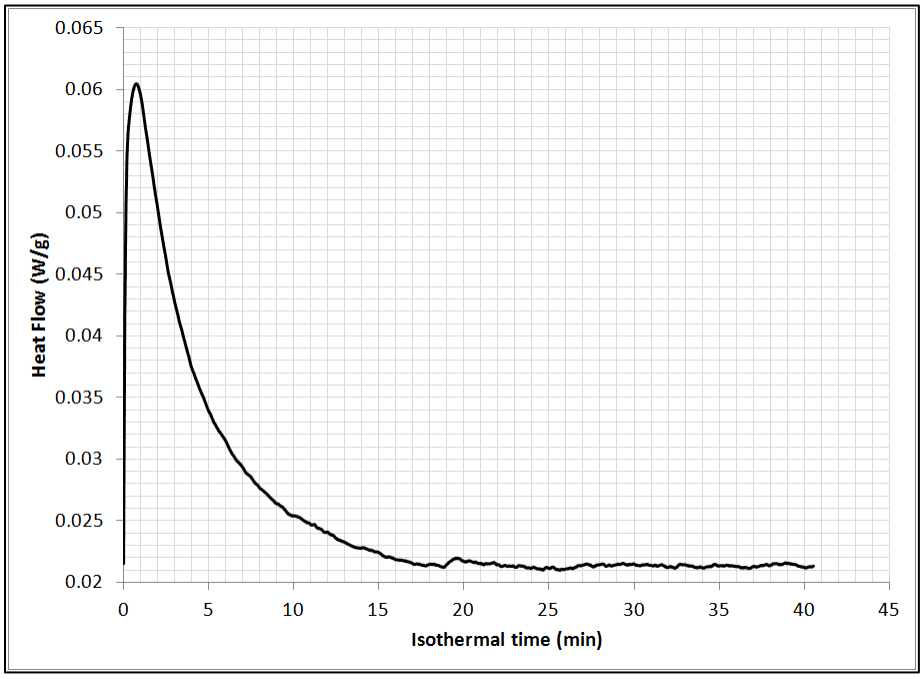

Figure 37 Isothermal Portion of DSC Heating Curve of Cryomilled Commercially Pure Aluminum at 300°C

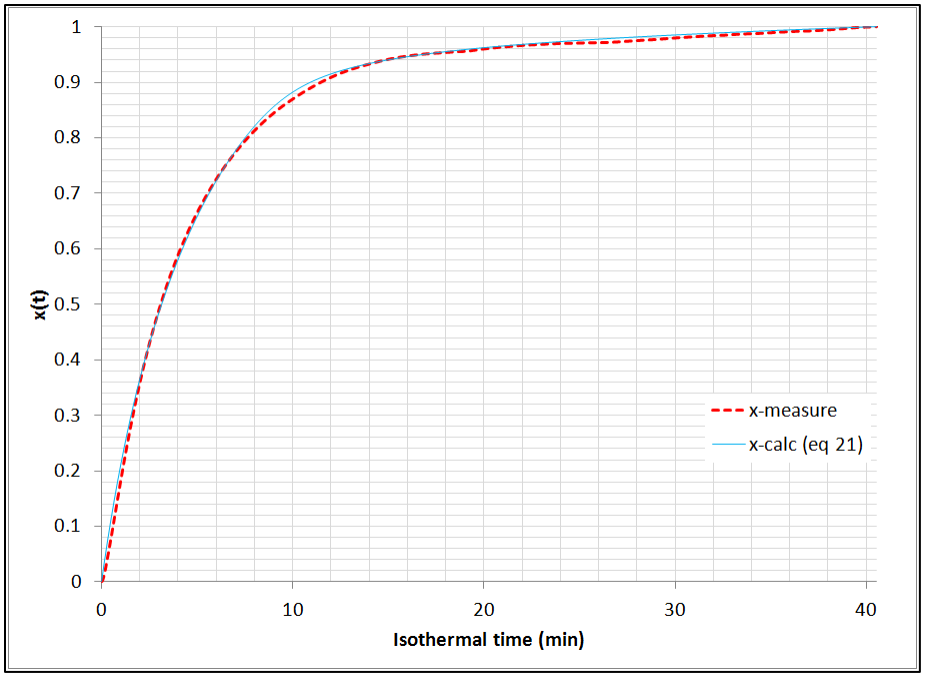

Figure 38 Curve Fitting of *x*(*t*) of Cryomilled Commercially Pure Aluminum

CHAPTER 4. DISCUSSION

4.1. DSC to Observe Grain Growth

4.1.1. General Observations

A typical DSC heating curve is shown in Figure 6 and a typical TGA curve is shown in Figure 4. Given what is known about the outgassing behavior of cryomilled aluminum, there is nothing unexpected in the shape of either curve (ref 31). In the DSC curve of Figure 6, there is a very broad peak centered around 100°C and a very sharp peak is seen around 500°C. The mass loss in Figure 4 starting around 100°C indicates that the first broad peak in Figure 6 is likely due to the evaporation of a species and, given the temperature range, this is likely a loss of water and any trapped light organics. Although it may appear that there is a sharp mass loss in Figure 4 at 273°C, this is likely an artifact of the heating program. The dip in Figure 4 around these temperatures coincides exactly with the sample being held isothermally for 2 minutes. Because the slope of the mass change in Figure 4 appears to be about the same before and after this dip, it's not expected that any sharp drop would have occurred there, meaning that no extra species was being noticeably lost at this temperature. Furthermore, there is a noticeable upward spike coinciding to the end of the 2 minute isothermal hold, again indicating temperature ramping based displacement in the measured weight. If the downward spike at the beginning of the isothermal hold and the upward spike at its end were both removed, the mass loss likely would be a continuous line so it can safely be assumed that whatever mass loss was already occurring as the temperature was being raised likely was just continuing during this isothermal hold. This is supported by the fact that there appears to be no peak in this range of

Figure 6. The final peak in Figure 6 at 500°C is the peak due to the isothermal grain growth. This same isothermal heat evolution is represented by the nearly flat line in part Figure 37, however the true shape of the isothermal heat evolution is obscured by the heat evolution during heating and cooling which is much larger in magnitude.

4.1.2. Stagnation of Grain Growth

Figure 37 shows the isothermal heat evolution on its own and, as can be seen, there is significantly more heat given off during the first 20 minutes of the isothermal hold time, which is presumed to be due solely grain growth. For this heat to have been due to grain growth, there must be a point in time at which the excess heat given off stops as it or, in other words, the line in Figure 37 becomes parallel to the time axis. The heat evolution due to grain growth can then be integrated with respect to the flat line representing stagnation of grain growth, and the heat of grain growth at any given time can then be used to find $x(t)$ in equation 21. If the line does not become flat during the isothermal hold time, it is possible that $x(t)$ will not be accurate as there will be no baseline to determine the heat given off from grain growth. To test this, the curve in Figure 37 was integrated as if the total isothermal hold time was 10, 15, 20, 30, and 40 minutes. It was found that although the $x(t)$ calculated for isothermal hold times of 10 to 20 minutes differed noticeably from what was calculated for 40 minutes, and $x(t)$ calculated for a 30 minute isothermal period was reasonably close to what was calculated for 40 minutes. Figure 39 shows $x(t)$ from integration with respect to the heat evolution at 10 to 40 minutes.

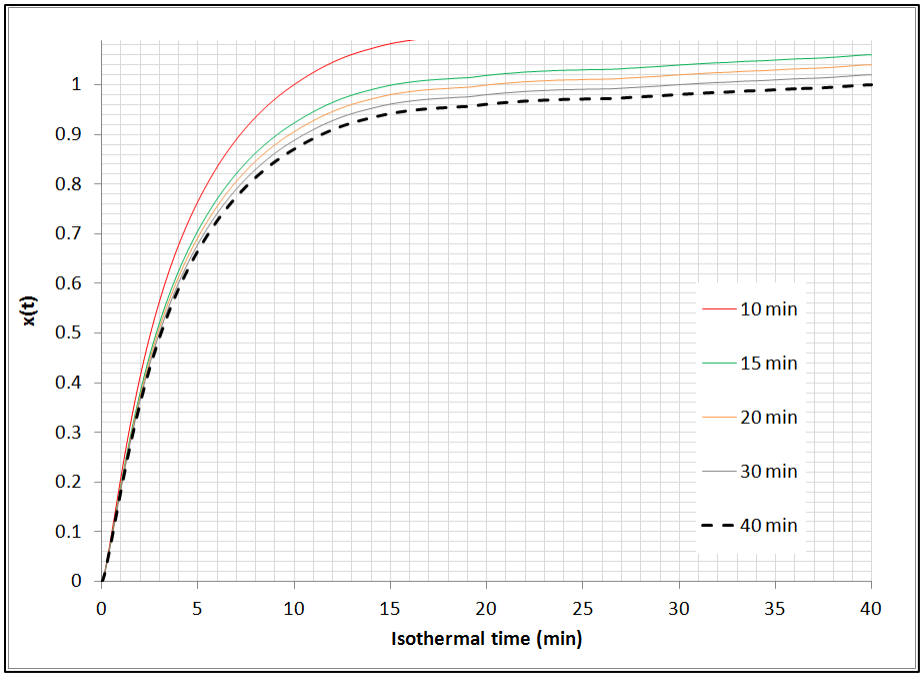

Figure 39 Effect of the Integration Period on the Shape of *x*(*t*)

The exercise of determining effect of the isothermal cutoff time (i.e. the value of t_f) on the shape of the measured $x(t)$ curve is important because of variability from one DSC run to the next. There is no set cut off time that ensures $x(t)$ is unaffected by the point from which an isothermal DSC curve is integrated. However, if the slope of the isothermal curve is plotted, the point at which the plot becomes nearly zero can be taken as the cutoff point for the particular DSC run. One such plot is shown in Figure 40, with the as-measured signal shown as the dotted gray lines and the signal averaged over the 50 points prior and 50 points following the energy measured at any instant shown as a thick black line for greater ease in following the line's trend.

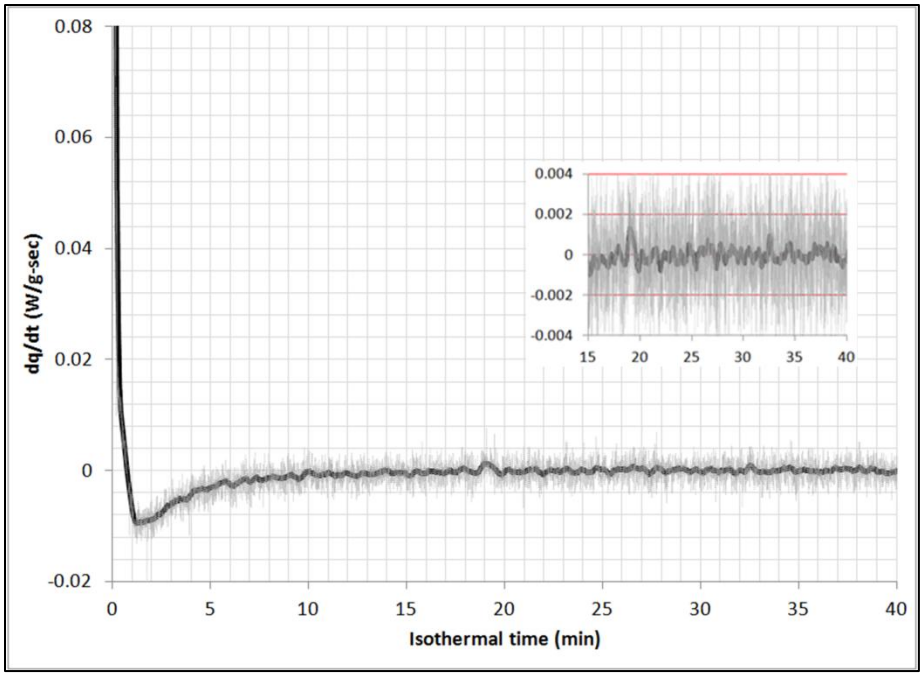

Figure 40 Example of Heat Evolution Rate During Isothermal DSC Hold. *The dotted gray line is the instantaneous slope and the thick black line is the average of the signal over 100 points. The average is centered at the plotted location, for example, the point plotted at 30 minutes includes the 50 points on the gray line before t = 30 minutes and the 50 points on the gray line after it.*

As can be seen from this plot and particularly from its inset, the slope of the isothermal heating curve becomes negative almost immediately and stays negative but nearly zero until nearly the end of the isothermal heating period. This implies that, despite the significant oscillation of the DSC signal during the period, the grain growth has nearly stagnated at the point when the oscillation tends to stay around zero, which is somewhere between 25 and 30 minutes. The wellness of fit of each $x(t)$ curve for $t_f < 40$ compared to $x(t)$ for the full 40 minute isothermal period can be found from the correlation coefficient between each as well. The correlation coefficients between $x(t)$ curves calculated for t_f of 40 minutes and t_f of 10, 15, 20, 25, 30, and 35 minutes are shown in Figure 41.

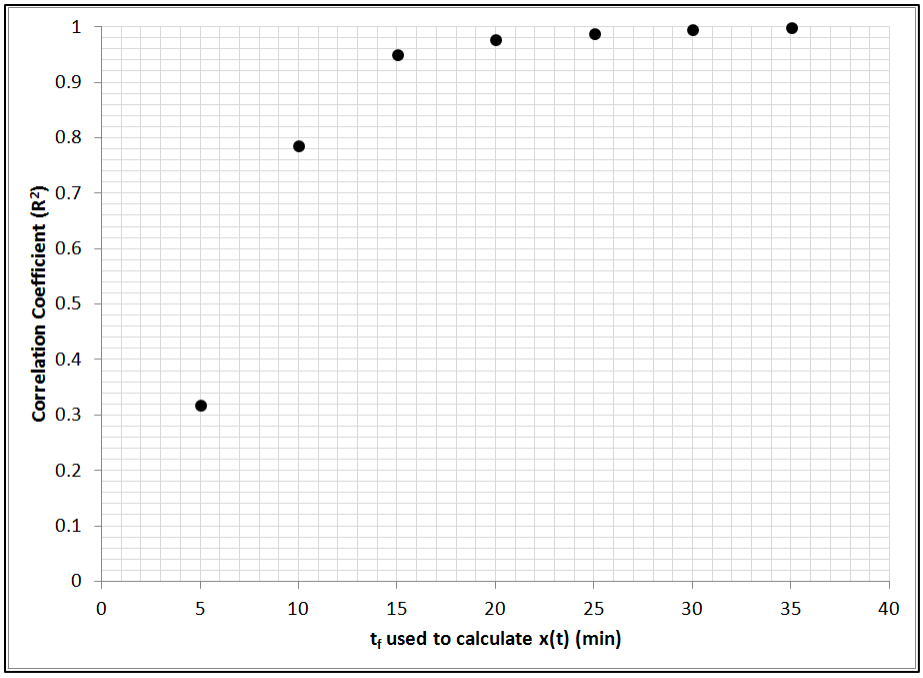

Figure 41 Correlation Coefficient Between *x*(*t*) curve calculated with an Integration Period Less Than 40 minutes and *x*(*t*) Integrated to 40 minutes

The fact that the correlation coefficient seems so close to 1 in for t_f of 20 or more minutes may seem surprising at first given that the $x(t)$ curve for t_f = 20 minutes in Figure 39 clearly has significant error compared to the curve measured against the full 40 minute isothermal period. This can be explained by the fact that nearly 300 data points were taken per second for a total of more than 12000 points during the run; by the sheer number of data points taken for correlation coefficient, it will more easily tend towards a value of one. Still, Figures 40 and 41 indicate that, after about 30 minutes, there is very little aggregate change in the heat evolution profile, which somewhat agrees with Figure 39 qualitatively. While Figure 40 offers a helpful visual aid to determine at what point grain growth stagnation has occurred, Figure 41 is a more numerical approach, the basis of which a standard can be set for determining if an isothermal DSC grain growth experiment was carried out over a sufficiently large amount of time. Because

each point from 30 minutes and beyond is close to 1 in Figure 41, it can be inferred that integration of Figure 37 with respect to any time greater than 30 minutes will yield $x(t)$ curves that are statistically similar enough that the grain growth kinetics should be not be dependent upon the chosen value of t_f.

Determining if grain growth has truly evolved to a point that it is no longer measurable by DSC was considered by Lu as well, and the chosen method in that work was validation by cooling of the sample and reheating such that the flat line obtained upon reheating provided the baseline for integration (ref 34). This method is entirely valid to verify stagnation of measureable grain growth as well, however, the methods illustrated in Figures 40 and 41 provide a means for checking completion of measurable grain growth that can be programmed with a Visual Basic or similar macro without the need for doubling the experimental time. Given that the stagnation of measurable grain growth occurred around 30 minutes of isothermal heating, any further heating can be considered unnecessary, although the entire 40 minute isothermal hold period will still be considered in later analyses. In general, measurable grain growth was seen to stagnate between 20 and 30 minutes in each run and, as a general rule, if it is estimated that measurable grain growth has stopped based on the flatness of an isothermal heating curve such as Figure 37 then a correlation coefficient check such as Figure 41 will yield the same result.

4.1.3. Meaning of Model Parameters

From equation 24, there are 6 parameters in the combined thermokinetic equation for grain growth, k_0, η, φ, D_{kin}, D_{eq}, and n; for convenience, these terms henceforth may be referred to individually or as a set, $\mathbf{\Lambda_i} = \{k_0, \eta, \varphi, D_{kin}, D_{eq}, n\}$. Two of the parameters in equation 24, D_{eq} and n, originate as thermodynamic terms from the grain boundary energy and, thus, are also used for the calculated value of $x(t)$ in equation 21. This is important to note because $x(t)$ also depends on the calculated value of $D(t)$, which gives the calculated $x(t)$ curve two-fold dependence on the values of D_{eq} and n. However, this is only a statement of how much D_{eq} and n affect the shape of $x(t)$ and not the actual meaning of the parameters.

Given the development of equation 17, the meaning of D_{eq} may be taken to be the grain size at which a partially soluble low concentration (i.e. alloying, contaminant, etc.) species has reached chemical equilibrium between the grain boundary and grain interior phases. Then, n may be taken as the rate change of grain boundary energy with respect to grain boundary area due to the changing concentration of soluble low concentration species in the grain boundary and grain interior. In other words, it describes the rate at which any given instantaneous grain size will change to approach D_{eq}. A larger value of n indicates a trend to approach to D_{eq} faster than a smaller n. Given that the four remaining parameters were introduced to modify and allow for a changing mobility term as described by equation 23, they must all be understood in terms of grain boundary mobility. Mathematically speaking, k_0 is the maximum value of k and $k_0(1-\eta)$ is the minimum value of k, meaning that both k_0 and η are the primary indicators of the mechanisms of grain boundary movement. As k_0 is proportional to the grain boundary mobility

at the initiation of grain growth (ref 10), its value can be assumed to be indicative of the physical mechanism by which grain growth begins. Then, η either can indicate how this growth-initiating physical mechanism dissipates or how the mechanism of grain boundary movement changes from the initial mechanism to another. Which of these interpretations of the meaning of η is correct can be determined by its value. As can be seen in Figure 42, a value $\eta = 1$ indicates that the grain boundaries become entirely immobile at some point, meaning that for $\eta = 1$ the boundary mobility is dissipating, thus implying that it likely remains the same mechanism during the entire process. On the other hand, for $\eta < 1$, the mobility approaches a non-zero value, which indicates that some mechanism different than the first must be available for grain boundaries to move.

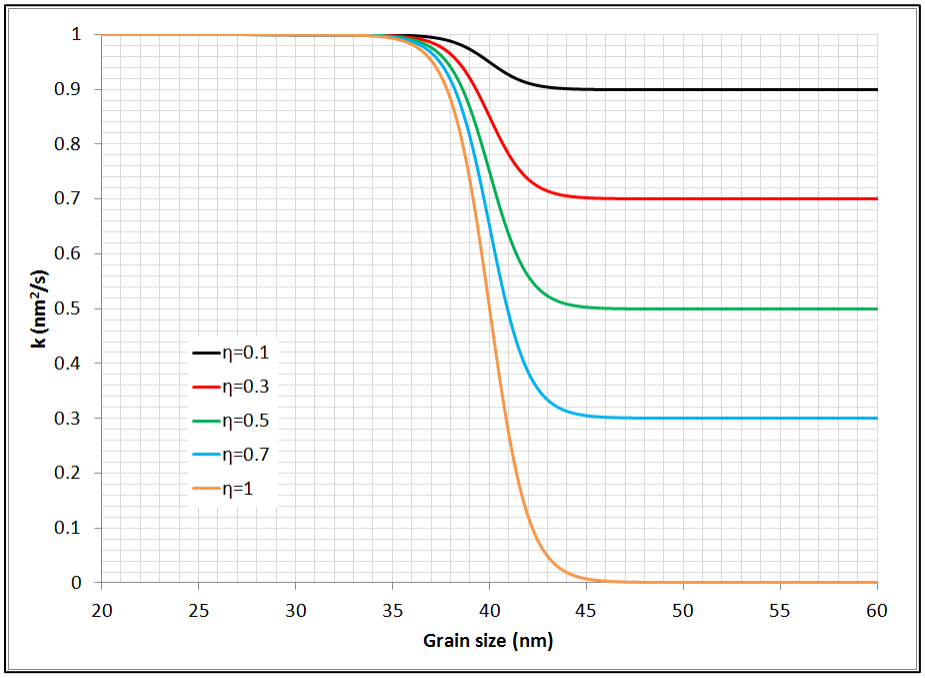

Figure 42 Effect of Eta on the Shape of *k(D)* Curves

Values of η greater than 1 would require that there be some grain size at which the boundary mobility is negative. Given that the mobility does not take the direction of movement into consideration, a negative mobility is not possible making $\eta = 1$ its upper bound. A value of η less than 0 should not be possible as it would indicate an increasing mobility with no limit, making $\eta = 0$ its lower bound. Therefore, $0 < \eta < 1$ must indicate a change in the mechanism of grain boundary movement, $\eta = 1$ indicates that the mechanism by which movement initiates dissipates during the growth process, and all other values are assumed to not be possible.

The value of D_{kin} may be understood as the grain size that is midway from the transition from k_{max} at $k = k_0$ and $D = D_0$ to k_{min} at $k = k_0(1 - \eta)$ and $D \rightarrow \infty$. How it effectively describes the grain growth behavior then depends on the meaning of η. For example, for $\eta = 1$, D_{kin} is simply the midpoint between k_{max} and k_{min}, which means it is only an indication of the grain size at which the boundaries are no longer mobile at $k_{min} = 0$. If, however, $0 < \eta < 1$ then D_{kin} indicates the grain size at which the second growth mechanism becomes more favorable than the first. As for its physical meaning, it is more than likely not an indicator of some characteristic grain size as the term implies. Although the mobility as described in equation 23 is dependent upon grain size, the grain size at any given time is a consequence of a driving force for grain growth, of which the rate is controlled by the mobility of the boundaries. In other words, the change in grain size and, thus, grain size itself is dependent upon grain boundary mobility despite equation 23 being stated in the opposite terms. Since the mobility is not dependent on the instantaneous grain size, it must be assumed that the mobility is not dependent upon D_{kin} either. Thus, the term D_{kin} in equation 23 is more likely to be represent a physical condition that

occurs at $D = D_{kin}$ which then will depend on the system at hand. Finally, it can be assumed that φ has no direct physical meaning. As can be seen in Figure 43, the effect of φ on the instantaneous mobility is to change the sharpness of the transition from k_{max} to k_{min}.

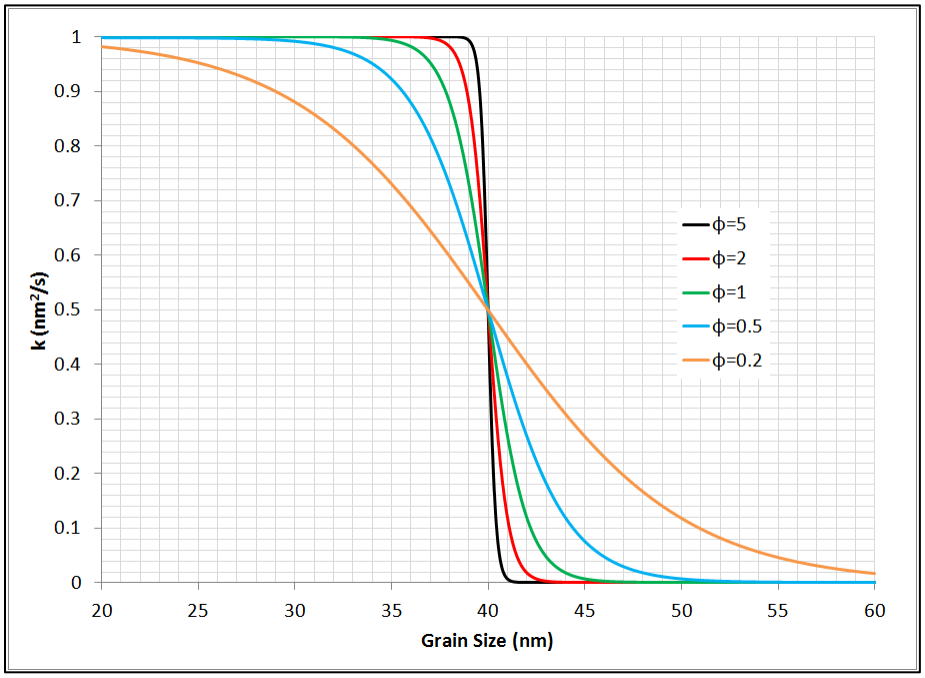

Figure 43 Effect of Phi on the Shape of *k(D)* Curves

If $\eta = 1$, then φ affects the rate at which the mechanism for boundary movement dissipates. If $0 < \eta < 1$, then φ affects the rate at which the initial mechanism of grain boundary movement transitions to the second mechanism. In both cases, the rate is mathematically stated as the rate with respect to grain size as indicated in Figure 43, but it must be understood that it is actually physically dependent upon the rate at which the grain size itself changes. Given that η and D_{kin} describe how the initial growth mechanism either dissipates or transitions to another mechanism, φ is only a consequence of the dissipation or change.

If using DSC only as tool for measuring grain growth, the actual meaning of the parameters becomes less important than the wellness of fit of the $x(t)$ curve that is afforded by the parameters. Setting aside the meaning of the parameters, the fact that six parameters are used for the least square error fit between calculated and measure $x(t)$ values makes the curve fitting quite easy. The number of parameters also lends to the possibility that several good fits between a calculated $x(t)$ curve and the measured $x(t)$ curve could exist without any indication if the fits are good as a mathematical coincidence or because they represent of a local minimum in energy. Thus, if DSC is only used to measure grain growth, a mathematical coincidence with no physical basis is still convenient if it yields a good fit. However, if the correct values of $\mathbf{\Lambda_i} = \{n, D_{eq}, k_0, \eta, D_{kin}, \varphi\}$ are used to calculate $x(t)$ then they may indicate more about how grain growth occurs and the set $\mathbf{\Lambda}$ may help to de-convolute the grain growth mechanism. If secondary verification of grain size is done, once the set of values $\mathbf{\Lambda}$ has been picked, $D(t)$ may be determined by stepwise integration of equation 24 and, if checked against known values of $D(t)$, will allow for better tuning of the parameters in the set $\mathbf{\Lambda}$. In particular, by accurately determining the thermal behavior of the variables in the set $\mathbf{\Lambda}$, the grain growth may be better understood.

Using the measured values for D_0 and D_f from grain sizes taken after cryomilling and after heating for 40 minutes, $D(t)$ was calculated from equation 24 by taking $n = 1$, $D_{eq} = 125$ nm, $k_0 = 59$ nm^2/s, $\eta = 0.965$, $D_{kin} = 37$ nm and $\varphi = 0.95$. The $D(t)$ values were then used to calculate $x(t)$ from equation 21, again using $n = 1$ and $D_{eq} = 125$ nm and compared to published values (ref

19). The $x(t)$ curve found with these values is shown in Figure 38 and the $D(t)$ curve with the previously published grain sizes is shown in Figure 44.

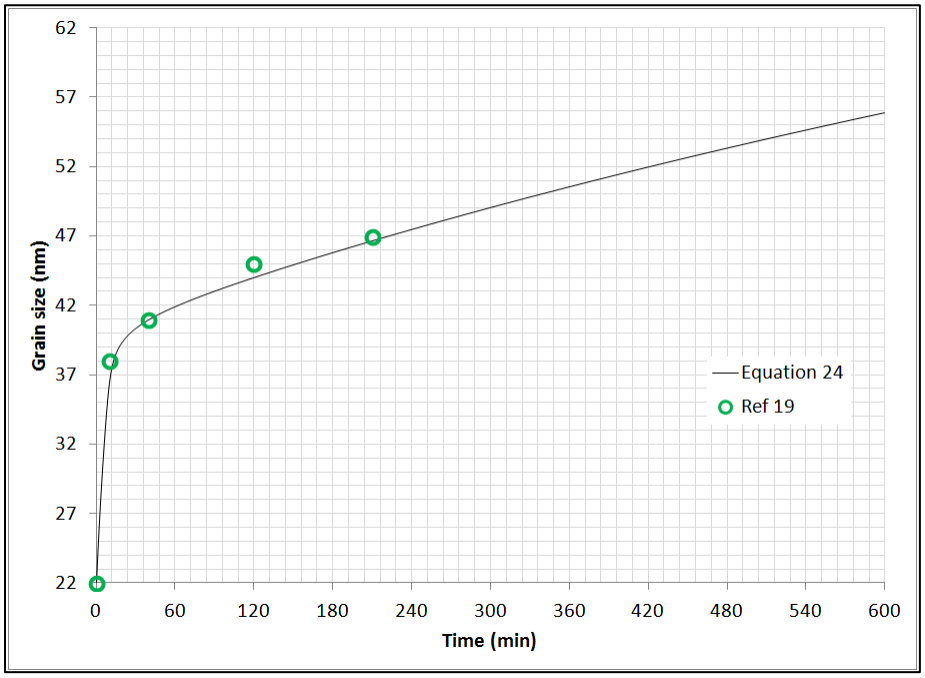

Figure 44 Calculated Grain Growth of Cryomilled Commercially Pure Aluminum Heated by DSC at 300°C

Calculating $x(t)$ and $D(t)$ for as-cryomilled CP aluminum without diamantane was repeated on a second sample from the same batch of powder as was produced for Figures 37, 38, and 44 and the result indicated a rather high variation of the heat evolution from one run to the next. This is reflected in Figure 45 which shows the difference in isothermal heat evolution curves for presumably identical samples.

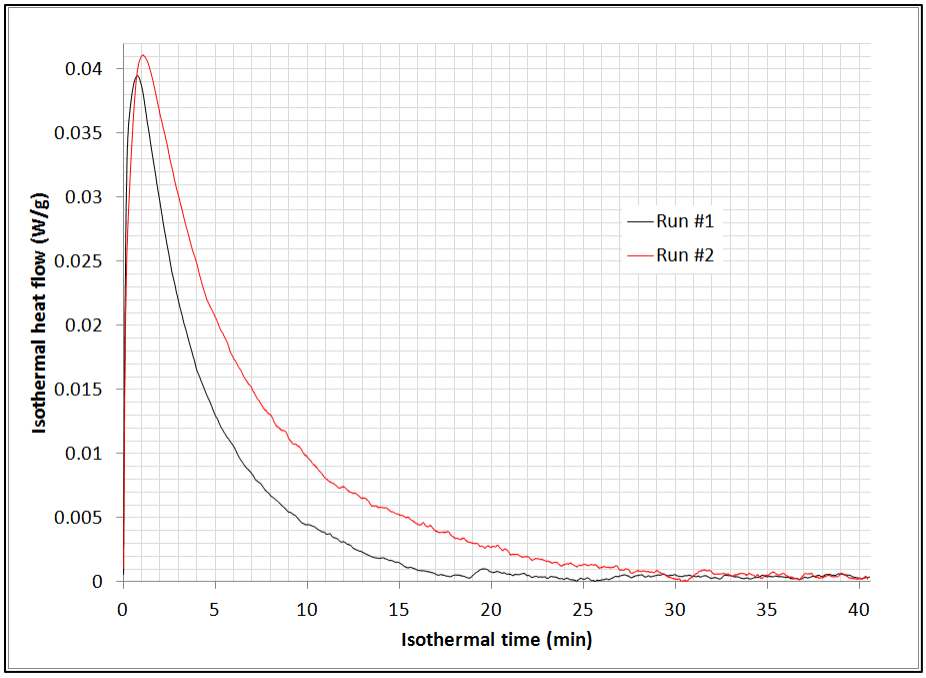

Figure 45 Comparison of Isothermal DSC Heating Sections of Cryomilled Commercially Pure Aluminum Samples from the Same Batch

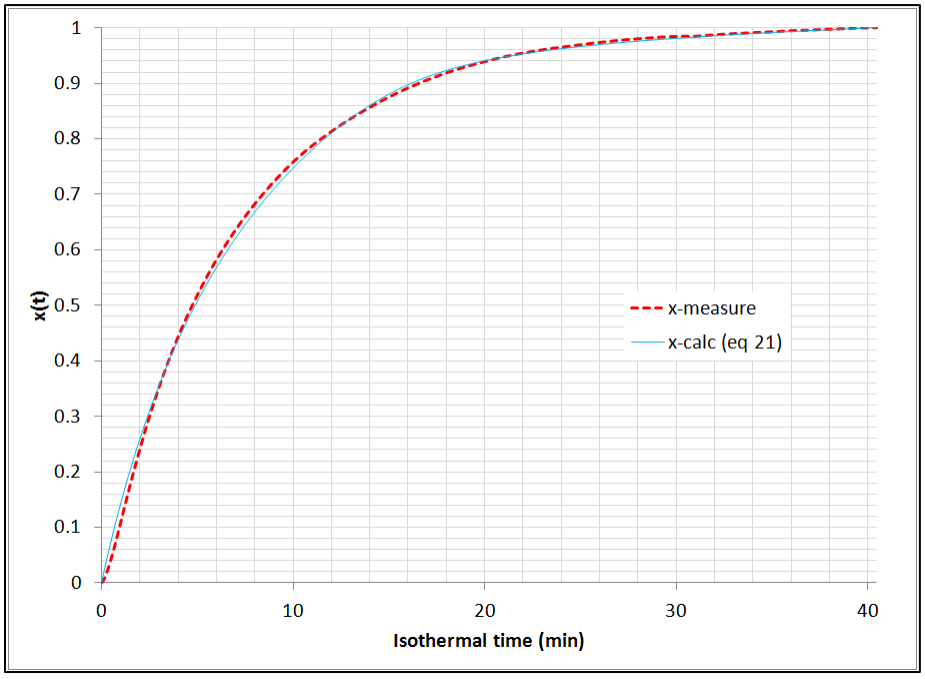

Figure 46 Calculated Grain Growth of Second Cryomilled Commercially Pure Aluminum Sample Held by DSC at 300°C

Compared to the $x(t)$ curve in Figure 38 that was calculated from run #1 in Figure 45, the $x(t)$ curve that results from run #2 has a more shallow slope in the first few minutes and a slower transition to the near-zero slope at the end of the isothermal period. Given the proposed meanings of the parameters in the set **Λ**, this indicates a smaller initial growth rate with a slower transition to the minimum growth rate. The values in the set **Λ** were adjusted to reflect this assumption, particularly that k_0 and φ were reduced, and the other parameters were adjusted accordingly to find reasonable fits of the calculated D (t) to measured grain sizes. The calculated $x(t)$ curve was fit to the measured curve for run #2 after this. The resulting curve for run #2 with n = 1, D_{eq} = 125 nm, k_0 = 38 nm^2/s, η = 0.95, D_{kin} = 38 nm, and φ = 0.92 is shown in Figure 46. Although the values of D_{eq}, n, D_{kin} and $k_{min} = k_0(1 - \eta)$ are very close for the curve fits in Figures 38 and 46, $k_{max} = k_0$ and φ are not. In fact, given that the isothermal heat flows are normalized to sample mass prior to making any calculation, the large difference in the values of k_0 from run #1 to run #2 seemingly indicate a difference in the mechanism that initiates grain growth, which may be a dubious claim. Whatever the actual definitions of k_0, η, φ, D_{kin}, D_{eq} and n are, for an identical system they should have identical values. If that is taken to be true, then the opposite must be true as well: differences in the values must indicate differences in the systems being measured. Small differences are reasonable in samples assumed to be the same, however, differences in mechanisms indicate dissimilar systems which is unlikely. Thus, the difference in the k_0 values measured between the first and second run are more likely the cumulative result of numerous small differences in the samples that are not captured by these particular fits. This particular case illustrates that additional caution must be exercise in choosing the parameters in the set **Λ** to fit $x(t)$ curves by acknowledging that the DSC method

can be sensitive to small material changes that appear to be random error. When choosing sets $\mathbf{\Lambda_i}$ to fit calculated $x(t)$ curves to their measured counterparts, in each of the following cases in the current work, values were attempted to be kept as constant as possible from one run to the next. For more on the uncertainty of the parameter values, see Appendix I.

Cryomilled aluminum was heated isothermally at 300°C, 375°C, 450°C, 500°C and 550°C with the heat signal measured by DSC. $x(t)$ was determined from the DSC signals for each isothermal hold periods and a set $\mathbf{\Lambda_i}$ was chosen for each DSC run to calculate grain size curves, D(t), and $x(t)$. The values in the sets $\mathbf{\Lambda_i}$ are shown in Table 6 and the resulting $D(t)$ curves are shown in Figure 47 with reported grain sizes if known.

Table 6 DSC Grain Growth Parameters of Cryomilled Commercially Pure Aluminum

Temp (°C)	k_0 (nm^2/s)	η	ϕ	D_{kin} (nm)	D_{eq} (nm)	n	k_{min} (nm^2/s)	R^2
300 (#1)	59	0.965	0.95	37	125	1	2.065	0.999
300 (#2)	38	0.95	0.92	38	125	1	1.9	0.998
375	46	0.94	0.9	41	145	1	2.76	0.995
450	45	0.9	0.9	45	150	1	4.5	0.991
*500**	*21*	*0.95*	*0.95*	*35*	*88*	*1*	*1.05*	0.998
550	260	0.45	0.9	90	190	1	143	0.996
**Values not included in subsequent analyses*								

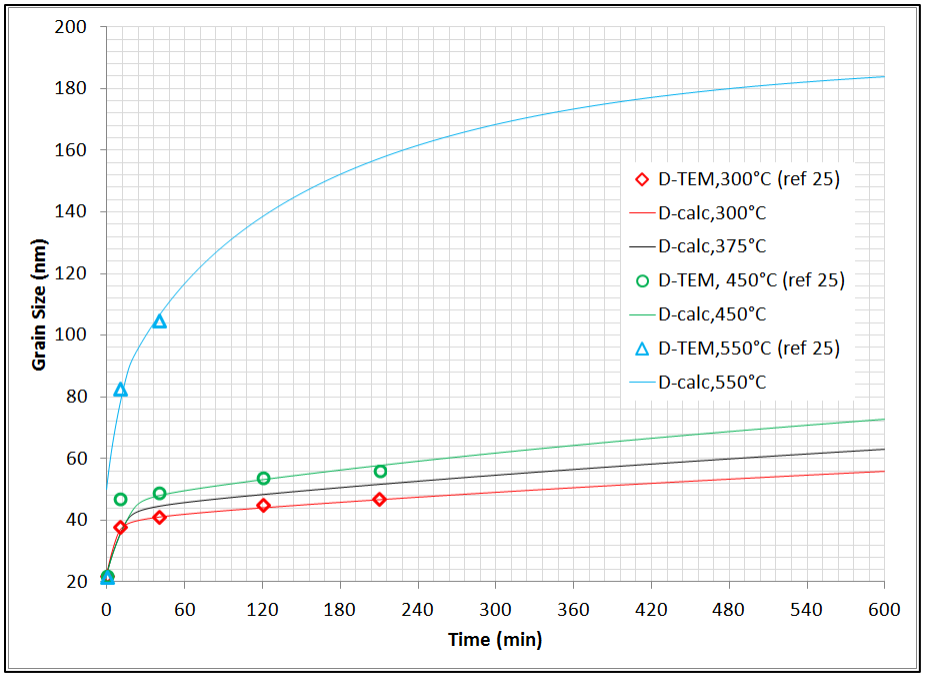

Figure 47 Calculated Grain Growth of Cryomilled Commercially Pure Aluminum Heated by DSC at Temperatures Between 300°C and 550°C

The values found for the best $x(t)$ fit for the samples heated isothermally at 500°C are shown in Table 6 and they were the only reasonable values that would yield a good fit of $x(t)$ to the measured curve. However, they clearly deviate from any trend that is indicated from other the values in the other $\mathbf{\Lambda_i}$ sets shown in Table 6 and, thus, are not included in any other part of the analysis. A total of three CP aluminum samples were heated at 500°C, for which the isothermal heating curve is shown in Figure 48. Shown for comparison is the isothermal heating curve at 550°C. As can be seen, the heat release curves of the samples held at 500°C have highly atypical shapes. The first sample at 500°C had an extremely large isothermal heat release, the second had what appeared to be two separate heating curves overlapping, and the third appeared to release small amounts of energy around 10 minutes and after 25 minutes, despite the initial energy release appearing to have stopped within 5 minutes. Because they were all prepared at

the same time with the same stock powder, it is likely that they were either contaminated during preparation or that they were improperly prepared, both of which could yield erroneous Λ_i values.

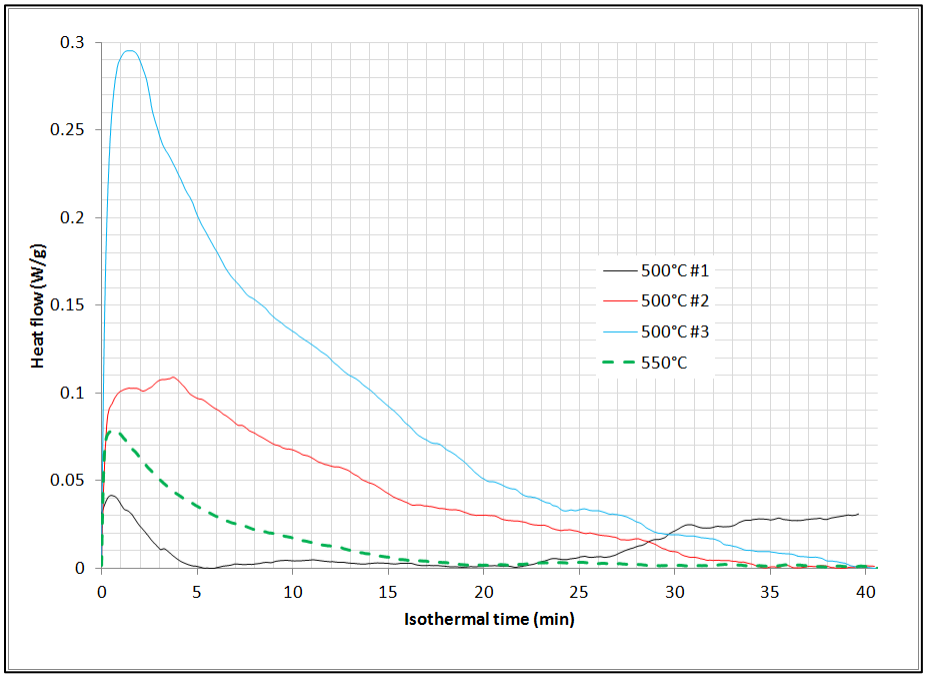

Figure 48 Isothermal Portion of DSC Heating Curves of Cryomilled Commercially Pure Aluminum at 500°C

Several of the values in Table 6 are plotted in Figures 49 through 52 to illustrate thermal and other dependences.

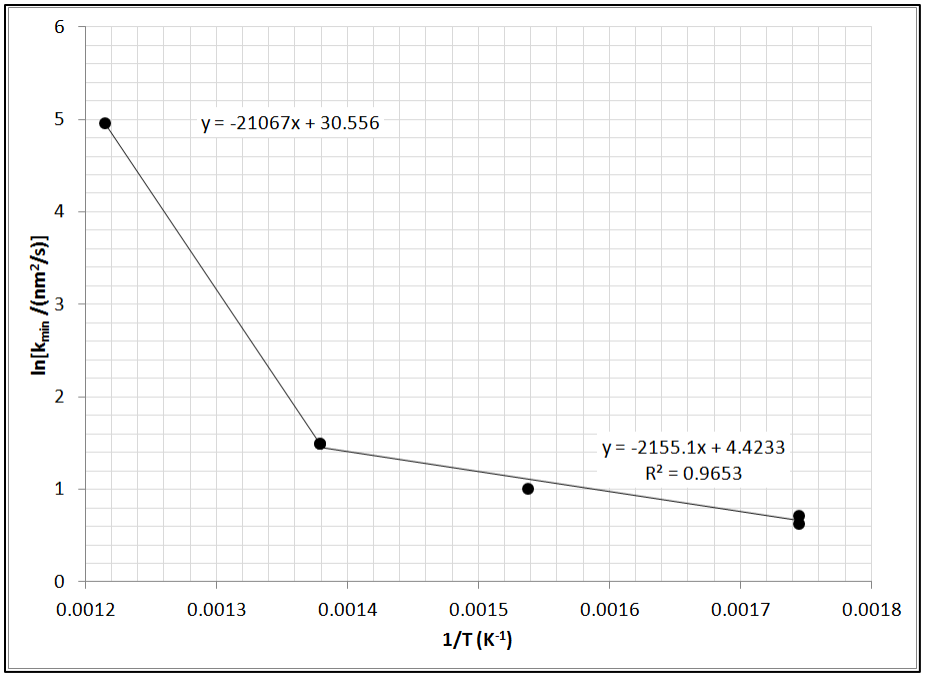

Figure 49 Thermal Dependence of k_{min} of Cryomilled Commercially Pure Aluminum

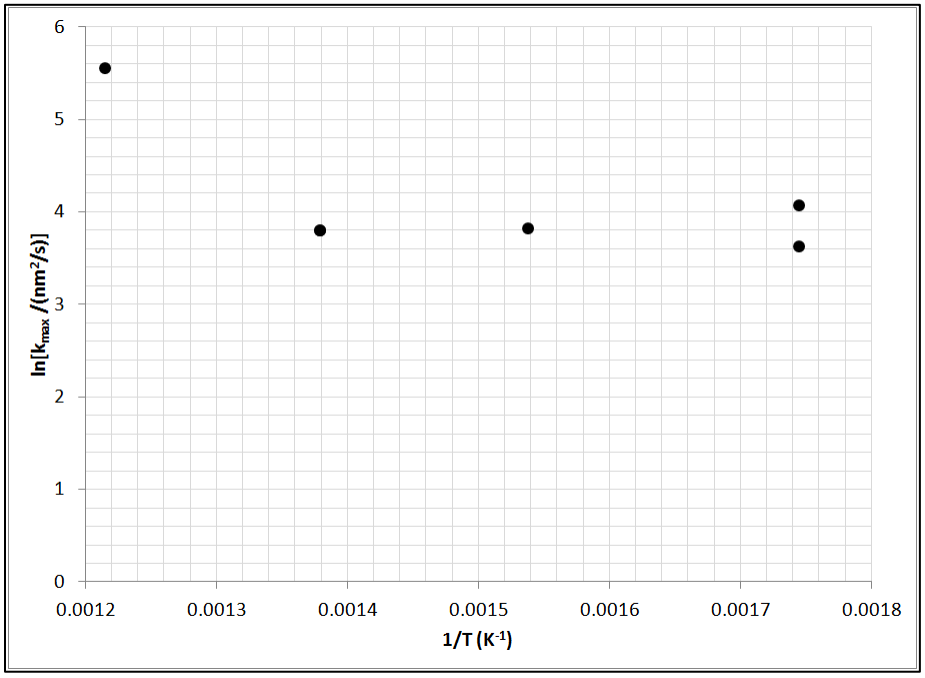

Figure 50 Thermal Dependence of k_{max} of Cryomilled Commercially Pure Aluminum

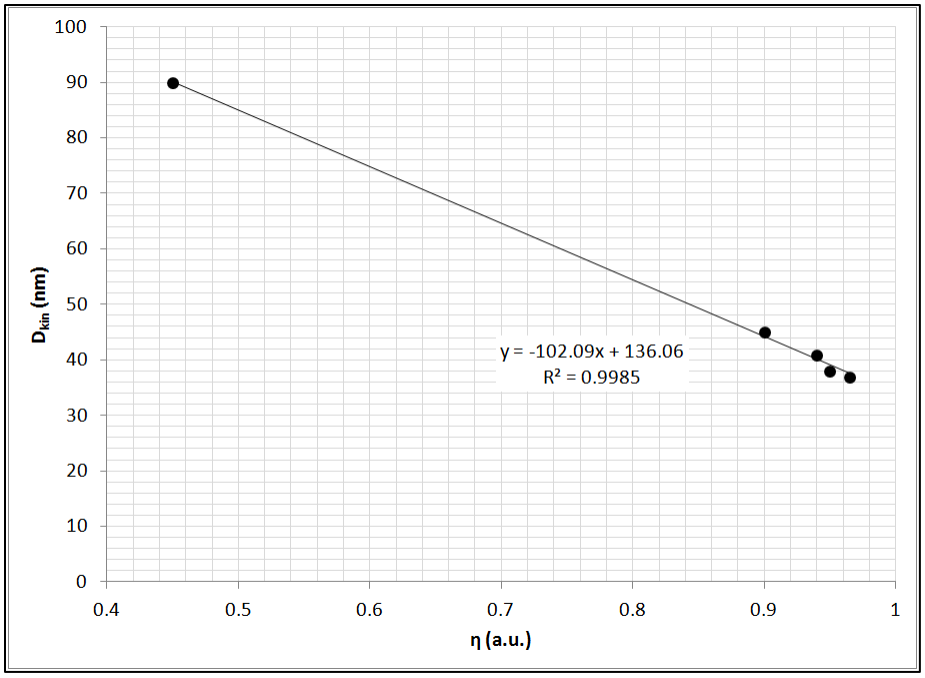

Figure 51 Observed Relationship Between D_{kin} and Eta in Cryomilled Commercially Pure Aluminum

Shown in Figure 49 is an Arrhenius plot of k_{min}, which represents the thermal dependence of the secondary mechanism for grain boundary motion. As can be seen, there is a switch in the secondary mechanism somewhere between 450°C and 550°C as indicated by the change in slope. Bearing in mind that the slope in the higher temperature regime is based on only two points and that the actual switching point between the high and low temperature regimes is not determined, the slope of the shown line corresponds to an activation energy of approximately 2.6 kJ/mol. The slope of the lower temperature regime which is more certain corresponds to an activation energy of 0.25 kJ/mol. Both values of activation energy are lower than what has been reported for cryomilled aluminum (ref 4). Given that the values were found with the assumption that grain boundary mobility changes during grain growth, lower values than what has been previously reported for a stabilized mobility would be expected. The dependence of $k_0 = k_{max}$ is shown in Figure 50. What is interesting about the trend shown is

that, below 550°C, there seems to be no thermal dependence of the initial grain boundary mobility, which may seem counterintuitive based on Figure 51. Figure 51 shows a strong correlation between D_{kin} and η. Defining η as $\eta = 1 - k_{min}/k_{max}$, this means that D_{kin} has a direct correlation to the ratio of k_{min} to k_{max}. Furthermore, the negative slope of the trend line in Figure 51 indicates that a larger value of k_{min} corresponds to a larger value of D_{kin}. What this means physically is that a faster secondary mechanism for boundary motion results in the switch from the primary to secondary mechanism occurring at a later point. Because D_{kin} is increasing with temperature as indicated in Table 6, this would mean that the initial mechanism for boundary motion is able to sustain longer when more heat is applied which is by definition a thermal dependence of k_0. However, Figure 50 clearly shows that, below 550°C there appears to be no thermal dependence on the initial boundary motion mechanism. Thus, what Figure 51 must indicate is that whatever is determined to be the *secondary* mechanism is active during the entire isothermal heating period and is occurring in parallel to the *primary* mechanism for boundary motion. For convenience, it may still be treated as a transition in grain boundary mechanisms, as the effect on $k(D)$ is the same.

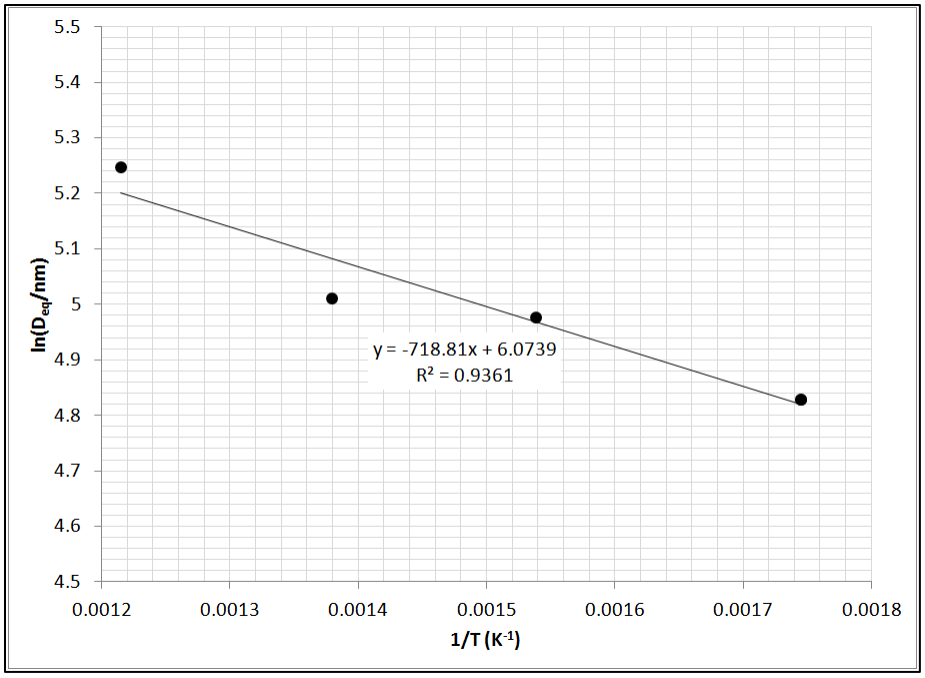

Figure 52 Thermal Dependence of D_{eq} of Cryomilled Commercially Pure Aluminum

Figure 51 shows an Arrhenius plot of equilibrium grain size, D_{eq}. The slope of the line indicates an activation energy of 86 J/mol which, given the nature of D_{eq}, must relate in some way to solute mixing.

4.1.4. Cryomilled Aluminum with Diamantane

Cryomilled aluminum samples with 0.5 wt% and 1.0 wt% diamantane were heated isothermally for at least 30 minutes at runs between 300°C and 550°C with the heat evolution signal measured by DSC. The isothermal heat evolution for each run typically had the shape of the isothermal heating curve in Figure 37, however, a few of the samples had a shape like that of run #1 of Figure 48, where excess heat appears to be given off after stagnation of grain growth. Only the more typical runs like in Figure 37 are taken into account in the following analysis. As was the case with commercially pure cryomilled aluminum, the isothermal heat evolution signal

was integrated over time and the instantaneous integrated value was normalized to the total heat evolved in the isothermal period to yield a $x(t)$ like Figure 38. Values in the set $\mathbf{\Lambda_i}$ were chosen for each run so that $D(t)$ could be calculated from equation 24, followed by $x(t)$ from equation 21. If values of $D(t)$ were known from independent measurements, they would be used for fitting of the $D(t)$ curve, and the calculated $x(t)$ curve was fitted to the measured $x(t)$ curve. The values for each sample were then compared based on diamantane content.

Cryomilled aluminum with 1.0 wt% diamantane was heated at 300°C and 500°C. The values in the sets $\mathbf{\Lambda_i}$ for several samples are shown in Table 7. Note that cryomilled aluminum with diamantane is particularly useful for demonstrating the validity of a variable mobility. For example, the #1 300°C sample in Table 7 when forced to a least-squares fit with $\eta = 0$ can only manage to be fit with a correlation coefficient between $x(t)$ curves, R^2, of greater than 0.99 with $k_0 > 1600$ nm^2/s, $D_{eq} = 28$ nm and $n = 0.04$. As indicated in Figure 55, a value of $D_{eq} = 28$ nm greatly undercuts the measured grain sizes for all samples measured after 40 minutes of heating. The only way the grains could grow 6 nm in under an hour and then only an additional 3 nm in the next 10 hours is by k_0 being reduced, meaning that the grain boundary mobility must change.

Table 7 DSC Grain Growth Parameters of Cryomilled Aluminum + 1% Diamantane

Temp (°C)	k_0 (nm^2/s)	η	ϕ	D_{kin} (nm)	D_{eq} (nm)	n	k_{min} (nm^2/s)	R^2
300 (#1)	10	0.99	0.6	25	40	1.8	0.1	0.996
300 (#2)	13	0.99	0.6	24	38.7	1.8	0.13	0.998
300 (#3)	13	0.99	0.7	24	38.5	2	0.13	0.998
500 (#1)	30	0.68	0.2	20	57	1.5	9.6	0.996
500 (#2)	42	0.75	0.2	20	58	1.5	10.5	0.995

Comparing Table 6 to Table 7, the first noticeable effect of the addition of diamantane is that the initial mobility appears to decrease. Furthermore, the observation from Table 6 that the initial mobility increases at higher temperatures is again seen in Table 7. As Table 7 only shows sets $\mathbf{\Lambda_{(1\%DM,300°C)}}$ and $\mathbf{\Lambda_{(1\%DM,500°C)}}$ so there can be no verification of athermal behavior in k_0 in the low temperature regime as was seen with commercially pure cryomilled aluminum. However, this does not eliminate the possibility that the initial grain growth could be athermal in cryomilled aluminum with diamantane below some characteristic temperature either. It can also be seen that the transition from the initial mechanism of grain growth to the second mechanism is slower and occurring sooner, as indicated by the smaller values of φ and D_{kin}. Furthermore, unlike with commercially pure samples, the samples with 1% diamantane have an apparent temperature dependence of φ. What can be inferred about the grain boundary mobility from the differences in k_0, φ and D_{kin} in Tables 6 and 7 is that the diamantane is hindering or slowing the initial growth mechanism, which is allowing the secondary growth mechanism to take place sooner, but that the overlap in mechanisms persists longer with diamantane added. Comparing the thermal stability parameters, D_{eq} and n, the addition of diamantane appears to decrease the equilibrium grain size significantly while increasing the value of n. This observation supports the idea that diamantane not only acts to impede grain boundary movement, it lowers grain boundary energy through chemical mixing potentials.

Aluminum cryomilled with 0.5 weight percent diamantane was heated isothermally at 300°C, 375°C, 450°C, 500°C, and 550°C. As with the commercially pure and 1% diamantane counterparts, the heat evolution in samples during isothermal holds was measured by DSC, $D(t)$

was calculated from chosen $\mathbf{\Lambda_i}$ sets, and the resulting calculated $x(t)$ curve was fit to the $x(t)$ curve calculated from the DSC profile. Sets of $\mathbf{\Lambda_i}$ parameters from the isothermal heating experiments are shown in Table 8.

Table 8 DSC Grain Growth Parameters of Cryomilled Aluminum + 0.5% Diamantane

Temp (°C)	k_0 (nm^2/s)	η	ϕ	D_{kin} (nm)	D_{eq} (nm)	n	k_{min} (nm^2/s)	R^2
300 (#1)	26	0.99	0.79	25	49	1.8	0.26	1.000
300 (#2)	26	0.99	0.79	25	49	1.8	0.26	1.000
375	30	0.98	0.28	32	53	2	0.6	0.998
450	35	0.96	0.2	33	50	2	1.4	0.996
500 (#1)	30	0.9	0.1	38	60	1.8	3	0.997
500 (#2)	30	0.93	0.1	36	62	2	2.1	0.994
550	75	0.3	0.05	45	80	2	52.5	0.992

Again, it can be observed from Table 8 that the initial mobility of grain boundaries, k_0, appears to be possibly athermal, with values somewhere between those found for commercially pure cryomilled aluminum (Table 6) and those found for cryomilled aluminum with 1% diamantane (Table 7). As was the case with samples cryomilled with 1% diamantane, the samples cryomilled with 0.5% diamantane appear to transition from the initial grain growth mechanism slower and sooner than the samples without diamantane. This supports the conclusion that diamantane is hindering the initial grain growth process. However, Table 8 also indicates that the transition from the initial to second growth mechanism is slower and occurs at a later point with 0.5% diamantane in the sample than with 1% diamantane in the sample. The observations of thermal stability imparted by diamantane made from Table 7 apply to Table 8 as well. D_{eq} and n are less for samples with 0.5% diamantane than commercially pure samples, but smaller than samples with 1% diamantane. This clearly supports the conclusion that diamantane is chemically

stabilizing grain boundaries by lowering the boundary energy, and that more available diamantane offers better thermal stabilization. That the values of *n* in Tables 7 and 8 are very similar is perhaps surprising, as this would mean that grain boundary change with solute species concentration in boundaries is much more dependent upon the species itself than the concentration of the species in the entire system at hand. Finally, it is again seen in Table 8 that the minimum grain boundary mobility is thermally dependent and exhibits low and high temperature regimes. Figure 53 shows an Arrhenius plot of k_{min} for cryomilled aluminum + 0.5 weight percent diamantane samples. The activation energies from the slopes of the two lines in the figure correspond to 4.7 kJ/mol in the high temperature regime and 0.6 kJ/mol in the low temperature regime.

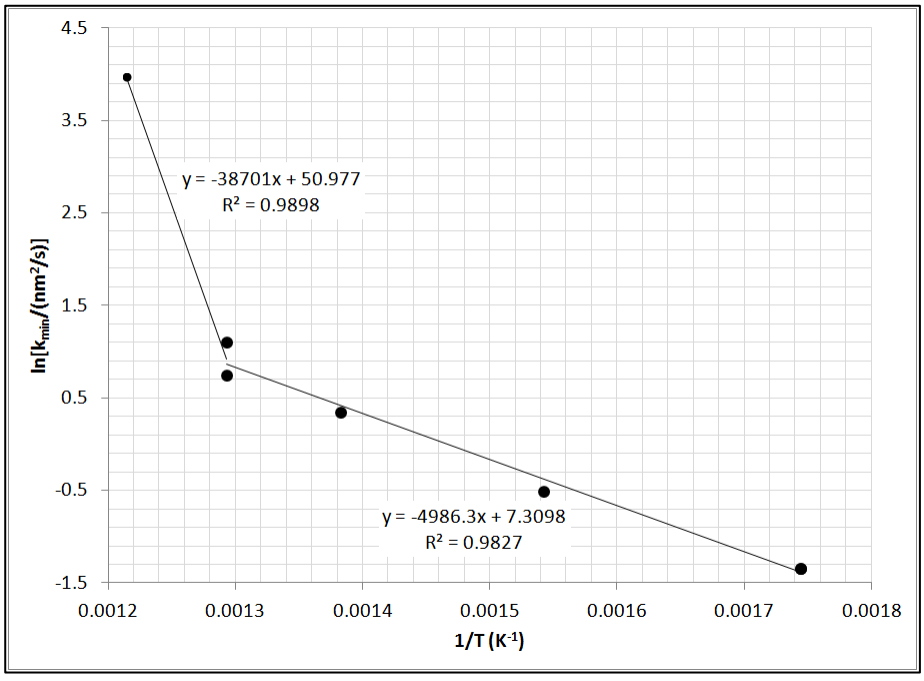

Figure 53 Thermal Dependence of k_{min} of Cryomilled Aluminum + 0.5% Diamantane

Figure 54 shows the Arrhenius plot of D_{eq} resulting from the values tabulated in Table 8. The activation energy indicated by the slope of the plot is 78 J/mol, which is higher than what was calculated for commercially pure samples from Figure 52. It must be kept in mind, though, that the linear trend is a relatively poor fit and that the true activation energy may be quite different.

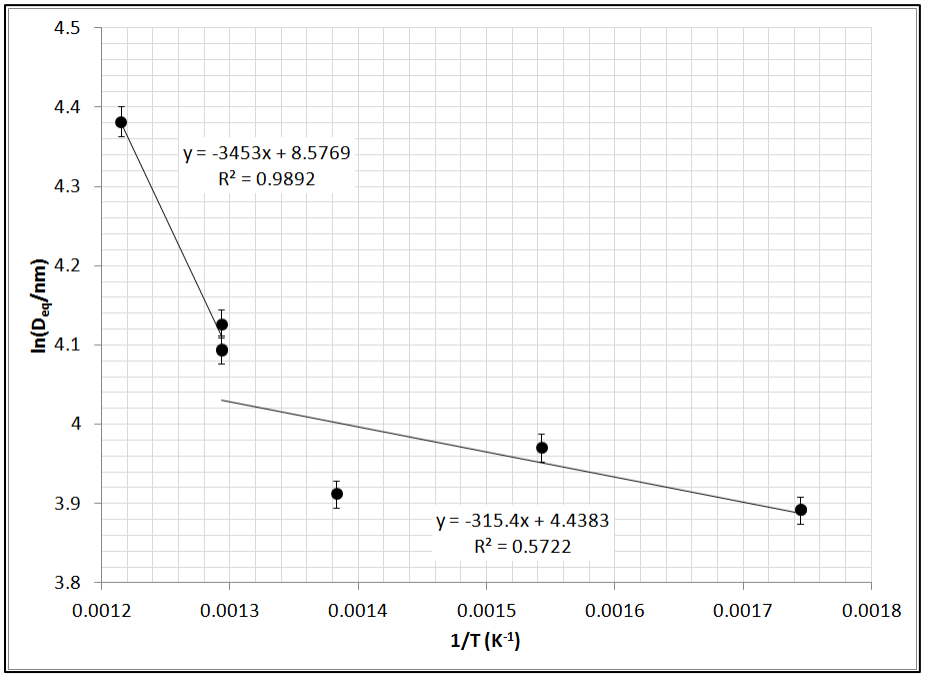

Figure 54 Thermal Dependence of D_{eq} of Cryomilled Aluminum + 0.5% Diamantane

The difference in activation energy in the commercially pure cryomilled samples and the cryomilled samples with 0.5% diamantane can be explained by the difference in solute atom species. The solute atoms in the commercially pure samples are likely to be trace elements from the stock powders such as copper, zinc, and silicon, and elements from the milling process such as carbon, nitrogen, and iron. The source of chemical stabilization of grain boundaries in samples with diamantane, of course, is the diamantane. If the activation energies calculated from the slopes of the trend lines in Figures 52 and 54 indeed do indicate a parameter related

to the mixing of solute atoms, it is to be expected that the activation energies would differ, as the mixing in commercially pure aluminum is expected to be with trace elements while the mixing with diamantane is with a larger, covalently bound compound. Furthermore, Figure 54 indicates that the mixing likely occurs in both a high and low temperature regime. One possible interpretation of this behavior is that ordering of diamantane changes at high temperatures. It is also reasonable that this behavior can be ascribed to decomposition of the diamantane at higher temperatures with the mixing of the products of the composition being less favorable than the mixing with diamantane.

The $D(t)$ curves calculated from the $\mathbf{\Lambda_i}$ sets in Table 8 are shown in Figures 55 through 58.

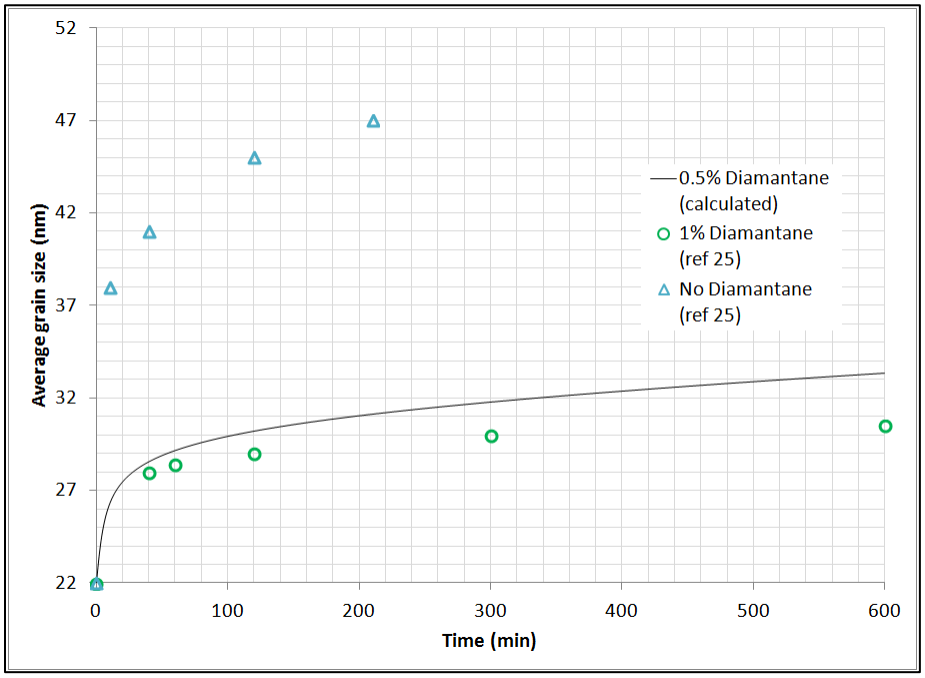

Figure 55 Estimated Grain Growth of Cryomilled Aluminum + 0.5% Diamantane at 300°C

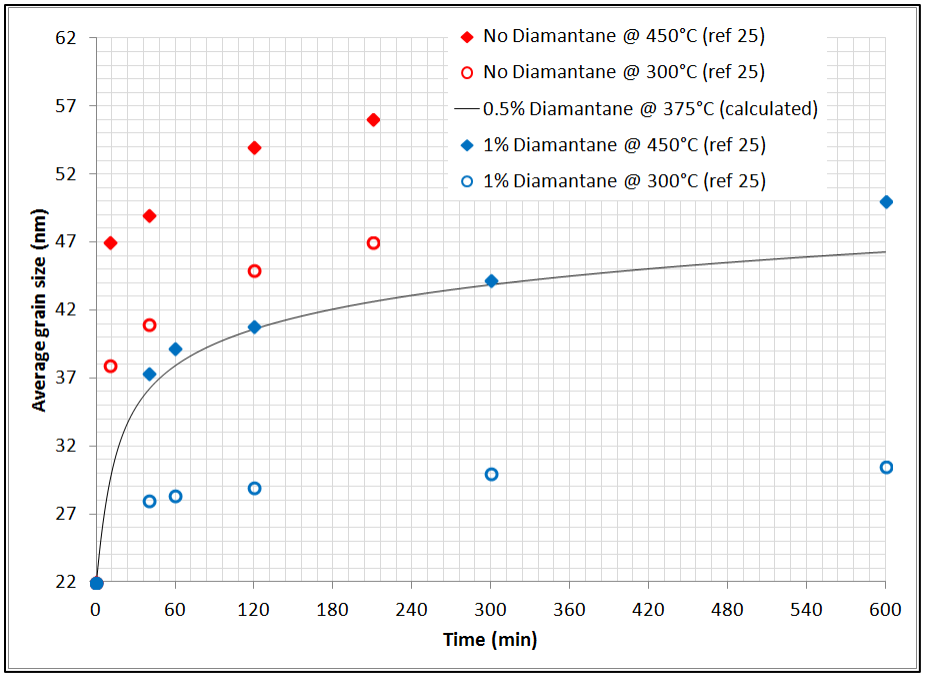

Figure 56 Estimated Grain Growth of Cryomilled Aluminum + 0.5% Diamantane at 375°C

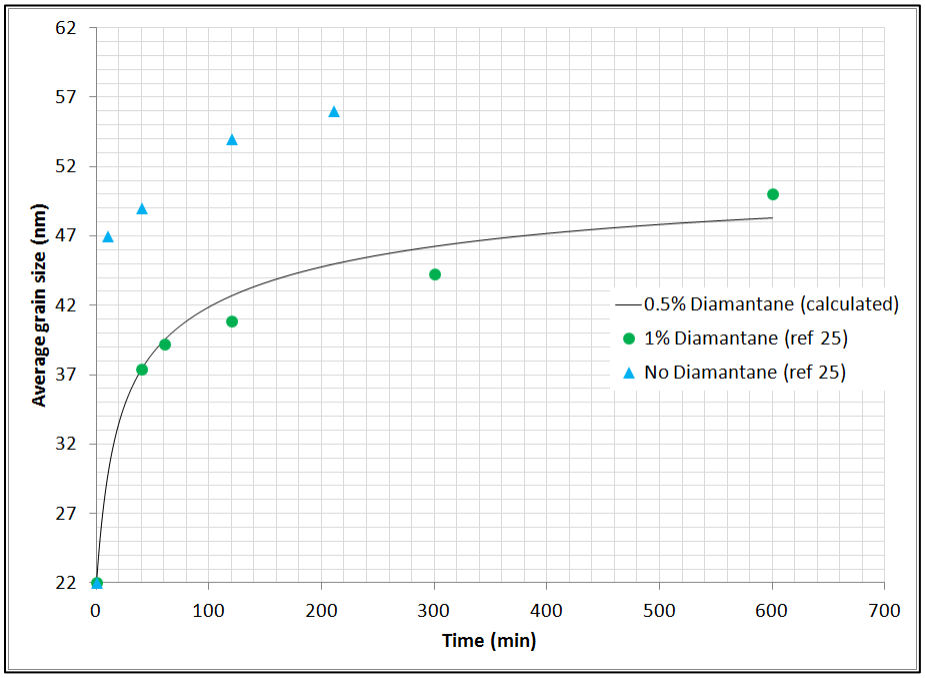

Figure 57 Estimated Grain Growth of Cryomilled Aluminum + 0.5% Diamantane at 450°C

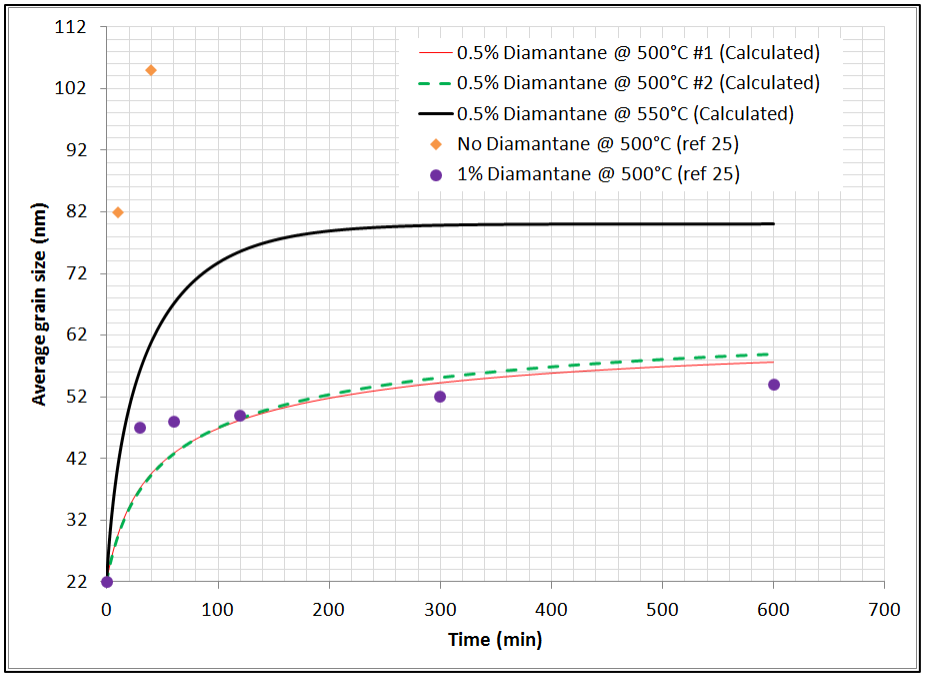

Figure 58 Estimated Grain Growth of Cryomilled Aluminum + 0.5% Diamantane at 500-550°C

What can be seen from Figures 55 through 58 is the ability of the DSC signal to predict grain growth behavior even in the absence of final grain size, D_f, in equation 21. In each of the growth curves in Figures 55 through 58, the grain size was calculated from equation 24 based on the set of variables $\mathbf{\Lambda_i}$ and the grain size predicted at the end of the isothermal hold period was used in equation 21 as the value of D_f. The known grain sizes and grain growth curves for samples without diamantane and with 1 weight percent diamantane were used for guidance in picking the initial values of the parameters in the sets $\mathbf{\Lambda_i}$, which were then adjusted to fit the calculated $x(t)$ curve to the measured $x(t)$ curve. Table 8 indicates a strong correlation between the $x(t)$ curves by the shown correlation coefficient values, R^2, and the grain growth behavior of 0.5% diamantane samples predicted in Figures 55 through 58 are reasonable compared to shown grain sizes from other works (ref 25).

Figures 55 and 57 also predict an interesting dependence of diamantane concentration on the grain growth behavior. In both of these figures, the predicted curve is compared directly to known grain sizes of commercially pure cryomilled aluminum and cryomilled aluminum with 1 weight percent diamantane as they are heated at the specified temperatures. Rather than lying halfway between the values shown for commercially pure cryomilled powders—in other words, 0% diamantane—and cryomilled powders with 1% diamantane, the powders cryomilled with 0.5% diamantane are predicted to have grain growth behavior much more similar to the 1% diamantane samples. This indicates that the initial half percent of diamantane added to the cryomilling mixture provides the majority of the thermal stability with very little added benefit of the second half percent. This is also seen in comparing Tables 7 and 8. While there is a noticeable decrease in equilibrium grain size at 300°C in the samples with 1% diamantane compared to the samples with 0.5% diamantane, the difference at 500°C is trivial.

The role of diamantane in grain growth can now be seen by comparing Tables 7 and 8 to Table 6. Perhaps the most useful conclusion that can be drawn is that that diamantane does actually impart thermal stability to the cryomilled material, as opposed to simply slowing grain boundary movement so much that they do not move appreciably over long periods of time. In addition, the smaller values of k_0 and k_{min} indicate that diamantane drags on grain boundaries as well, effectively lowering their rate of movement. The values of D_{kin} and φ decrease by adding diamantane as well. Thus far, the actual mechanism by which grain growth starts and the mechanism to which it transitions have not been discussed, but the fact that k_0, k_{min}, D_{kin} and φ all decrease by adding diamantane gives some indication of the physical role of

diamantane in grain growth. The model for grain growth in equation 24 was developed with a stated assumption that grain boundary movement is accomplished by diffusion of atoms in some position at one grain edge diffusing to a lower energy position at the opposite grain edge (ref 10). The idea that grain growth could transition from one mechanism to another does not agree with this physical description as one scenario requires one mechanism and the other requires two. However, the development of equation 24 does not preclude its use as a general description of grain growth with multiple rate constants.

Remembering that below some temperature the initial growth mechanism seems athermal, the initial growth mechanism could be a process such as grain growth accommodated by concerted dislocation motion, grain rotation, recrystallization, and so forth. Each of these phenomena have been reported or theorized in nanocrystalline materials and given the large number of dislocations generated during cryomilling, any of these could explain the initial very fast movement of grain boundaries (refs 40-43). Rather than postulate the exact nature of the phenomenon that occurs, it will be more beneficial to describe it as a brief process that begins after an initial barrier is overcome, after which it continues athermally until there is a slight shift in equilibrium of the entire system to a lower energy state. This description may be used as a generalization of any of the previously mentioned processes. At the same time, grain growth accommodated by detachment of atoms from one grain boundary, diffusion, and attachment to the opposite grain boundary can occur. However, it must be taken as an assumption that only one of these processes can occur in a grain boundary at any given time. Furthermore, it will be assumed that the as-cryomilled grain boundaries have a set population that can only

grow initially by the initial process, a set population that can only grow by the attachment/detachment mode, and another population that could grow by either mode. With this description, the effect of diamantane would be expected to be as acting as a physical hindrance to the initial process and to the standard detachment-attachment mode of grain growth. If diamantane acts as a greater hindrance to the initial process than to the detachment-attachment process, then the initial process becomes less favorable more quickly. This would be reflected in smaller D_{kin} values when diamantane is present, which is the case. The smaller values in φ which indicate the transition from the first mechanism to the second takes longer implies that it is the diamantane that is responsible for the slower transition of mechanisms. This can be explained by the fact that the attachment-detachment grain growth process is thermally activated. As the initial growth mechanism is slowed by diamantane, the thermally activated grain growth is still occurring at a steady rate in parallel. Since fewer boundaries are being brought towards equilibrium by the initial mechanism, more are having energy lowered by the standard grain growth in the meantime. This would present as an apparent broadening of the range over which the transition takes place, which means a lower φ value.

4.2. Effect of Low Diamantane Concentrations

4.2.1. Thermal Stability

The thermal stability imparted by diamantane in a cryomilled aluminum material was demonstrated to be significant with powders heated between 300°C and 550°C predicted to reach an equilibrium grain size below 100 nm with 0.5 and 1.0 weight percent additions. This is, of course, thermal stability demonstrated for unconsolidated powder heated in a closed system

and, as larger grain sizes have been reported in consolidated aluminum cryomilled with diamantane than in powders, the consolidation process shifts equilibrium (refs 4, 25). Thus it must be understood that the previous description of the effect of diamantane on grain growth that was discussed could change when the material is stressed. With this in mind, Table 3 may be reviewed in light of the previous discussion of thermal stability in powders investigated by isothermal DSC experiments. The consolidation temperature for the samples used characterized by TEM and shown in Table 3 520°C. As this is somewhere between the temperatures of 500°C and 550°C in Table 8, it is to be expected that the equilibrium grain size is somewhere between the value of D_{eq} = 61 ± 1 nm at 500°C and D_{eq} = 80 nm at 550°C. Using the trend line in Figure 54, the equilibrium grain size at 520°C is expected to be approximately 65 nm. As the average grain size of the consolidated sample in Table 3 from the same stock powder was measured to be 74 nm, equilibrium is indeed affected by the isostatic pressure, high speed extrusion, or both. In comparing Table 3 to Tables 6 and 8, the same trend of larger grain sizes due to the consolidation process is to be expected.

As was noted previously, the primary benefit in thermal stability is imparted by the first 0.5 weight percent of diamantane and the second 0.5 weight percent offers only marginally improved thermal stability. Comparing the HIP + Trap Extrude samples in Table 3 with no diamantane, 0.1% diamantane, 0.2% diamantane, and 0.5% diamantane, it is confirmed again that diamantane offers significant thermal stability as the average grain size measured with no diamantane is significantly larger than any of the samples with diamantane. Interestingly, the 0.2% and 0.5% diamantane samples have nearly the same reported average grain size, and the

0.1% diamantane sample has the smallest average grain size of the three. This seems to be in direct conflict with the observation in the isothermal DSC experiments that, albeit only marginal improvement in thermal stability, greater diamantane concentrations still do impart greater thermal stability. However, the grain sizes in Table 3 are not equilibrium grain sizes and, thus, are not directly comparable to the D_{eq} values reported in Tables 7 and 8. In fact, an average grain size of 61 nm after consolidation of 0.1% diamantane powders does not preclude that it will have a much larger equilibrium grain size that is closer to the equilibrium grain size for the commercially pure cryomilled material. For this to happen, grain growth must occur slower in the material cryomilled with 0.1% diamantane than the other samples containing diamantane. In terms of the parameters in equation 24, this is occurs if k_0 is small, D_{kin} is small and η is close to 1, and when n is small. Physically speaking, k_0 being small represents diamantane slowing the postulated initial growth mechanism. Although the amount by which k_0 is reduced at 300°C seems dependent upon diamantane concentration, Tables 6 through 8 indicate a somewhat concentration-independent reduction in k_0 at 500°C. As the samples in Table 3 were consolidated in the higher homologous temperature range, it is reasonable to assume that the value of k_0 during the consolidation process was not significantly different in samples with 0.1%, 0.2%, and 0.5% diamantane. In samples without diamantane and with 0.5 weight percent diamantane, there was an apparent transition in the secondary mechanism for grain growth represented by k_{min}, a phenomenon which has been observed before (ref 4). The transition temperature predicted by Figure 53 from the intersection of the trend lines is at 499°C and although the transition temperature cannot be predicted from Table 7 for the material with 1% diamantane, a value of 450°C has been reported (ref 25). From this trend, diamantane

concentration is lowering the transition temperature. Thus, it is reasonable to assume that the material with 0.1% diamantane was consolidated below the transition temperature while the materials with 0.2% diamantane and 0.5% diamantane were consolidated above the consolidation temperature.

From the development thus far, it cannot be determined whether or not the value of *n* for consolidated samples would be approximately 2 or not. It was previously postulated that the value of *n* was approximately the same for powders with 0.5% and 1% diamantane because the grain boundary excess depends on the solute species but not its concentration. For *n* to be less than 2 for the consolidated sample with 0.1% diamantane, it is possible that this assumption breaks down and thus requires greater explanation for why the value of *n* is near 2 for samples with 0.5% and 1% diamantane, but it is less for material with 0.1% diamantane. One example explanation for this behavior would be that whatever effect leads to a value of $n = 2$ for the grain boundary excess parameter saturates at or before a diamantane weight concentration of 0.5%, such as if the ratio of diamantane between grain interiors to grain boundaries approaches a constant value at or around 0.5% by weight. Alternatively, the assumption that the chemical mixing only depends on species and not concentration may hold true at lower concentrations, but that at lower concentrations the chemical mixing is controlled by both the contaminants and diamantane and at higher concentrations it is dominated by diamantane alone. Comparing the slopes of the trend lines in Figures 52 and 54, the lower activation energy for the process assumed to be associated with chemical mixing in the material with diamantane implies that the mixing process is more favorable with diamantane than with the contaminant atoms and

supports the possibility that the value of *n* is dependent upon the ratio of diamantane to contaminant atoms.

4.2.2. Mechanical Behavior

Table 5 shows the measured Vickers hardness of several consolidated samples with and without diamantane. From the previous discussion, it was concluded that consolidated material with 0.1% diamantane likely have an equilibrium grain size larger than what is reported as the as-consolidated measured average grain size. Furthermore, it was concluded that a combination of factors lead to particularly slow grain growth at very low diamantane concentrations. Thus it may be assumed that the consolidated material with 0.1% diamantane in Table 5 that is heated at 300°C begins with the grain size reported in Table 3 and that the grain size increases very slowly with the 40 min and 120 min annealing. In the traditional Hall-Petch model, softening is a consequence of grain growth as stated earlier. In the very low diamantane concentration regime, the hardness results indicate traditional Hall-Petch behavior with very slight softening observed after heating.

The effect of final consolidation can be seen in Tables 3 and 5 as well. As shown in Table 3, swaging of materials with diamantane results in a larger average grain size. Comparing material consolidated with 0.1% diamantane by trap extrusion and swaging in Table 5, the swaged material is softer. Given the larger observed grain size, this again supports traditional Hall-Petch behavior in material with very low diamantane concentration. The difference in hardness of swaged material with 0.1% diamantane and 0.2% diamantane after annealing is trivial, although

there is a possible real increase in hardness with annealing time in the 0.2% diamantane material. The as-consolidated grain size of material with 0.2% diamantane was slightly larger than the material with 0.1% diamantane and, given the assumption that the material with 0.1% diamantane experiences slower grain growth, it is expected that the grain size after 120 minutes of annealing would be larger in the material with 0.2% diamantane than the material with 0.1%. In that case, Table 5 indicates that the material with 0.2% diamantane hardens as it is annealed while the material with 0.1% diamantane softens. The inverse Hall-Petch behavior indicated in the 0.2% diamantane sample has been previously reported, however, Table 3 suggests that inverse Hall-Petch behavior is dependent upon diamantane concentration (ref 4). This does not mean that inverse Hall-Petch behavior is not also dependent upon grain size, but the transition point from inverse to traditional Hall-Petch behavior may change with diamantane concentration.

The inverse Hall-Petch behavior was previously assumed to be accommodated by dislocations with sliding of grains along their boundaries (ref 4). In that work, the physical and chemical nature of diamantane was not considered, rather the transition of deformation mechanism was justified based on the domain size through which dislocations may pile up. Above some critical size, stress is carried by dislocations at a pile up propagating through a grain boundary and continuing to carry deformation to the other side while below the critical stress, grains slide more easily along their boundaries to carry deformation. It should be expected, though, that the ability of a dislocation to be carried across a grain boundary is going to be affected by the presence of diamantane. Not only will it present a physical boundary to dislocation

propagation, the atoms around the dislocation may in some way interact with the diamantane, which would again change the behavior of the dislocation. It would then a reasonable assumption that dislocations are affected by the amount of diamantane in the entire system, and by the amount present at the grain boundary. In addition to the diamantane stabilizing grain sizes and thus lowering the length along which dislocations may pile up, increased diamantane concentration will provide fewer locations in a grain boundary across which a dislocation may propagate. Both effects would lower the characteristic grain size for the transition from traditional to inverse Hall-Petch behavior.

4.3. Effect of Magnesium (Al-5Mg)

4.3.1. Thermal Stability

Table 2 shows the average grain size of as-milled powders mechanically alloyed with 5 weight percent magnesium and some with diamantane. For the sake of comparison, the same equipment scanning as-milled commercially pure powders resulted in an average grain size of 42 ± 2 nm. Grain size was determined by the Scherrer equation (eq. 26) applied to the same peaks used to determine the grain sizes in Table 2. The first line of Table 2 shows is that of the grain size calculated by equation 26 when applied to as-received powders. Since these are assumed to be coarse grained, there is apparently significant machine broadening in the peaks of all samples shown in Table 2. For this reason, the values are shown for comparative purposes only, including the value of 42 ± 2 nm for commercially pure cryomilled powders. Even by comparison, it can be seen that cryomilled powders with 5% magnesium tend to be smaller than those without. The value determined for as-milled commercially pure aluminum is about

1/3 larger than what was calculated for the powder cryomilled with 5% magnesium. Aluminum-magnesium powders with 0.2% diamantane were predicted to have approximately the same as-milled grain size as the powder without diamantane, although the aluminum-magnesium powder with 0.5% diamantane had a larger grain size. While the difference in as-milled grain sizes could be from variation in milling temperature that affects the amount of recovery during the process, if the runs are assumed to be identical then the magnesium must be affecting recovery. In fact, other reports have indicated a slight decrease in as-milled grain size with magnesium additions, which is further affected by other alloying elements (ref 20). Since the as-milled powder with 0.5% diamantane has a larger grain size than powders with 0.2% diamantane and no diamantane, the increased presence of diamantane is likely the cause for the increase in grain size. By correlation, this must mean that the decrease in as-milled grain size is due to the presence of magnesium at the grain boundary. Without magnesium or diamantane present at the grain boundaries, liquid nitrogen is necessary when cryomilling aluminum to prevent heating that would lead to recovery and grain growth. By adding magnesium to the milling mixture, the alloyed material is even more effective at doing this and, if there is grain boundary involvement, it is likely that magnesium's presence at grain boundaries is preventing dislocation annihilation. Solute mixing has already been well established as a means of lowering grain boundary energy to slow grain growth, and this explanation serves for why as-milled aluminum-magnesium powders have smaller grain sizes in general as well. As the boundary movement is expected to be inhibited by the presence of the highly soluble magnesium atoms, grain growth should be hindered, and with two means of preventing grain growth during cryomilling the as-milled grain size should be smaller. As more

diamantane is added to the milling mixture and ends up on the grain boundaries, the effect is apparently reduced and the as-milled grain size of aluminum-magnesium with 0.5% diamantane is closer to the as-milled grain size of commercially pure aluminum.

Table 3 shows the average grain size for consolidated aluminum-magnesium material with and without diamantane. As expected for material without diamantane, the presence of magnesium at the grain boundary is affording some degree of thermal stability, with the grain size of aluminum with 5% magnesium nearly 1/3 less than commercially pure aluminum. However this is not the case in the presence of diamantane. With 0.5% diamantane added to the mixture, aluminum with 5% magnesium is about 1/6 larger than material without magnesium. As was noted before, Table 3 makes no indication of equilibrium grain size and only lists the grain size measured after the indicated consolidation. This leaves open the possibility that aluminum with 5% magnesium and 0.5% diamantane is more thermally stable than aluminum with just 0.5% diamantane. Whether or not this is the case cannot be determined from the data presented alone, however, it can be surmised that this might be the case. An assumption was stated earlier that as-milled powders with magnesium have a smaller average grain size than as-milled powders without it because of the presence of magnesium at the grain boundaries, and that the effect of magnesium is reduced by much more diamantane occupying space at the grain boundaries. This explanation does not require that the grain boundary volume is entirely saturated by diamantane and, in fact, because magnesium must also establish a chemical equilibrium between the grain interiors and boundaries, there still should be some magnesium in the grain boundaries. This leads to a picture of both magnesium

and diamantane present at the grain boundaries in the aluminum-magnesium with 0.5% diamantane material, with the likelihood that the diamantane volume is greater than the magnesium volume due to a preferential presence at the grain boundary. Given that the consolidated average grain size of aluminum with diamantane is much less than that of aluminum with magnesium, diamantane is clearly much more effective at limiting grain growth than magnesium. Thus, a mixture of mostly diamantane and only some magnesium should have grain growth thermokinetics somewhere between material without diamantane and material without magnesium. This encompasses the effect of magnesium on the thermal stability of cryomilled aluminum and cryomilled aluminum with diamantane.

4.3.2. Mechanical Behavior

If indeed grain boundary sliding is the dominant deformation mechanism of commercially pure aluminum in the sub-100 nm grain size regime, then the limiting rate in the process in that range would be the climb velocity of dislocations in grain boundaries (ref 30). One may consider the effect of dislocation motion, though, by evaluation of the rate equation with which the behavior is modeled:

$$\dot{\gamma} = 9\,(b/D)^3\,(\bar{D}_{GB,0}/b^2)\exp(-Q_{GB}/RT)\,[\exp(2M\tau b^3/kT) - 1] \qquad \text{(eq. 28)},$$

where $\dot{\gamma}$ is the strain rate of deformation, b is the Burger's vector, D is the average grain size, $\bar{D}_{GB,0}$ is the grain boundary diffusivity, Q_{GB} is the activation energy for grain boundary diffusion, M is the stress concentration factor of sliding grains blocked by triple junctions, and τ is the applied stress. The stress concentration factor at triple points and the Burger's vector likely would not change if diamantane is present at grain boundaries, unless of course excess

diamantane tends to segregate to triple junctions. Furthermore, because the stress concentration at triple points is the source of dislocation generation, then so long as *M* is not influenced by the presence of diamantane, then the rate of dislocation generation and dislocation concentration both should remain unchanged as well. With an understanding of how diamantane influences the grain growth and deformation processes, the question at hand turns to the influence of magnesium. In a coarse grained alloy, magnesium at concentrations low enough to not form Al-Mg precipitates will simply form a solid solution, which is the well-known strengthening mechanism in 5XXX series of aluminum alloys. However, if the energetic cost for dislocation pile up has already become so high compared to that of ensemble movement of grains along their boundaries—as is expected in the grain boundary sliding process—then strengthening of grain interiors through solid solution strengthening would not provide any benefit. To the contrary, it could be imagined that if the magnesium is present in the grain interiors and its only influence was as a solute strengthener, then the outcome of its presence would a shift to larger values of the characteristic grain size at which deformation switches from the inverse to the traditional Hall-Petch mechanism. However, by comparing Tables 4 and 5 it is seen that aluminum-magnesium consolidated materials exhibit Hall-Petch behavior down to at least 88 nm grain size. With the switching point from inverse to traditional Hall-Petch behavior reported to be 110 nm for pure aluminum, the switching point apparently shifts downward from the addition of magnesium. Thus, the magnesium must work in another way than just solid solution strengthening when it is cryomilled to with Al.

It has been shown through molecular dynamics simulation as well as microscopic methods that, in low sigma aluminum grain boundaries, magnesium will preferentially sit in the larger sites

(ref 44–45). Given that magnesium is larger than aluminum, this makes sense as it allows for more relaxation in the grain boundary by sitting at these sites. Although there is no reason to expect a large concentration of low sigma grain boundaries in aluminum cryomilled with diamantane, the idea that magnesium would always prefer the most open sites at boundaries persists. If one imagines a structure without magnesium, the most open sites would provide a mean by which important grain boundary sliding steps such as dislocation climb and the sliding itself are primarily accommodated. Thus, if these otherwise open sites are occupied by magnesium instead, or if they are affected by the presence of magnesium in another way, the means by which GBS could occur are eliminated. Although not necessarily proving that grain boundary sliding would absolutely be eliminated by the presence of magnesium at the grain boundaries, the elimination of some free volume by the presence of magnesium would result in an increase of activation energy for any grain boundary sliding step that requires diffusion parallel to the plane of the grain boundaries. If such an increase in activation energy was great enough, its result would be a return to traditional Hall-Petch behavior, which appears to be the case. The ratio of hardness of O-temper 5083Al to that of 1100Al is about 3 to 1, so the strengthening afforded by the solid solution with magnesium increases the hardness of the aluminum up to 3-fold (ref 46–47). Comparing this to the same ratio for the cryomilled diamantane-free samples shown in Table, the strengthening is about 1.5-fold, noticeably less. Although the efficacy of solid solution strengthening need not be free of dependence from grain size, the difference in the ratio still indicates that the reason the 5Mg sample is stronger than that of the commercially pure sample is at least partly due to a change in deformation mechanism. More notably, though, the addition of diamantane to the aluminum-magnesium

sample results in a smaller and more thermally stable grain size such that the increased hardness validates the idea that the deformation mechanism in aluminum-magnesium system is traditional Hall-Petch behavior.

CHAPTER 5. CONCLUSIONS

A theory has been developed for the heat released during grain growth due to both the loss of grain boundary volume and the changing chemical potential of low-concentration solute atoms that lower the specific boundary energy. In addition, the mobility of grain boundaries is assumed to change. The form of the mobility change is chosen as a sigmoidal form empirically so as to allow for a smooth transition from one constant mobility to another. The variable mobility and variable grain boundary energy are applied to curvature-driven grain growth to yield equation 24.

The reduction of specific grain boundary energy and grain boundary volume are measured as an exothermic heat signal when held isothermally between $0.6T_m$ and $0.9T_m$, after which the heat signal is integrated over time and normalized to the total amount of heat released during was is taken to be the measurable grain growth period. With the initial and final grain sizes measured independently, equation 24 can be applied with assumed grain growth parameters and the instantaneous grain size during each point of isothermal heating can be used to calculate the integrated and normalized heat flow at that time. The assumed grain growth parameters are then adjusted to fit the calculated integrated and normalized heat flow to the actual heat flow. The result of a least squares fit is a grain growth curve characterized by the final values of the parameters in the equation 24 model. This method is advantageous because it allows for a highly time resolved grain growth curve that captures features that are otherwise missed by methods that only capture grain size at several points in time during isothermal

heating. Grain growth parameters were compared based on isothermal temperature and the amount of diamantane added to the cryomilling mixture.

Following the isothermal DSC experiments, aluminum was cryomilled with very low concentrations of diamantane. The as-consolidated grain size and mechanical behavior were characterized to determine the effects of diamantane when it is only lightly dispersed at the grain boundaries. Magnesium was added to the cryomilling mixture at a concentration of 5 weight percent of the mixture as well. The as-consolidated grain size and mechanical behavior were again characterized with the goal in mind to determine how the effects of diamantane on aluminum are affected by the presence of magnesium. The results also indicate how diamantane might alter the thermal stability and mechanical behavior of cryomilled aluminum alloys.

From the current work completed, the following conclusions may be drawn:

1. The assumed sigmoidally-varying grain boundary mobility during isothermal heating tends to allow for very good fits of the DSC integrated heat profiles. The initial grain boundary mobility in several samples seeming to be relatively independent of temperature indicates that the boundary motion is initiated athermally. This is observed in powders both with and without diamantane, meaning that the behavior is due to having been cryomilled and not due the presence of impurities or other solute species. Because of the high dislocation concentration and random grain boundaries present after cryomilling, the initial growth mechanism is implicated as a process such as grain rotation, or reordering or recovery of dislocations. The

initial athermal growth mechanism then transitions to a thermally activated mechanism. The sigmoidal dependence of mobility on grain size indicates that the transition in mechanisms is due to both mechanisms acting in parallel, where the thermally activated mechanism becomes dominant once the source of the initial growth mechanism is consumed.

2. The initial grain growth mechanism is observed to be athermal, but it is affected by diamantane concentration. Because diamantane is necessarily present only at grain boundaries at the start of grain growth, the diamantane concentration affects how much of the grain boundary volume is initially occupied. This means that the initial grain growth mechanism relies on the free volume present in the grain boundaries, which again implicates grain rotation, reordering and recovery. Regardless of the actual grain growth mechanism, it may be concluded that grain growth is initially hindered by the presence of diamantane at the grain boundaries. The thermally activated grain growth mechanism is also seen to be dependent upon diamantane concentration, so the conclusion carries through that the presence of diamantane at grain boundaries hinders grain growth. As the second grain growth mechanism is assumed to be the desorption-diffusion-adsorption mode, it is most likely that diamantane pins grain boundaries in the second growth mechanism.

3. Grain growth is affected by the presence of diamantane due to chemical stability as well. As is expected, the grain boundary excess of diamantane is affected by the diamantane concentration, which lowers the equilibrium grain size at increasing diamantane

concentrations. It is also concluded that the grain boundary excess parameter, *n*, is affected by the chemical species involved in the mixing but not its concentration.

4. The second grain growth mechanism exhibits two possible behaviors, which depends on the heating temperature. In the low temperature regime, the secondary growth mechanism has a lower activation energy than in the high temperature regime. The transition point between the low and high temperature regimes is shown to be affected by the diamantane concentration as well, with the consolidation temperature used, 520°C, the switching point for a diamantane concentration between 0.1 and 0.2 weight percent. The previously reported Inverse Hall-Petch behavior in cryomilled aluminum-diamantane system is also inferred to be dependent upon diamantane concentration, not only because of the difference in thermal stability imparted to the material but also because of the grain boundary free volume dependence on diamantane concentration.

5. As-consolidated grain size and mechanical behavior of aluminum-magnesium samples with and without diamantane indicates that, like diamantane, magnesium imparts some thermal stability due to chemical mixing. Furthermore, the magnesium competes to some degree with diamantane for presence in the grain boundaries due to magnesium's affinity for larger grain boundary sites. The resulting thermal stability is that of a mixture between the effects of magnesium and those of diamantane. The presence of magnesium in the grain boundary is able to open up enough space to allow for Hall-Petch strengthening, such that aluminum-

magnesium consolidated samples with diamantane are not susceptible to Inverse Hall-Petch softening at the observed grain sizes.

CHAPTER 6. FUTURE WORK

The body of work presented in this dissertation has answered a few questions, introduced some interesting possibilities and shed some light on some previously reported phenomena. But to a greater extent, the current work has led to more questions than the answers originally sought. There are, of course, many routes one could take to follow up this work, but what may be the seven topics most closely related to the current research are presented below.

Application of the DSC Model to Other Systems The DSC grain growth model developed in equation 21 is an extension of Lu's report in the late 1980s and early 1990s on the application DSC as a means of measuring grain growth (ref 34). While the work of Lu has been followed up by other works, a full model has yet to be developed to account for impurities and small amounts of alloying elements that will affect grain growth via the thermodynamic parameter, grain boundary excess (ref 48-49). In the current work, the development of equation 24 allows for some estimation of grain growth based on physically relatable parameters and descriptions. To fully develop this model, it must be applied to other systems in a controlled manner. Chapter 4.1 applies the model to cryomilled aluminum with and without diamantane, essentially two similar but distinct systems. The influence of internal strain on the applicability of the model can be tested by measuring grain growth of aluminum formed by a method that does not require plastic deformation to make a nanograins, for example pulsed electrodeposition. The influence of pinning media on the model may be investigated by changing the milling diamondoid additive from diamantane to adamantane and triamantane, in separate experiments. Applicability to other materials can be tested by applying the model to

other cryomilled metals, such as copper and nickel. Moreover, application of the DSC grain growth model to other systems can help to further explain the meanings and relationships between the $\mathbf{\Lambda_i}$ parameters. The current work has explored the meanings and relationships in the aluminum-diamantane system, but it has only scratched the surface.

Bicrystal Studies with Diamantane Because of the possibility of interaction between carbon and aluminum, as well as the likelihood that at least a small amount of terminating hydrogen is liberated from diamantane molecules, it should be determined in a much more controlled manner the degree of exothermic (or endothermic) interaction between aluminum and diamantane. If, for example, there is indeed some exothermic interaction measured by DSC that is void of any relation to grain growth behavior, then the thermal signature of this process will be measured along with any grain growth. Then, if this is measured primarily at the start of the isothermal heating experiment, the real amount of heat released at the onset of heating from grain growth alone would make the initial slope of the $x(t)$ curves much less than what is shown in the figures in Chapters 3 and 4. Effectively, this would mean all k_0 parameters would have been overestimated.

To determine if there is an additional process being measured by DSC, grain growth must be removed entirely. This could be done by measuring the DSC signal from fully annealed powders cryomilled with diamantane. Alternatively, a more conclusive result would be obtain with a bicrystal experiment. In such a study, an aluminum bicrystal formed with two single crystals would have a layer of diamantane introduced at their boundary before cold pressing together

to form a somewhat coherent boundary. A DSC sample would be cut from the bicrystal sandwich, which would then be heated isothermal. Any signal would indicate not only an additional thermal process, but experiments at multiple temperatures could be used to determine its contribution to the thermal activation on isothermal heating.

Inverse Hall-Petch Behavior To date, all data published on the mechanical behavior of consolidated cryomilled aluminum with diamantane has indicated that the material is softer than its corollary without diamantane. There is no doubt that the diamantane is somehow softening the material and, because of much greater ductility in tensile samples made from the material with diamantane than without, grain boundary sliding is the choice deformation mechanism for the material (ref 4). This is, however, the first work to show evidence that the concentration of diamantane has any effect on transition grain size from Inverse Hall-Petch behavior to traditional Hall-Petch behavior. Strength or hardness versus grain size plots are needed for cryomilled aluminum with varying amounts of diamantane to absolutely determine if the transition grain size is dependent upon grain size. If it is proven to be the case, a cause for this must be determined. Doing so is absolutely the best way to determine the amount of diamantane and grain size necessary to optimize the strength of commercially pure aluminum.

Secondary Growth Mechanism Like the transition from Inverse Hall-Petch to traditional Hall-Petch behavior, the current work has provided some evidence that the transition temperature from one secondary grain growth mechanism to another secondary grain growth mechanism is dependent upon diamantane concentration. This work will require a better understanding of

the DSC model, as the k_{min} parameter was revealed through that model. Once there is a better understanding, after which there is a higher confidence in the correctness of k_{min} values, a series of Arrhenius plots can be used to determine the transition temperature of k_{min} for different diamantane concentrations. This knowledge will be particularly useful for material design, for example in allowable heat treatments, maximum service temperature, and so forth.

Primary Growth Mechanism From the k_0 values determined from DSC data, it was inferred that below certain temperatures k_0 represents a thermally activated process. Although not certain, the lack of any evident trend in k_0 with temperature as well as the spread in k_0 values being within acceptable experimental error has led to this inference that grain growth begins with an athermal process. This process, which typically would begin to dissipate after only a 10-15% increase in grain size has yet to be reported in any other work of thermally stabilized cryomilled aluminum. Thus, more data is needed for secondary validation that this is not an artifact of the curve fitting. Absolute validation of this behavior would be even more beneficial, which could be done by TEM observation of cryomilled powders heated in-situ on a heating stage.

Other Alloys This and previous works have presented results primarily using commercially pure aluminum. Aluminum with 5 percent magnesium was introduced towards the end of the current work although, strictly speaking, this does not represent any one particular alloy. The benefit of doing the work with just aluminum and magnesium is that it removes the influence of other alloying elements. This concept may be extended to study the effects of diamantane in a precipitation hardened system. Likely copper or zinc would be cryomilled with the starting

powder instead, and the same analyses used herein could be applied to the selected system. In addition to generally being stronger than 5XXX aluminum, the 2XXX (Cu) and 7XXX (Zn) aluminum alloys would be expected to have precipitates that could interact in unique ways with diamantane, and with grain boundary sliding during deformation.

Once the range of aluminum alloys has been studied, other alloys may benefit from the same analysis. In particular, copper alloys, the range of titanium alloys, zirconium alloys, zinc alloys, and Superalloys may see some benefit from thermal stabilization after cryomilling. Although many titanium alloys and Superalloys are already considered high strength for most applications, increase in strength offers opportunity for further reduction in volume, which ultimately may offer cost savings. Many of these materials are particularly corrosion resistant as well and, for the same reason as aluminum, would benefit from strengthening by cryomilling.

Other Stabilizing Media In addition to testing thermal stability offered by higher order diamondoids, similar diamond-cubic materials such as nano-sized silicon could be used. In particular, silicon is pointed out both because of its similarity to diamond and because it tends to terminate in oxygen rather than hydrogen. As pointed out earlier, some hydrogen is likely to be released from diamantane. Although the same could happen in silicon by releasing oxygen, oxygen is less detrimental to the aluminum structure than hydrogen, which can cause embrittlement.

Diamantane could also be introduced into cryomilled aluminum and other metals after functionalization. On the one hand, functionalization may encourage or discourage interaction with aluminum, which will of course change how it interacts during grain growth and deformation. On the other hand, functionalized diamantane in cryomilled biocompatible metals may be necessary to improve biocompatibility from the diamantane portion of the structure.

REFERENCES

1. Hall, E.O., *Proceedings of the Physics Society of London* 64, 1951, pp 747-753.

2. Petch, N.J., *Journal of the Iron and Steel Institute of London* 173, 1953, pp 25-28.

3. Meyers, MA., et al, *Progress in Materials Science* 51, 2006, pp 427-556.

4. Maung, K., et al, *Acta Materialia* 60, 2012, pp 5850-5857.

5. Bezok, N. and E. Oktay, *Materials Science and Engineering* 576A, 2013, pp 82-90.

6. Horn, R.M. and R.O. Ritchie, *Metallurgical Transactions* 9A, 1978, pp. 1039-1053.

7. Ma, D., et al, *Science and Technology of Advanced Materials* 14 (2), 2013, No. 02500.

8. Callister, W.J., *Materials Science and Engineering: An Introduction (6th Ed.)*. John Wiley and Sons: New York, 2007. Print.

9. R. Mahmudi, *Scripta Materiala et Metallurgica* 32 (5), 1995, pp 781-786.

10. Burke, J.E. and D. Turnbull, *Progress in Metals Physics* 3, 1952, pp 220-297.

11. Lee, K.J., et al., *Nanotechnology* 17, 2006, pp 2424-2428.

12. Wu, N.-L., et al., *Science* 285, 1999, pp 1375-1376.

13. Jorge Jr., A.M., et al., *Metallurgical and Materials Transactions* 40A, 2009, pp 3314-3321.

14. Gertsman, V.Y. and R. Birringer, *Scripta Metallurgica et Materialia* 30, 1994, pp 577-581.

15. Li, JCM, *Physics Review Letters* 96, 2006, No 215506.

16. Witkin, D.B. and E.J. Lavernia, *Progress in Materials Science* 51, 2006, pp 1-60.

17. Tellkamp, V.L. et al, *Metallurgical and Materials Transactions* 32A, 2001, pp 2335-2343.

18. Huda, Z. and T. Zaharinie, *Journal of Alloys and Compounds* 478, 2009, pp 128-132.

19. Roy, I., et al., *Metallurgical and Materials Transactions* 37A, 2006, pp 721-730.

20. Hanna, W., et al., *Advances in Materials Science and Engineering*, 2014, No. 921017.

21. Ma, K., et al., *Acta Materialia* 62, 2014, pp 141-155.

22. Aerodyne Alloys, "6Al-4V Titanium Bar (UNS R56400)," AMS 4928 Ti-6Al-4V datasheet, last accessed 27 Sep 2014 <http://http://www.aerodynealloys.com/pdf/6a1-4v-titanium-bar.pdf>

23. Gao, J. et al., *Acta Materialia* 45, 1997, pp 3653-3658.

24. Wurschum, R., et al., *Advanced Engineering Materials* 5, 2003, pp 365-372.

25. Maung, K., et al., *Journal of Materials Science* 46, 2011, pp 6932-6940.

26. Dahl, J.E. et al., *Science* 299, 2003, pp. 96-99.

27. Bokari, W., "Diamond Molecules--Building Blocks for Nanotechnology." First International Symposium on Nanomanufacturing. Massachusetts Institute of Technology. 25 April 2003. Presentation. <http://web.mit.edu/nanosymposium/www/Presentations/Bokhari.pdf>

28. Fecht, H.J., *Nanostructured Materials* 6, 1995, pp 33-42.

29. Yamasaki, T., *Materials Physics and Mechanics* 1, 2000, pp. 127-132.

30. Mohamed, F.A. and M. Chauhan, *Metallurgical and Materials Transactions* 37A, 2006, pp 3555-3567.

31. Zhang, Z., et al., *Metallurgical and Materials Transactions* 41A, 2010, pp 532-541.

32. Zhong, Y., et al., *Journal of Alloys and Compounds* 476, 2009, pp 113-117.

33. Simoes, S., et al., *Nanotechnology* 21, 2010, No. 145701.

34. Lu, K., *Scripta Metallurgica et Materialia* 25, 1991, pp 2047-2052.

35. Weissmuller, J., *Nanostructured Materials* 3, 1993, pp 261-272.

36. Kirchheim, R., *Acta Materialia* 55, 2007, pp 5129-5138.

37. Li, J., et al., *Scripta Materialia* 60, 2009, pp 945-948.

38. Michels, A., et al., *Acta Materialia* 47, 1999, pp 2143-2152.

39. Bernardini, J., et al., *Proceedings of the Royal Society of London* 379A, 1982, pp 159-178.

40. Farkas, D., et al., *Physical Review Letters* 98, 2007, No. 165502.

41. Li, H., *Advanced Engineering Materials* 7, 2005, pp 1109-1110.

42. Gutkin, M. Yu., et al., *Scripta Materialia* 58, 2008, pp 850-853.

43. Han, B.Q., et al., *Journal of Materials Science* 42, 2007, pp 1660-1672.

44. Liu, X., et al., *Journal of Physics: Condensed Matter* 17, 2005, pp 4301-4308.

45. Shamsuzzoha, M., et al., *Interface Science* 3, 1996, pp 227-234.

46. ASM Aerospace Specification Metals Inc., “Aluminum 5083-O”, Technical Specification, Last accessed 23 Nov 2014. <http://asm.matweb.com/search/SpecificMaterial.asp?bassnum=MA5083O>

47. HM Wire International Inc., “Aluminum 1100-O”, Product Specification Sheet, Last accessed 23 Nov 2014. <http://www.hmwire.com/New%20PDFs/Aluminum_1100_Information.pdf>

48. Eckert, J., et al., *Journal of Materials Research* 7, 1992, pp. 1751-1762.

49. Lu, K. and Z. Dong, *Journal of Materials Science and Technology* 13, 1997, pp. 491-494.

APPENDIX I. UNCERTAINTY IN DSC PARAMETERS

The primary source of uncertainty in the values of the set **Λ** (k_{min}, k_{max}, φ, D_{kin}, D_{eq}, and n) is the natural variation in the system. The quantity of material being measured is small and thus should be sensitive to variations both from run to run, as well as variation within the run. For instance, if a specific few powder particles become contaminated with iron from the milling media towards the end of a run, then it is possible that one DSC sample could have these powders in it while another would not. In addition, there are many user-controlled variables in the production of the powders that can affect the DSC heat flow, for example, exposure to air after milling or position of the thermocouple used during the run. While the uncertainty from random variations in user-controlled parameters and sequences, and the variation within a run should constitute the majority of the uncertainty, the error inherent to the DSC measurement must be considered as well.

There is a single source of error inherent to the DSC measurement, which is from noise in the signal and can be assumed to be related to the precision of the instrument. The calorimetric precision of the instrument (TA Instruments DSC Q2000) is ± 0.05% and the temperature accuracy is ± 0.1°C, or ± 0.013% at 500°C. Because the calculated curve is fit to the measured curve, the true value of the variables will depend on the actual heat flow; furthermore, the experiments are isothermal, making the precision of the heat flow much more important than the accuracy of the temperature due to the fact that one parameter—heat flow—is variable during the experiment and the other—temperature—is constant. Therefore, a 0.05% uncertainty due to the precision of the instrument can be assumed. However, as indicated

before this is expected to be much less significant than the random error originating from the samples.

Random error is introduced due to the nature of the material. This random error is dependent upon, for example, the uncertainty in the initial grain size of the specific sample being measured, variation in powder chemistry from run to run, and variation in the amount of gas trapped in the sample during the experiment. The variation in the initial grain size must be considered across several independently calculated average grain sizes, though, because the DSC model already assumes an average grain size that will have a standard deviation associated with it. Thus, variation of initial grain size is best quantified by the standard error of the mean grain size. Because the same stock powder is used from run to run, variation in powder chemistry could only come about from one of two sources. Either the amount of impurities will be changing from run to run, or the as-milled powder will not be entirely homogenous and DSC samples are taken from different portions of the inhomogenous powder. The amount of gas trapped is somewhat affected by the milling, particularly if water is adsorbed onto the powder surfaces. However, the trapped gas is primarily influenced by how the powders are packed into the aluminum pans. Of the sources of random error introduced on a per experiment basis, only the effect of uncertainty in the initial average grain size can be estimated directly. The remaining sources of random error can only be estimated from formulations that had more than one sample tested.

Error in the model parameters originating from uncertainty in the initial average grain size can be estimated by determining the model parameters of a range of starting grain sizes and relating the change in model parameters to the change in initial grain size. The percent change of each model parameter was compared to the percent change in initial grain size and a correlation between the percent change in a parameter against the percent change in initial grain size was taken as the "slope" between the model parameters and initial grain size. Although many of the relationships between starting grain size and model parameters were not actually linear, a linear assumption was made to estimate how much each parameter is affected by the starting grain size for any given data set. Table A1 summarizes the optimized model parameters and slope compared to the starting grain size. The correlation coefficient between calculated and measured *x(t)* curves is shown as well to compare wellness of fit in each case.

Table A1 Change in DSC model parameters as the initial grain size used in the calculation is changed.

D_0 (nm)	D_f (nm)	k_0 (nm^2/s)	η	ϕ	D_{kin} (nm)	D_{eq} (nm)	n	k_{min} (nm^2/s)	R^2
20	28	10.57	0.97	0.67	24.19	39.90	2.07	0.35	0.9983
21	28	10.26	0.97	0.73	24.83	40.07	1.94	0.34	0.9982
22	28	10.01	0.98	0.62	25.01	40.00	1.80	0.22	0.9967
23	28	10.00	0.98	0.62	25.01	39.18	2.17	0.17	0.9975
24	28	10.00	0.98	0.61	25.00	38.97	2.22	0.15	0.9959
	Slope	-0.3056	0.1191	-0.8438	0.1594	-0.1512	0.6386	-5.6533	
	% Error (est)	0.373	0.145	1.029	0.194	0.184	0.779	6.895	

A slope of less than zero indicates an inverse relationship and an absolute value of a slope greater than one would indicate that the model parameter changes faster than the initial grain size. Given that, except for the minimum mobility, k_{min}, all absolute values of slopes are less than 1, these parameters may all be considered somewhat insensitive to changes in the starting

grain size, for the given range of starting grain sizes shown. The only parameter with a slope that takes an absolute value greater than 1 is the minimum mobility, k_{min}, which is estimated to change more than 5 times for each percent change in starting grain size. The reduction in maximum mobility, η, is least sensitive to changes in the starting average grain size.

The assumed starting grain size of 22 nm is from ref [25], wherein the average grain size from 500 measurements was 22 ± 6 nm. This yields a standard error of the mean as 0.27 nm, or 1.2% of the calculated mean. From this, the percent error for each of the parameters was estimated from the "slope" by taking the product of the parameter's "slope" and the standard error of the mean. The estimated percent error of each variable is shown. The data used for the calculation was the #1 sample of cryomilled aluminum with 1% diamantane.

The preceding calculations are one example of how one source of random error leads to uncertainty in the model parameters. The effect of the final grain size in the calculations, D_f, could be estimated as well, however, it is less useful because the final grain size is estimated but not calculated in some cases. Instead, the most useful and practical way to estimate uncertainty in the measurements is by simply taking repeated measurements and characterizing the standard deviation of the values that come about from the resulting DSC curves and model parameters fit to those curves. The greatest number of DSC isothermal heat flow measurements taken on any given material in this work was on cryomilled aluminum with 1% diamantane. This is particularly useful for this evaluation because the six measurements were taken over two different batches of powder, three samples from each batch. Table A2

summarizes the estimated standard deviation for the model parameters based on the six isothermal experiments.

Table A2 Six sets of DSC parameters for cryomilled aluminum with 1% diamantane.

Temp (°C)	k_0 (nm^2/s)	η	ϕ	D_{kin} (nm)	D_{eq} (nm)	n	k_{min} (nm^2/s)	R^2
300 (#1)	10	0.99	0.6	25	40	1.8	0.1	0.996
300 (#2)	13	0.99	0.6	24	38.7	1.8	0.13	0.998
300 (#3)	13	0.99	0.7	24	38.5	2	0.13	0.998
300 (#4)	13	0.99	0.35	22.8	39	2	0.13	0.988
300 (#5)	13	0.95	0.35	22.4	39	1.7	0.65	0.999
300 (#6)	13	0.99	0.45	24	38.7	2	0.13	0.999
Avg	12.5	0.98	0.51	23.70	38.98	1.88	0.21	
Std Dev	1.2	0.02	0.15	0.94	0.53	0.13	0.22	
% Dev	9.8	1.7	28.8	4.0	1.4	7.1	101.6	

The estimated percent deviation from these six runs may be compared to the estimated uncertainty due to the error in the starting average grain size. Interestingly, the overall error is roughly proportional to the error due to the starting grain size. Note, however, that the estimated percent deviation in k_{min} of more than 100% is primarily due to a single value from run #5 that was much more than any of the five other runs. This may be considered an outlier due to the fact that, if excluded from the calculation of the average and standard deviation, k_{min} = 0.65 nm^2/s from run #5 is nearly 40 standard deviations away from the mean. When the value from run #5 is omitted, the value of k_{min} from the remaining 5 runs may be taken as k_{min} = (0.124 ± 0.013) nm^2/s, or k_{min} = 0.124 nm^2/s ± 10.8%. Even after removing the value from run #5, the percent deviation is the second greatest for k_{min}, which is similar to what was observed from the errors associated with the starting grain size. This exercise provides a means by which the uncertainty in the DSC model parameters may be estimated. Except for φ, each variable in

the model may be safely assumed to be up to 10% uncertain, and φ may be assumed to be up to 30% uncertain.